# Compatibilization of PMMA/PS blends by nanoparticles and block copolymers: effect on morphology and interfacial relaxation phenomena

par

Julie GENOYER

THESE PRESENTEE EN COTUTELLE A L'ECOLE DE
TECHNOLOGIE SUPERIEURE ET A L'INSTITUT MINES TELECOM
LILLE DOUAI COMME EXIGEANCE PARTIELLE A L'OBTENTION
DU DOCTORAT EN GENIE
Ph. D.

MONTRÉAL, LE 14 MARS 2018

ÉCOLE DE TECHNOLOGIE SUPÉRIEURE
UNIVERSITÉ DU QUÉBEC

**N° d'ordre : 42585**

**IMT Lille Douai**
École Mines-Télécom
IMT-Université de Lille

**ÉTS**
Le génie pour l'industrie

**Université de Lille**
1 SCIENCES ET TECHNOLOGIES

**THÈSE en co-tutelle**

présentée en vue d'obtenir le grade de

**DOCTEUR**

en

Physique et science des matériaux

par

**Julie GENOYER**

COMPATIBILIZATION OF PMMA/PS BLENDS BY NANOPARTICLES
AND BLOCK COPOLYMERS : EFFECT ON MORPHOLOGY
AND INTERFACIAL RELAXATION PHENOMENA

Manuscrit déposé le 14 Mars 2018

Soutenue le 19 décembre 2017 devant le jury d'examen :

| | | |
|---|---|---|
| Rapporteur | **John DEALY** | Prof., McGill University, Montréal |
| Rapporteur | **Jean-Charles MAJESTÉ** | Prof., Université Jean Monnet, St Étienne |
| Examinateur | **Alan CARTER** | Prof., ÉTS Montréal |
| Examinateur | **Philippe CASSAGNAU** | Prof., Université Claude Bernard, Villeurbanne |
| Examinateur | **Pierre LAFLEUR** | Prof., Ecole Polytechnique de Montréal |
| Directeur | **Nicole DEMARQUETTE** | Prof., ÉTS Montréal |
| Directeur | **Jérémie SOULESTIN** | Prof., IMT Lille Douai |

# ACKNOWLEDGMENT

drinks on weekends became a nice ritual. I would like to thank Amulya for her friendship through my last year in Douai.

A special thanks to my roommates: Erwan, Mathieu, Lola, Lucas, JP, Pierre, Marie and Lucien who made my stay in Montreal unforgettable.

Finally, I would like to thank my parents who always support me, push me to do my best and to surpass myself.

**TABLE OF CONTENTS**

Page

# INTRODUCTION

Blends of polymers are commonly used in the plastic industry. The usual polymers are often not sufficient for the actual demand of consumers that always want better performance. To meet this need of multi-functional materials, a range of polymer blends has been developed. Blending polymers of different type is a relatively easy and cost-effective way to obtain materials that combine contradictory properties compared to the development of a new molecule. Indeed, it only requires a simple process (batch mixer, extruder…) to mix the preexisting polymers compared to a chemical synthesis, which is more expensive, more complex and less evident to set up. In particular, immiscible polymer blends are technologically interesting since their mechanical, thermal, electric, magnetic, transport, and optical properties strongly depend on their microstructure. Very often, polymer blends morphology develops during processing, and at the same time, the polymer blends processability is influenced by the microstructure. The interplay between flow, morphology, and rheology is therefore a key point if one aims at tailoring the final material properties by mixing two immiscible fluids.

The incompatibility between polymers has led the researchers to develop strategies to improve the adhesion between the phases. Over the years, several methods have been found. The most common remains the addition of block copolymer in which each block is chosen to be compatible with one of the phases so that the copolymer localizes itself at the interface. Another route, often preferred in industry, is the addition of reactive polymers. In this case, two polymers react in situ during processing directly at the interface. More recently, immiscible blends have been shown to be stabilized by nanofillers as well. The use of those colloidal particles results in what is called "Pickering emulsion" such as in water/oil emulsions. Even though the stabilization mechanism remains unclear, the stabilization by nanoparticles can offer advantages compared to copolymer compatibilization: solid particles are usually less expensive than block copolymers and can bring additional properties to the material (thermal, electrical, optical…) if necessary. At the present time, the influence of fillers on polymer blends morphology is still a matter of intensive investigation.

The rheology–morphology mutual interaction was studied experimentally, theoretically, and numerically, focusing on both concentrated systems and dilute ones using mostly small amplitude oscillatory shear (SAOS) in the linear regime. The works that link microstructure with flow and rheology are numerous. Linear rheology is a powerful way to characterize polymer blends: morphology, interfacial tension between the components, relaxation phenomena after small deformations can be inferred from a simple shear measure in the linear regime.

However, in real processing conditions, polymer blends encounter more complex flows and higher deformations. Extensional flow, for example, is an important part of several processes. As such, the extensional properties of polymer melts are of great interest. Extensional flow is usually used to evidence a strain hardening behavior of branched polymers or exfoliated clay nanocomposites. However, there is very few studies of polymer blends behavior under extensional flow.

The main objective of this thesis was to use rheology to study the effect of adding nanoparticles to polymer blends. To do so, clay nanoparticles were chosen as they can come in varied sizes and shapes. Moreover, they can be easily organo-modified to disperse well in polymers. PMMA and PS were chosen as together they form a model polymer blend which rheological behavior is already well known and appropriate for the use of rheological models.

Several steps in the process of understanding the effect of adding nanoparticles and a possible compatibilization mechanism induced by them were conducted:

- The first goal was to understand more deeply the mechanism taking place in the compatibilization of PMMA/PS blends with conventional compatibilizers: PS-b-PMMA block copolymers and Cloisite 20A, a commercially available organoclay.

- The second step was to study the effect of adding different clay nanoparticles: Montmorillonite, laponite and halloysite which differ only by their size and shape and study their effect under both shear flow (low deformations) and extensional flow (so high deformations).

# CHAPTER 1

## POLYMER BLENDS & THEIR RHEOLOGICAL BEHAVIOR

This literature review covers generalities about immiscible polymer blends, the compatibilization using block copolymers or nanoparticles and the use of shear and extensional rheology to characterize polymer blends behavior.

### A.    Polymer blends: Generalities

The final properties of blends depend on the composition, but also on the interfacial properties and morphology. Over the years, numerous works on simple blends of two Newtonian fluids allowed the understanding of the different microstructural changes. Depending on the concentration in dispersed phase, the blend can have different morphologies such as in FIG. 1.1.



FIG. 1.1 Evolution of a blend morphology as a function of concentration [1]

For example, dilute systems usually display a droplet like morphology whereas both phases can create domains of uncertain shape when the concentration of dispersed phases increases. Our study focuses on the dilute or semi-dilute blends that exhibit a droplet like morphology. In this case, the creation of the microstructure is mainly governed by droplet breakup and coalescence under flow and after cessation of flow which are all described below.

### 1.    Droplet breakup

Taylor [2], [3] and Rumscheidt and Mason [4] studied the dispersion of a Newtonian fluid into another Newtonian fluid subjected to small deformation. In such field, the droplets are deformed into an elongated shape in the direction of the flow. Taylor suggested that at low stress in a steady uniform shear flow, the deformation degree of a droplet is a function of

- The capillary number Ca

$$Ca = \frac{F_{viscous}}{F_{interfacial}} = \frac{\eta_m \dot{\gamma} R_v}{\alpha} \tag{1.1}$$

- The viscosity ratio p of the dispersed phase and the matrix

$$p = \frac{\eta_d}{\eta_m} \tag{1.2}$$

Applying a flow can lead to droplet breakup when the interfacial tension forces cannot balance the viscous forces. That is what happens above a critical value of the capillary number: $Ca_c$. Below this value the droplets will not break anymore. Grace [5] provided data about this phenomenon by plotting $Ca_c$ as a function of p for both simple shear and extensional flow (FIG. 1.2). The critical capillary number is significantly higher in simple shear than in elongation. In fact, in an elongational flow, droplet breakup can occur at any p whereas for a simple shear flow and a $p \geq 4$, it is not possible to break the droplets anymore. Also, the weaker p, the higher $Ca_c$ will be, which means that it will be more difficult to break the droplets of low viscosity in a highly viscous matrix. The lowest $Ca_c$, in other words the range where breakup is the easiest, is found for $0.1 \leq p \leq 1.0$.
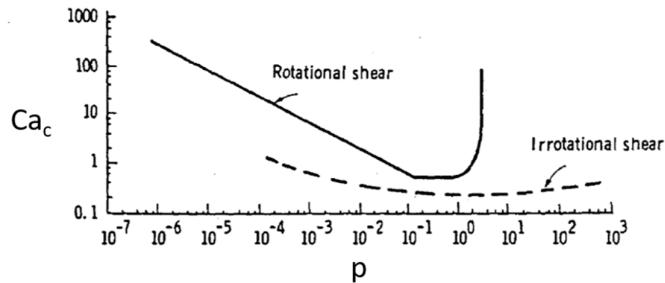


**FIG. 1.2 Effect of the viscosity ratio on critical capillary number in rotational shear and irrotational shear fields** [5]

A simple empirical fit of this curve has been given later by De Bruijn [6] (see equation ( 1.3 )):

$$logCa_c = -0.506 - 0.0995logp + 0.124(logp)^2 - \frac{0.115}{logp - log4.08} \tag{1.3}$$

## 2.   Coalescence

Coalescence is a process in which two or more droplets merge into one, resulting in a bigger droplet. Two types of coalescence can be distinguished:

- Flow driven coalescence where droplets are brought close by the flow (FIG. 1.3).
- Static coalescence which involves only Brownian motion.
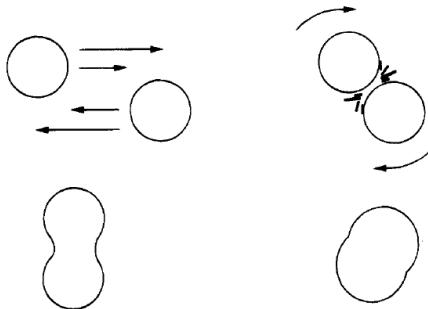
**FIG. 1.3 Idealized shear induced coalescence** [7]

When two droplets collide, they develop a flat interface over which they are separated by a thin film of matrix fluid. If its thickness falls below a critical value $h_c$ (usually around 10 nm) then the film ruptures and the droplets coalesce [6]. Sundaraj and Macosko [7] showed that coalescence decreases if the matrix phase viscosity is above a critical value and the dispersed phase volume fraction under a critical value. The shear rate can also have an influence on the coalescence process: Van Puyvelde et al. [8] and Lyu et al. [9] both agreed that increasing the shear rate decreases coalescence which is in good agreement with the definition of the critical capillary number (equation ( 1.1 )).

### 3.        Morphological hysteresis

The interactions between breakup and coalescence produce a phenomenon of morphological hysteresis illustrated in FIG. 1.4 [6]. In this figure, the coalescence limit under which coalescence occurs and the breakup limit above which breakup occurs can be visualized. The coalescence limit and breakup limit meet at a critical shear rate $\dot{\gamma}_c$. Above this value of shear rate, the steady state drop size is determined by a competition between coalescence and breakup (point 1 for example), here both can occur but the fastest one dominates. Below this critical number there exists a range of drops in the hysteresis region where the two phenomena cancel each other out (point 2, 3, 4, 5 and 6). In this region we observe neither coalescence nor breakup.

If we only want to observe coalescence, as Vinckier et al. [10] and many others did, it is possible to use the hysteresis present in these blends to do so. First, the blend undergoes a pre-shearing at high shear rate to generate a fine morphology and then the shear rate is lowered in step to below a critical value (point 1 to 2 for instance) allowing us to observe only coalescence.
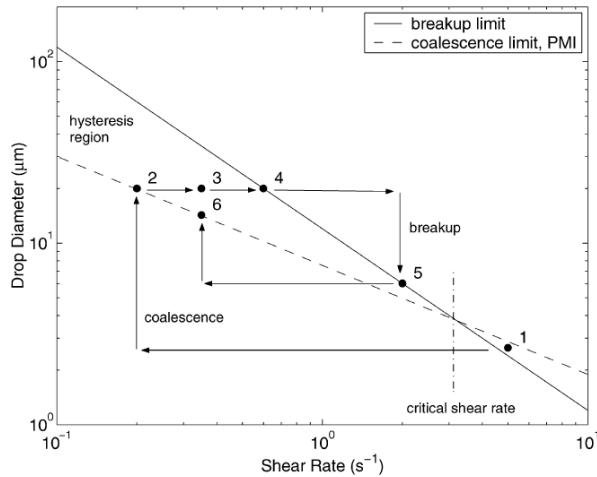
**FIG. 1.4 Typical history of droplet size versus shear rate, illustration of morphological hysteresis** [6]

### B.      Compatibilization of polymer blends

In order to obtain a fine and stable morphology, what is called compatibilizers can be added. They are expected to settle at the interface between the polymers and stabilize the morphology. Numerous papers focus on the use of block copolymer as compatibilizer. Recently, nanoparticles such as silica, clay or carbon nanotubes have been shown useful as well. Below the different types of compatibilizers that are commonly used in polymer blends are presented.

### 1.      Block copolymers

The compatibilization effect of block copolymers is a subject that has been widely studied. It has become a usual way to stabilize polymer blends. They enhance the adhesion between the phases and allow to obtain finer dispersions by settling at the interface. There are two ways to compatibilize a blend: add a pre-synthesized block copolymer in the blend, or create it in-situ during the process the compatibilizer. The first option has the advantage of allowing a better control the molecular architecture of the compatibilizer. The second option is called reactive compatibilization. To directly generate the copolymer at the interface both polymers must have reactive groups. The main advantage of this option is that the compatibilizer is created directly at the interface so the problem of locate it there is no longer a concern. However, in this case, it is difficult to control the amount and the architecture of the compatibilizer [11], [12]. Most of the articles deal with the compatibilization with a pre-synthesized polymer, however, reactive compatibilization is often the solution chosen by the industry.

The presence of block copolymers at the interface can induce one or several of the following effects:

- reduction of the dispersed phase size [13]–[15]
- decrease of interfacial tension [7], [14]–[16]
- inhibition of the droplet's coalescence [7], [17]–[20]

Sundararaj and Macosko [7] were the first to suggest that the addition of a copolymer causes suppression of coalescence rather than reduction of interfacial tension. Two physical mechanisms both illustrated in FIG. 1.5 have been proposed to explain coalescence suppression.

The first one (FIG. 1.5a) is based on the Marangoni effect. When two droplets approach each other, the matrix flows out from the gap between the approaching droplets and when it happens the compatibilizer is dragged along. This results in a gradient in compatibilizer concentration on the droplet surface, so in an interfacial tension gradient. Because of that, Marangoni stresses appear to make the compatibilizer come back homogeneously around the droplets and in doing so, prevents coalescence. This mechanism was elegantly evidenced by Jeon and Macosko [21] who showed gradients in block copolymer concentration during flow by visualizing a fluorescent PS-PMMA copolymer at the surface of a PMMA droplet in a PS matrix. The minimum coverage of block copolymer necessary to completely suppress coalescence by considering Marangoni stresses can be estimated using equation ( 1.4 ) [22].

$$\sum_{min} = \frac{5}{32}\frac{2R_v\eta_m\dot{\gamma}}{kT} \qquad (1.4)$$

The second mechanism (FIG. 1.5b), proposed by Sundararaj and Macosko [7], explains coalescence suppression by steric hindrance. When two droplets approach each other, the block copolymer is squeezed in between them. It leads to repulsion between the droplets because a change in the conformation of the copolymer chain leads to a gain in entropy. This hypothesis is consistent with the observations of Van Hemelrijck et al. [23], and Lyu et al. [20] that showed that the length of the diblock in the matrix influences coalescence in such a manner that the longer the block, the more coalescence is suppressed. This theory assumes that the block copolymer cannot move at the interface. By equating

the Van der Waals force with the steric force, the minimum coverage of block copolymer can be estimated by the following expression [20]:

$$\sum_c = \frac{20}{27\pi < r_0^2 >}$$

(1.5)

Where $< r_0^2 >$ is the square mean end-to-end distance of the chains of block copolymers. Originally, this steric hindrance theory was developed to explain suppression of static coalescence, thus it is independent of shear rate.



(a)                (b)
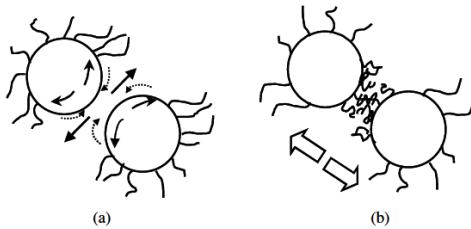
**FIG. 1.5 Two possible mechanisms preventing coalescence : a) Marangoni effect b) Steric hindrance** [24]

These two phenomena could also be present at the same time. On this subject, Fortelny [25] assessed that steric hindrance can act only if the Marangoni effect is negligible, suggesting that Marangoni stresses usually dominates.

All this is valid if the block copolymers settle only at the interface, however, some researchers evidenced that micelles can be present in the blends, decreasing the efficiency of the compatibilizers [22]. The efficiency is then linked to the quantity of block copolymer at the interface, thus to the surface coverage.

## 2.      Nanoparticles

### a)      Generalities

Nanoparticles have been used as modifiers in polymer materials for many years. Their ability to improve elastic, thermal or electric properties is particularly appreciated. The nanoparticles have the advantage of offering a wide variety of chemistry, size and shape. Their efficiency is less dependent on the chemistry they offer compared to block copolymers which need a tailored chemistry for each blend. Also, their greatest advantage is to be cheap. Among others, silica, clay, carbon nanotubes have been shown to induce a stabilization of morphology [19].

Particles localization, established during processing, has a non-negligible impact on the final properties. To estimate it theoretically, the wetting parameter described in FIG. 1.6 can be calculated. It takes into account the interactions between the three components (two polymers and one filler).

$$\omega_{AB} = cos\theta = \frac{\gamma_{S-B} - \gamma_{S-A}}{\gamma_{AB}}$$
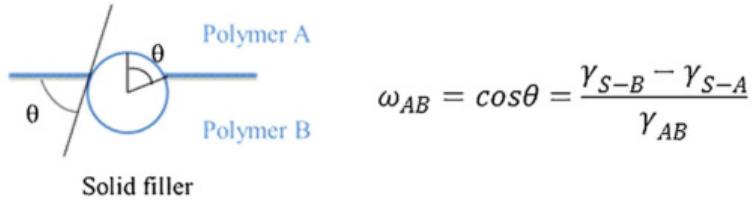
**FIG. 1.6 Representation of the interface between polymer A, polymer B and a particle and the equation of the wetting parameter, where Θ is the contact angle, $\gamma_{S-B}$ and $\gamma_{S-A}$ the interfacial tension between particle and polymers, and $\gamma_{AB}$ the interfacial tension between the polymers A and B** [26]

According to Fenouillot et al. [27], if $\omega_{AB} > 1$ the particles are present in polymer A, if $\omega_{AB} < -1$ the particles are present only in polymer B and if $-1 < \omega_{AB} < 1$ the particles are located at the interface.

The interfacial tension between two polymers can be found using several methods such as the breaking thread method, the retraction of deformed drop method, the pendant drop method and rheological methods based on linear viscoelastic measurements [28]. Each method has its advantages and limitations, but the experimental error increases in the following order: equilibrium methods < dynamic methods < rheological methods.

However, the interfacial tension between particles and polymers are more difficult to obtain. It is difficult to obtain reliable values between polymers and fillers in general because of the special surface structure of fillers. This induce some difficulties to calculate the wetting parameter and be able to predict the localization of nanoparticles.

The wetting parameter can help predict where the nanoparticles would be located at equilibrium, but the final localization of the filler in the blend is also strongly influenced by dynamic processes. The sequence of mixing of the components during processing or the viscosity of blends components can have an influence. For example, Elias et al. [29] have selected different sequences of addition for PP/EVA/hydrophilic silica blends. The components were either loaded simultaneously, or silica was premixed with PP and then PP/silica was blended with EVA. They showed that in the first case silica was located in the EVA phase, whereas in the second case silica particles were at the interface. Gubbels et al. [30] also varied the sequence mixing of PE, PS and carbon black to localize the carbon black at the interface. They showed that the kinetic of transfer of the carbon black from the less preferred phase to the other one can be used to allow the migration of the filler to the interface. It allows one to stop the mixing procedure at the right time to have carbon black

at the interface. The kinetics of this transfer depends on the shear forces and the rheology of each polymer under the processing conditions.

The rheology hence the viscosity ratio of the polymers is also a key factor for the determination of the final morphology. Elias et al [31] showed the influence of the molecular weight of two EVA on the final morphology of PP/EVA blends with hydrophilic silica and hydrophobic silica. The three components were loaded simultaneously but as the EVA melt before PP the filler is first placed in EVA. In the case of hydrophobic silica, which has better affinity with the PP matrix, they showed that the migration of silica toward the PP phase depended on the EVA molecular weight: it was easier with low viscous EVA.

The efficiency of nanoparticles as compatibilizers depend on, obviously, their chemical nature but also their size and shape. For example, Elias et al. [32] added hydrophobic and hydrophilic silica in PP/PS blends. They showed that hydrophilic silica tends to disperse in PS phase whereas hydrophobic silica localized itself at the interface and in PP phase. Similarly, Du et al. [33] functionalized multi-walled carbon nanotubes (MWCNT) with copolymers of methyl methacrylate and styrene P(MMA-co-S) of different molecular weight. Consequently, the molecular weight of the grafted copolymers had an influence on the localization of the MWCNT is SAN/PPE blends: low molecular weight copolymer grafted MWCNTs were localized at the interface whereas higher molecular weight led the nanoparticles to dispersed in PPE phase. It is quite common to modify the surface chemistry of the whole nanoparticle. Indeed, the nanoparticles are inorganic, and the modification mostly consists into making them more compatible with polymers to achieve a good dispersion. Usually, carbon compatibilizers don't need to be modified even if graphene is often oxidized and carbon nanotubes' surface can easily be functionalized.

The size of nanoparticles has proven to be an important parameter in the compatibilization as well. The particle radius $R_p$ should be of the same order of magnitude than the gyration radius $R_g$ of the polymer. If $R_p$ is similar to $R_g$ the particles begin to influence entropy of the chains. With a much higher $R_p$, the role of entropic surface tension become stronger and lead to phase separation (particle-rich and polymer-rich phases) [27]. To investigate the influence of nanoparticle size, Yurekli et al. [34] used three clays of different sizes (laponite which is around 300 Å, montmorillonite which is 0.5-1.0 μm and fluorohectorite 10 μm). They showed that laponite and montmorillonite had a satisfying

compatibilization effect whereas fluorohectorite had no effect. This is believed to be because fluorohectorite is too big.

**TABLE 1.1 Different type of nanoparticles used as compatibilizers and their characteristics** [26]

| Nanoparticles | Shape | Average particle size (nm) | Specific surface area (m²/g) | Treatment surface |
|---|---|---|---|---|
| Fumed silica | Spheres | 3–250 | 50–400 | Hydrophilic (naturally) or hydrophobic (after modification) |
| MMT and O-MMT | Platelets | – | – | Organically modified to adjust the affinity with the polymer |
| LDH (magnesium aluminum) | Platelets | $D_{50} < 10\,\mu m$ | – | Modified with a $RCOO^-$; modified with interstitial $OH^-$ |
| CaCO₃ | Unknown | 80 | 12 | No treatment |
| Carbon black | Spheres | 12; 18 | 1487; 180–250 | No treatment |
| Carbon nanotube (MWCNT) | Rods | Outer: 20–30: inner: 5–10 Length: 10–50 μm | – | Often functionalized to render the surface more organophilic |
| Graphite oxide | Isometric, irregular spheroids | $D_{90} < 5\,\mu m$ Thickness = 100 nm | 26 | Oxidized |
| Graphene | Platelets | – | – | Oxidized |
| Gold nanorods (CdSe) | Rods | 18*48 nm; 8*30 nm | – | Poly(ethylene glycol)-thiol modified; coated with trioctylphosphine oxide |
| TiO₂ | Spheres | 300; 15 | – | – |

As it can be seen in TABLE 1.1, the nanoparticles can have different shapes: platelets, spheres or rods. Very few articles deal with the influence of shape. Among those few we can notice Huang and Guo [35] who studied the influence of the shape of Janus particles. Janus particles are nanoparticles which contain two compartments with different surface chemistry. The use of those particles follows the same logic than block copolymers: eache surface chemistry has more affinity with a different phase. Huang and Guo studied Janus nanospheres, nanodiscs and nanorods with different dividing surface design. Their main conclusion is that spheres and discs were the most efficient.

Among the nanoparticles, clays have particularly attracted interest because most of them are natural, recovered from soils, easily modified by simple ionic exchange, and present less health hazard than carbon-based nanoparticles.

**b)      Clays**

Especially, montmorillonite has already been used as a compatibilizer for polymer blends. Montmorillonite is a layered silicate which structure is described in FIG. 1.7. Its sheets have two siloxane tetrahedral sheets sandwiching an aluminum octahedral sheet. The silicate layers are negatively charged, which is counterbalanced by exchangeable cations such as $Na^+$ and $Ca^{2+}$ placed in the interlayer. When associated with polymers, the interlayer cations are usually exchanged with quaternary ammonium salts which increase the basal spacing [36], [37]. The intercalation of such organic surfactants changes the surface

properties of clays in such a way that they have better affinity with polymers and disperse better. Because of its popularity, several modified montmorillonite are already commercially available.
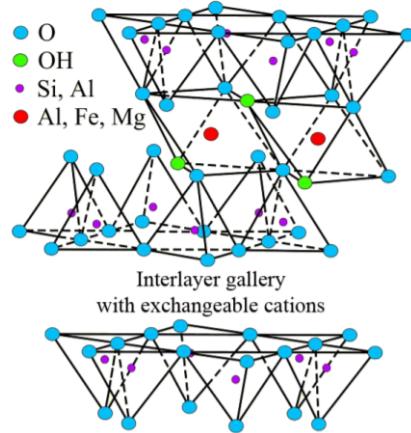


**FIG. 1.7 Structure of montmorillonite**

As for other clays like laponite or halloysite, the modification is possible but modified Laponite or halloysite are rarely available commercially. Laponite is a synthetic clay shaped in discs of around 30 nm of diameter [38] which has the same structure than montmorillonite (see FIG. 1.7). As such, the same organic modification can be done. The only difference is that Laponite has a smaller Cation Exchange Capacity (CEC) than montmorillonite. Laponite CEC can be found in the literature between 47 and 75 meq/100 g [39]–[41] whereas montmorillonite CEC is 92.5 meq/100g (information of supplier). Contrary to montmorillonite, Laponite was not extensively used for polymer blend compatibilization. Recently, Tang and Alavi [38] discovered by blending starch, PVOH and Laponite RD that apart from enhancing the properties of the material, Laponite also had a function of crosslinker and compatibilizer between Starch and PVOH.

Halloysites are natural rod nanoparticles that have started to get some interest in nanocomposite quite recently [42]. Halloysite is a silicate bi layer which is rolled into a cylinder as described in FIG. 1.8. The outside layer of the nanotubes, made of $SiO_2$, is negatively charged whereas the $Al(OH)_3$ inner lumen is positively charged. Thanks to this difference in the external and internal chemical composition, a selective modification is favored: cations can adsorb around the nanoparticles whereas anions can place itself inside the tube (see FIG. 1.9).
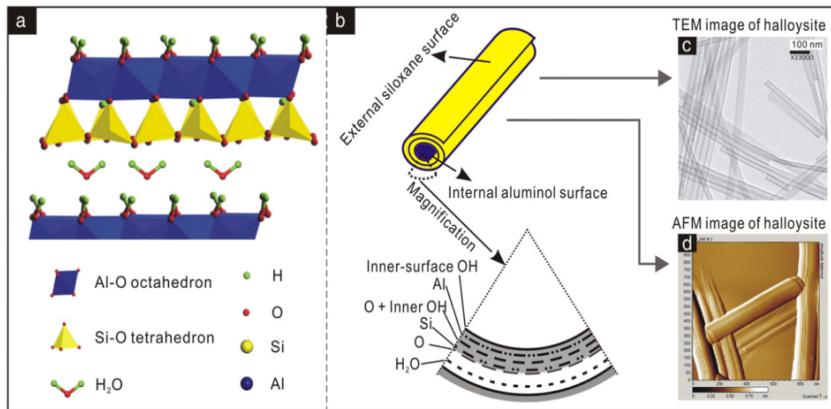
**FIG. 1.8 Halloysite structure** [43]

Halloysite can be used for flame retardant, corrosion protection or optical and electrical properties. Because of its tubular structure, halloysite was also used as nanocontainer for drug release [44]. However, very few articles deal with the compatibilization of blends using Halloysites. Pal et al. [45] studied the influence of adding Halloysites in a blend of polyoxymethylene/PP. They found out that the Halloysite induced a reduction in the average droplet radius. They also were able to show that modified Halloysites had more effect than the pure unmodified ones. Kundu et al. [46] also evidenced the effectiveness of Halloysites as compatibilizers. The Halloysites used were also organically modified.
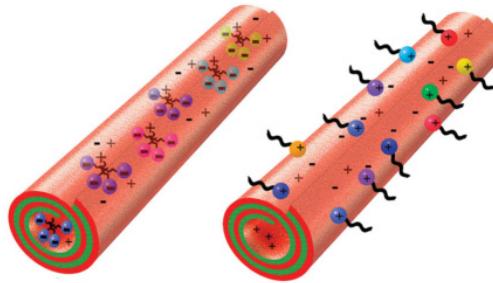


**FIG. 1.9 Selective absorption of anionic and cationic molecules** [47]

C.    **Linear shear rheology**

Linear viscoelasticity is the simplest behavior that molten polymers can exhibit in rheology. It occurs at very small and very slow deformation. It can be easily characterized by using the storage modulus, loss modulus and complex viscosity of standard SAOS experiments. Deformation in the linear regime is mainly useful to obtain data about the

molecular structure of the product. It can give us the molecular weight distribution and information about branching.

### 1.    Experiments

In the case of polymer blends, SAOS results are particularly useful to assess the morphology and study the relaxations. As can be seen in FIG. 1.10, the storage modulus of a pure polymer blend presents a shoulder (dashed line) compared to a simple polymer which storage modulus would have a slope of 2 (pointed line). This shoulder is due to the relaxation of the droplets after shearing. When the blend is compatibilized, the presence of compatibilizer at the interface causes a complex interfacial rheology. Several research teams discovered an additional relaxation process in small amplitude oscillatory shear than for a common polymer blends as shown (see FIG. 1.10) [48], [49].
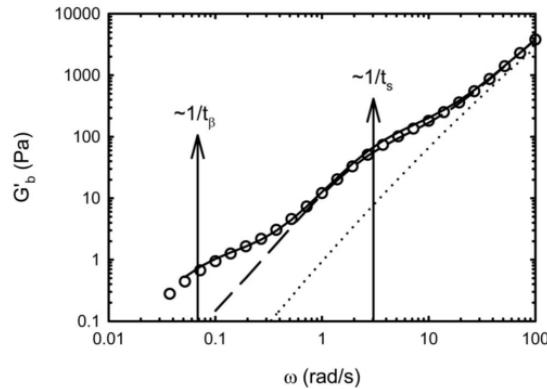


**FIG. 1.10 Storage modulus of a PI/PDMS blend compatibilized with 0.1% of a bloc copolymer. The dashed line is the PI/PDMS blend without compatibilizer.** [23]

Inferring the relaxation spectra from SAOS results is a way to evidence clearly those relaxations. Honerkamp and Weese [50] developed a mathematical methods to do so. On a classical relaxation spectrum, the following relaxations can be vizualized:

- At small times, the relaxation of the chains of polymers. One or several relaxations, depending on the number of polymers involved and if the relaxations overlap or not.
- At medium times, the relaxation of the droplet's shape happening at $\tau_1$(but usually referred as $\tau_F$) in FIG. 1.11.
- In some cases, at long times, the relaxation due to Marangoni stresses ($\tau_F$ in FIG. 1.11) [15], [16], [51].

All those relaxations were predicted by the Palierne model [52]. But the first to fit this model to experimental results showing those two relaxation processes were Riemann

et al. [48]. They found values for $\tau_F$ and $\tau_\beta$ that will be described again later on by Jacobs et al. [49]. Van Hemelrjick et al. [53] studied the influence of the compatibilizer concentration on these times. They showed that $\tau_\beta$ strongly depends on the concentration of compatibilizer whereas $\tau_F$ depends more on the concentration of the dispersed phase. This last relaxation time only happens for blends compatibilized by copolymers and is believed to be due to the presence of copolymer at the interface.
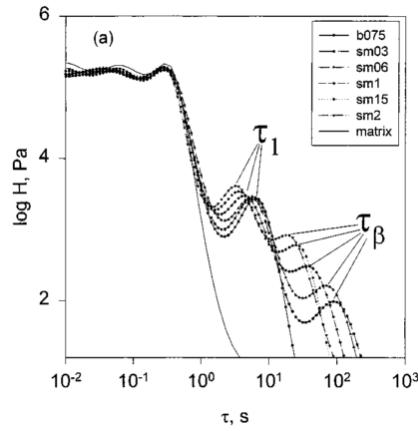


**FIG. 1.11 Relaxation spectra of PMMA/PS blends compatibilized by block copolymers** [48]

Apart from characterizing polymer blends, linear shear rheology can be used to study shear induced coalescence. The experimental procedure is based on the hysteresis described in Part I.A.3. Generally, pre-shearing the blend at high rate to generate a fine morphology and then lowering the shear rate to a value favoring coalescence is the chosen procedure [10], [17], [19], [54]. A typical coalescence tests is shown in FIG. 1.12b. During coalescence tests, the shearing is stopped to conduct SAOS experiments in order to probe morphology at a certain time.
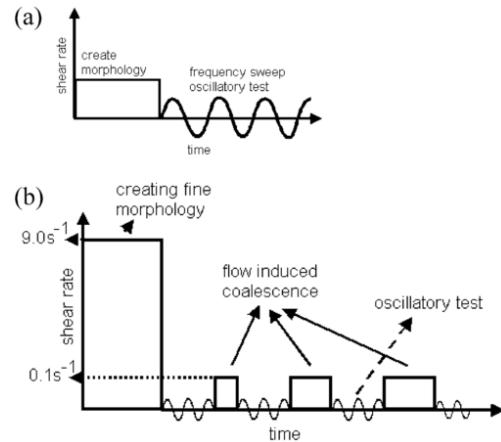


**FIG. 1.12 Usual procedure (a) to investigate the effect of pre-shearing, and (b) to investigate the coalescence process. Extracted from** [19]

### 2. Models

Several models were developed to link the microstructure of a polymer blend to its rheological behavior. One such model is Palierne's model [52] which is used to describe the rheology of viscoelastic polymer blends with or without compatibilizer.

To enable the use of this model, several conditions have to be respected:

- The droplets of dispersed phase should be small enough so that bulk forces such as gravitation and inertia are negligible

- All inclusion should have the same environment which is true when they are regularly stacked such as in a monodispersed emulsion.

- Interactions between particles other than dipole-dipole are not considered in the model. As such, the blend should be dilute to avoid those interactions.

- The experiments must be carried out at small strain amplitude because only linear phenomena are considered here.

- The surface energy is dependent on the variation of area and resistance to shear.

With all these conditions and approximations taken into account in the calculations, Palierne proposed the following expression for the complex modulus of the blends depending on the moduli of the matrix $G_M^*$ and the inclusion $G_I^*$, on the interfacial tension $\alpha^0$, on the radius of the droplets R and on two surface parameters $\beta'$ and $\beta''$:

$$G_b^* = G_M^* \left[ \frac{1 + \frac{3}{2}\sum_I \frac{\Phi_I E_I}{D_I}}{1 - \sum_I \frac{\Phi_I E_I}{D_I}} \right] \tag{1.6}$$

$$E_I = 2(G_I^* - G_M^*)(19G_I^* + 16G_M^*) + \frac{48\beta'\alpha^0}{R} + \frac{32\beta''(\alpha^0 + \beta')}{R^2}$$

$$+ \frac{8\alpha^0}{R}(5G_I^* + 2G_M^*) + \frac{2\beta'}{R}(23G_I^* - 16G_M^*) \tag{1.7}$$

$$+ \frac{4\beta''}{R}(13G_I^* + 8G_M^*)$$

$$D_I = (2G_I^* - 3G_M^*)(19G_I^* + 16G_M^*) + \frac{48\beta'\alpha^0}{R} + \frac{32\beta''(\alpha^0 + \beta')}{R^2}$$

$$+ \frac{40\alpha^0}{R}(G_I^* + G_M^*) + \frac{2\beta'}{R}(23G_I^* + 32G_M^*) \qquad (1.8)$$

$$+ \frac{4\beta''}{R}(13G_I^* + 12G_M^*)$$

Special cases of this expression are listed below. Some of them have been given in the literature even before the creation of this model and are special cases or limit cases recovered by this expression. Others are simplified version used later on in different works.

When $\alpha^0 = \beta' = \beta'' = 0$, we can find the Kerner result in case of incompressible media [52]. This expression describes the rheological behavior only in high frequency region where the interfacial tension has no effect.

For Hookean spheres in a Newtonian matrix, i.e. for $G_I^*$ constant and real and $G_M^*$ Newtonian ($G_M^* = i\omega\eta_M$), the expressions gives Frohlich and sack result [52].

If we consider that both inclusion and matrix are Newtonian liquids, then the result of Oldroyd is found with these equations [52].

The Palierne model is meant to be used on a blend where all the droplets are identical so for monodisperse blends. If we have a wider range of droplet size, R should be replaced by a size distribution v(R) leading to the expression below.

$$G_b^* = G_M^* \left[ \frac{1 + \frac{3}{2}\int_0^\infty \frac{E(\omega, R)}{D(\omega, R)}v(R)dR}{1 - \int_0^\infty \frac{E(\omega, R)}{D(\omega, R)}v(R)dR} \right] \qquad (1.9)$$

To simplify the model in the case of polydispersed blends, Graebling et al. [55] showed that the use of a volume average radius $R_v$ rather than a size distribution can be done up to a polydispersity of 2.3, leading to a simplified version:

$$G_b^* = G_M^* \left[ \frac{1 + \frac{3}{2}\Phi\frac{E(\omega, R_v)}{D(\omega, R_v)}}{1 - \Phi\frac{E(\omega, R_v)}{D(\omega, R_v)}} \right] \qquad (1.10)$$

$\beta' = \beta'' = 0$ corresponds to a constant interfacial tension despite the possible addition of interfacial agents. This version of Palierne is the most simple one and the most used [55], [56]. It is often used to fit the storage modulus in order to find the interfacial tension or the average radius of droplets. To do so, the following expression of the droplets shape relaxation time can be easily used:

$$\tau_F = \frac{\left(\frac{R\eta_M}{4\alpha}\right)(19p + 16)\left(2p + 3 - 2\Phi(p-1)\right)}{10(p+1) - 2\Phi(5p+2)}$$ ( 1.11 )

Palierne's model was also modified by Jacobs et al [49] who noticed that the two interfacial parameters β' and β'' of the original version had symmetrical roles in the equations. In regard of this, they decided to consider only one of them and set the other to zero. They decided to set the interfacial dilatation modulus β' to zero and consider the interfacial shear modulus β'' constant. This approach requires the existence of an additional shape relaxation time other than the drops relaxation time and also that the $\eta_0$ values depend only on the amount of dispersed phase and not the interfacial nature.

Following the work of Jacobs et al., Van Hemelrijck et al [53]. found the corresponding expression for $G_b'$ with only two parameters : $\frac{\alpha}{R}$ and $\frac{\beta''}{R}$.

This work gave the following relaxation times:

$$\tau_F = \frac{\lambda_{12}}{2}\left(1 - \left(1 - \frac{4\lambda_{11}}{\lambda_{12}}\right)^{0.5}\right)$$ ( 1.12 )

$$\tau_\beta = \frac{\lambda_{12}}{2}\left(1 + \left(1 - \frac{4\lambda_{11}}{\lambda_{12}}\right)^{0.5}\right)$$ ( 1.13 )

With :

$$\tau_{11} = \frac{R_v\eta_m}{4\alpha} \frac{(19p + 16)(2p + 3 - 2\Phi(p-1))}{10(p+1) + \frac{\beta_{20}}{\alpha}(13p + 12) - 2\Phi\left((5p+2) + \frac{\beta_{20}}{2\alpha}(13p+8)\right)}$$ ( 1.14 )

$$\tau_{12} = \frac{R_v\eta_m}{8\beta_{20}} \frac{10(p+1) + \frac{\beta_{20}}{\alpha}(13p + 12) - 2\Phi\left((5p+2) + \frac{\beta_{20}}{2\alpha}(13p+8)\right)}{(1 - \Phi)}$$ ( 1.15 )

The relaxation time $\tau_\beta$ corresponding to Marangoni stresses was clearly identify by this work. As can be seen in FIG. 1.13, De Souza et al. [16] showed that $\tau_F$ does not depend on the value of $\beta_{20}$. However, $\tau_\beta$ decreases with increasing $\beta_{20}$.
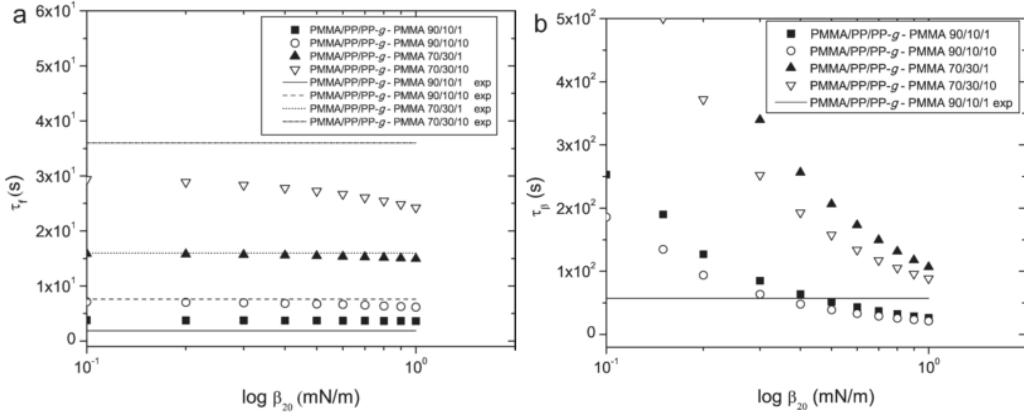
**FIG. 1.13 (a) τf values as a function of β$_{20}$ estimated using eqs.( 1.12 )-( 1.15 ), for PMMA/PP/PP-g-PMMA blends. (b) τβ values as a function of b20 estimated using eqs. ( 1.12 )-( 1.15 ), for PMMA/PP/PP-g-PMMA blends**[16]

Other models can be used to link the morphology with linear rheology. They are not described in details here but among them can be found Lacroix et al.'s [57] version of the Lee and Park model [58], Bousmina's model [59] which is very similar to Palierne's model and Yu et al.'s model [60] based on Grmela et al.'s work [61].

### D.    **Extensional Rheology**

Extensional rheology is of significant importance as nearly all polymer process subject the material to elongational flow. The dominance of extensional flow is accentuated in processes such as blow molding or melt spinning. Extensional deformations are very sensitive to macromolecular structure of the polymers such as the degree of branching, the molecular weight distribution, and cross-linking [62].

### 1.    **Measurement devices**

Measuring the properties of polymer melts under extensional flow has been a technical challenge for researchers for decades. The first way to evaluate the extensional properties of melts was to use the entrance pressure drop of the flow through a contraction by using a conventional capillary rheometer [57]. Several analyses exist to infer the extensional viscosity from the entrance drop pressure. According to Padmanabhan and Macosko [63] these analysis, which are approximations of the complex reality, can lead to very different results. As such, this method is not the most reliable one.

Later on, a uniaxial elongational rheometer (RME) was developed by Meissner and Hostettler [64]. The sample, floating horizontally on a cushion of nitrogen or argon gas

heated to the measuring temperature, is stretched by four rotating belt clamps at the required constant rate of strain (constant rotational speed of the clamps).

Another device was developed by Munsted et al.[65] where the sample is vertically suspended in a heated oil bath which compensates for much of the specimen's gravity and apply an homogeneous temperature distribution. One end of the sample is fixed to a load cell located in the oil bath and its other end is fixed to a thin metal tape which can be rolled up by a disk.

The last device that is going to be described here is the Sentmanat extensional rheometer (SER) [66] described in FIG. 1.14. This miniature rheometer is a device that can be installed on a conventional rotational rheometer. It consists in two paired drums, a master drum (A) and a slave drum (B) on which the sample is attached using clamps (I). The rotation of the drive shaft (F) results in a rotation of the master drum and an opposite rotation of the slave drum which results in the stretching of the sample.
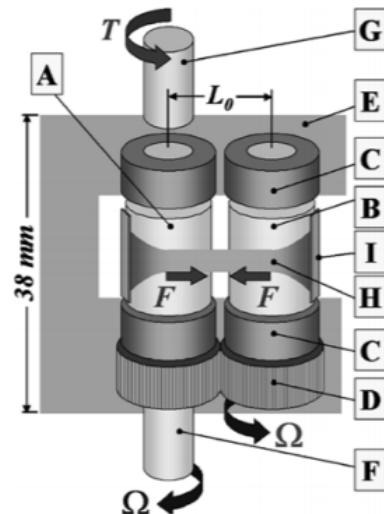


FIG. 1.14 Sentmanat Extensional Rheometer device. A: Master drum, B: slave drum, C: bearings, D: intermeshing gears, E: chassis, F: drive shaft, G: torque shaft, H: sample, I: securing clamps. Extracted from [66].

During a uniaxial elongational test, the sample of length $L_0$, witdh $W_0$ and thickness $B_0$ is stretched at a constant strain rate $\dot{\varepsilon}$ defined by equation ( 1.16 ) and the resulting force F is measured as a function of time.

$$\dot{\varepsilon} = \dot{\varepsilon}_0 h(t)$$
( 1.16 )

with $h(t) = 0$ for $t < 0$ and $h(t) = 1$ for $t > 0$. $\dot{\varepsilon}_0$ is constant.

The magnitude of stretching is usually defined by the Hencky strain as follow:

$$\varepsilon^H = \int_{L_0}^{L(t)} \frac{dL}{L} = \ln(\frac{L(t)}{L_0}) \qquad (1.17)$$

To have a constant strain rate $\dot{\varepsilon}_0 = \frac{\partial \varepsilon^H}{\partial t} = \frac{\partial \ln(\frac{L(t)}{L_0})}{\partial t}$, the dimensions of the sample must vary exponentially.

Generally, the elongational viscosity is the studied feature under uniaxial elongation. Like the shear viscosity, it is a function of the shear rate. However, in the case of elongational flows, it is difficult to measure the steady state value. In experiments, it is only possible to access a time dependent value $\eta_E^+(t)$ which is the tensile stress growth coefficient (also called the transient elongation viscosity) defined as follow:

$$\eta_E^+(t) = \frac{\sigma^+(t)}{\dot{\varepsilon}_0} = \frac{F(t)/A(t)}{\dot{\varepsilon}_0} \qquad (1.18)$$

Where A(t) is the cross section of the sample.

The elongational viscosity is defined as the asymptotic value of this coefficient for large times (t → ∞).

## 2.    Strain hardening

The most studied feature in extensional flow is the strain hardening behavior of some polymer melts [67]–[70]. An example of a linear and crosslinked PMMA's tensile stress growth coefficients are shown in FIG. 1.15. It can be seen that crosslinked polymers exhibit a strong increase compared to the linear region whereas linear polymers have a linear behavior meaning that their transient elongational viscosity curve follow the curve representing three times the shear viscosity (see FIG. 1.15a). Long-chain branching, and broadness of molecular weight distribution are also factors that are known to enhance strain hardening of polymers.

The presence of exfoliated or intercalated organoclays can enhance strain-hardening behavior of polymers as well. Okamoto et al. [72] were one of the first to show the influence of layered silicate on the elongational viscosity. They showed by observing samples using TEM that the exfoliated clays formed what they called a house of cards structure during extensional experiments. They attributed the strong strain hardening to the silicate layers perpendicular to the flow direction.  Park et al. [73] concluded that exfoliated systems were able to display strain hardening whereas intercalated systems were not. Their results are represented in FIG. 1.16 where exfoliated clay (FIG. 1.16a) clearly induce a strain hardening phenomenon whereas intercalated structures did not (FIG. 1.16b).
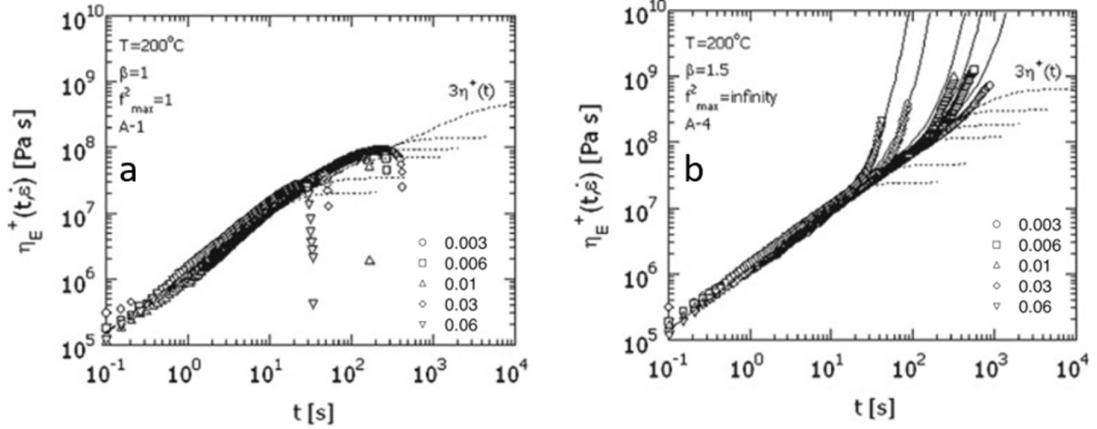
**FIG. 1.15 Tensile stress growth coefficients of a (a) linear PMMA, (b) cross-linked PMMA. The viscoelastic limit is indicated by 3η⁺, the other dotted lines and plain lines are the predictions of various models not described here. Extracted from** [71]
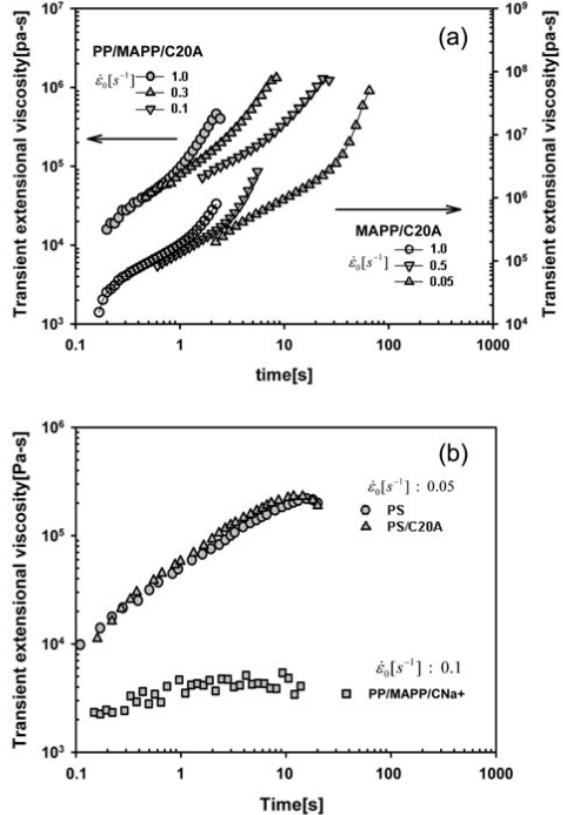


**FIG. 1.16 Transient elongational viscosities of (a) exfoliated PP nanocomposites, (b) intercalated PS nanocomposites and PP microcomposite. Extracted from** [73]

However, Li et al. [74] evidenced a subtle strain hardening in the case of intercalated systems as can be seen in FIG. 1.17. They found that modified clays could induce an increase in the transient elongational viscosity (indicated by an arrow in FIG. 1.17) attributed to a strain hardening behavior. They also evidenced that the higher the strain rate, the earlier the strain hardening behavior occurs.
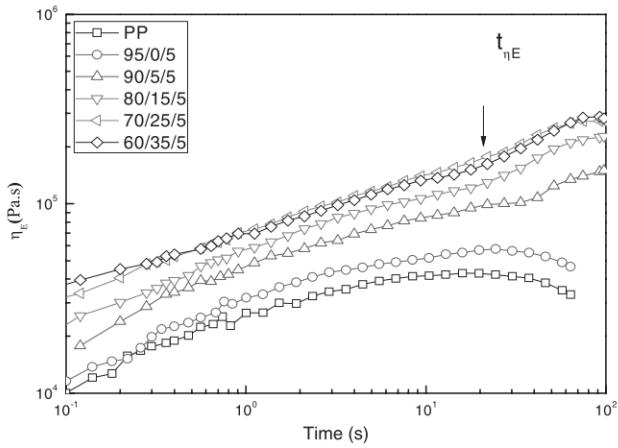
**FIG. 1.17 Transient elongational viscosities of pure PP and its nanocomposites with different amounts of surfactant. Extracted from** [74]**.**

### 3.    Polymer blend behavior

The behavior of polymer blends pure or compatibilized under elongational deformation is still very rare in the literature. The pioneering works of Taylor [2], [3] and Grace [5] described previously helped to understand the deformation of emulsion and polymer blends under flow. As can be seen in FIG. 1.2, under irrotational shear, such as extensional flow, the value of $Ca_c$ is very low and not significantly dependent on the viscosity ratio. As such, elongational flow is likely to induce breakup.

Works describing the evolution of blend morphology during elongational flow is still quite rare. Delaby and al. [75], [76] showed the droplets deform less than the sample if it has a higher viscosity than the matrix and more than the sample if it is lower, in the case of large capillary number. Heindl et al. [77] studied the evolution of the extensional viscosity of PS/PE blends. They found that the extensional viscosity is greatly influenced by the matrix PS at low content of PE. They also showed that after shape recovery of the droplets, droplet breakup did not occur, but coalescence did, leading to a coarse morphology.

Indeed, the blend morphology can be unstable after mixing or processing during the cooling step. As such, understanding what is happening in the blends after cessation of flow is also of importance. On that matter, Gramespacher and Meissner [78] studied the elongational flow behavior as well as the recovery behavior of PMMA/PS blends. They showed that the elongational viscosity did not display notable differences between blends, but the recovery behavior did: the recoverable elongational strains increased with the PS

concentration. Also, when the viscoelastic recovery is reached, the droplets are not yet totally relaxed. From this moment, the interfacial tension is the only force acting to relax the droplets back to a spherical shape. Gramespacher et al. used the following equation to infer the interfacial tension between the components of the blends using the relaxation time of the droplets.

$$\tau_{relax} = \frac{\eta_{0,b} d_0}{\Phi \alpha}$$

(1.19)

Where $\eta_{0,b}$ is the zero-shear viscosity of the blend, $d_0$ the diameter of the droplets, $\Phi$ the volume concentration of dispersed phase and $\alpha$ the interfacial tension. The resulting interfacial tension were in good agreements with information extracted from linear shear rheology. This expression can be used on the contrary to estimate the relaxation time of the droplets.

Handge and Potschke [79] also evidenced such a two-step recovery. They also applied the Handge model [80] made to describe the recovery behavior samples and had good agreement with experiments at high capillary number. Mechbal and Bousmina [81] also studied the behavior after elongation and the following relaxation of PMMA/PS blends. They chose to compare experimental data with the model of Yu et al. [82] and found that the model described fairly well the morphological evolution. As far as they are concerned, Stary et al. [83], [84] showed that in a PS/LLDPE blend, during elongation followed by a free recovery experiment, the fibrils can undergo breakup due to Rayleigh disturbance or necking. They also showed that the relaxation experiments, where the sample length is kept constant after cessation of flow, led to substantially higher frequency of droplet breakup resulting in a finer morphology than in the case of free recovery.

Actually, most polymer blends commercially used are compatibilized, however, the works on compatibilized polymer blends under elongational flow are extremely rare. Stary et al. [85] showed that the presence of compatibilizer at the interface suppressed droplet breakup and promoted the shape recovery of the droplets after cessation of flow. They explained it by the presence of Marangoni stresses at the interface. Mechbal and Bousmina [86] also explained their results by the presence of Marangoni stresses. Stone et al. [87] studied the breakup after elongation of a droplet. They found that the stretch ratio ($L_{fib}$ length of the ellipsoids divided by the initial diameter $d_0$) must be above a critical value for

the droplet to break. They were able to plot experimentally $\frac{L_{fib}}{d_0}$ as a function of the viscosity ratio as shown in FIG. 1.18.
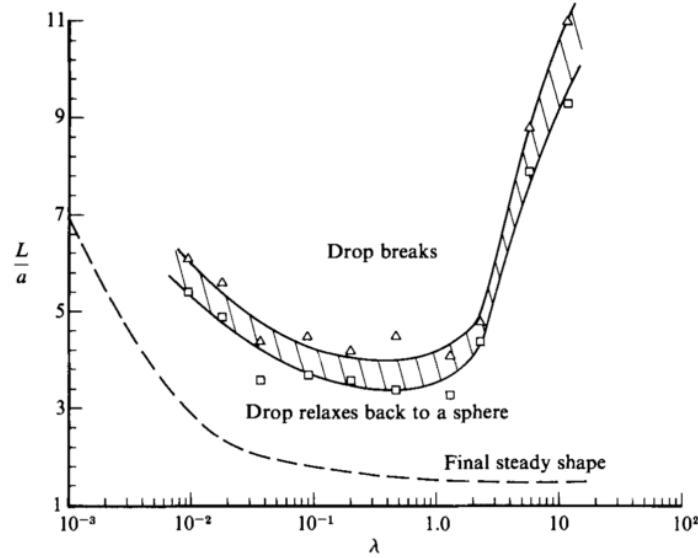


**FIG. 1.18 Critical elongation ratio ensuring breakup after cessation of flow. Triangles denote the smaller ratio for which droplet breakup was observed, squares denote the highest ratio for which the droplets relaxed back to a sphere without breakup. Extracted from** [87]

All the results found in the case of compatibilized polymer blends used block copolymers. No study concerning the behavior of polymer blends compatibilized by nanoparticles under elongation flow could be found.

E.     **Conclusion**

Through this literature review, the works already done on rheology of polymer blends were presented. This subject has already attracted a lot of attention in the past 20 years. However, there is still room for improvement and research. Usually, a stabilization of morphology can be obtained by adding a so called compatibilizer, which can be a block copolymer or nanoparticles. Nanoparticles have the advantage to be cheaper and do not need to have a tailored chemistry for each type of blend. Generally, the addition of compatibilizers at the interface leads to a decrease in the droplets size, a decrease of interfacial tension and an inhibition of coalescence. In the case of block copolymers, the apparition of Marangoni stresses can also be evidenced.

On the one hand, linear shear rheology can be used to characterize polymer blends morphology but also study the coalescence phenomenon. Indeed, small angle oscillatory shear results can be used to find the interfacial tension of the blend or the morphology by using linear models such as the Palierne model. It is then particularly useful to observe a refinement of the droplets size, a decrease in interfacial tension or to assess the evolution of morphology during coalescence tests. The relaxation spectra inferred from SAOS results can help in evidencing an additional relaxation time corresponding to Marangoni stresses for polymer blends compatibilized by block copolymers.

On the other hand, extensional flow allows to study polymer melts and their blends under high deformations. Generally, extensional flow is used to study the strain hardening behavior of polymer melts or nanocomposites. However, the deformation of the droplets under uniaxial elongation can also be studied as well as the relaxation of the droplets after cessation of flow. No articles could be found on the behavior of polymer blends compatibilized by nanoparticles under elongational flow.

# CHAPTER 2

# ARTICLES ORGANIZATION

The literature review of Chapter I investigated the current knowledge about polymer blends, their compatibilization and their rheological behavior. This thesis aims at extending the knowledge on polymer blends compatibilized by nanoparticles and their rheological behavior. A total of 3 papers were written to contribute to the scientific knowledge in the following order:

Chapter 3 presents the first article entitled *"Compatibilization mechanism induced by organoclay in PMMA/PS blends"*. Those preliminary results on PMMA/PS blends compatibilized by Cloisite 20A, a commercial organo-modified clay, evidenced for the first time that nanoparticles could also induce Marangoni stresses when located at the interface. This innovative result led to think that clay nanoparticles acted similarly to block copolymers and was published in *Journal of Rheology* in May 2017.

After discovering that Marangoni stresses could occur in the case of clay nanoparticles, PMMA/PS blends with block copolymers of different molar masses were investigated. The goal was to have a deeper knowledge about the compatibilization mechanism induced by block copolymers and to be able to compare with nanoparticles. As such, the variation of interfacial tension, the coalescence phenomenon and the relaxations happening in the blends were studied. Particularly, the evolution of the relaxation due to Marangoni stresses during coalescence generated interesting results. Those results led to a second article entitled *"Compatibilization mechanism induced by block copolymers with different molar masses in PMMA/PS blends",* currently under review in *Journal of Rheology*.

Chapter 5 presents the third article entitled *"Comparison of Montmorillonite, Laponite and Halloysite as compatibilizers in PMAM/PS blends"*. This work focuses on the use of 3 types of clay: montmorillonite, laponite and halloysite, to compatibilize PMMA/PS blends. This work first presents the modification of clays and their dispersion state in polymers. The results on PMMA/PS blends to which clays were added were greatly influenced by the localization of clays and their dispersion state. As in Chapter 4, the

variation of interfacial tension, the coalescence phenomenon and the relaxations happening in the blends were studied but led to different results. The results were used to write a third article submitted to the *European Polymer Journal*.

As Chapter 1 evidenced, the behavior of polymer blends compatibilized by nanoparticles under elongational flow is still little known. As such, the last chapter's goal was to study the behavior of the same blends as Chapter 5 under elongational flow. The influence of addition of the 3 clays on the tensile stress growth coefficients of PMMA and PS nanocomposites and the relaxation of the droplets after high elongational deformation were studied. This last chapter is particularly innovative as the relaxation of the droplets of polymer blends after elongational deformation compatibilized by nanoparticles was never studied before to our knowledge. Those results are written as a thesis chapter rather than an article.

# CHAPTER 3

## COMPATIBILIZATION MECHANISM INDUCED BY ORGANOCLAY IN PMMA/PS BLENDS

Julie GENOYER[1,3], Marcio YEE[2,*] Jérémie SOULESTIN [1], and Nicole R. DEMARQUETTE[2,3]

[1] *Mines Douai, Department of Polymers and Composites Technology & Mechanical Engineering, Douai, France*
[2] *University of São Paulo, Metallurgical and Materials Engineering Department, São Paulo, Brazil*
[3] *École de technologie supérieure, Department of Mechanical Engineering, Montreal, Canada*
[*] *Presently at Federal University of São Paulo, Department of Sea Sciences, Santos, Brazil*

### Abstract

In this work, the effect of adding organoclay (Cloisite 20A) to a poly(methyl metacrylate) (PMMA)/polystyrene (PS) blend was evaluated in order to understand the compatibilization mechanism taking place. The blend morphology was quantified using micrographs obtained by Scanning Electron Microscopy, and observed by transmission electron microscopy (TEM). The state of dispersion of the clay was studied using Small Angle X-ray Scattering (SAXS) and Wide Angle X-ray Scattering (WAXS) and by applying the Carreau-Yasuda with a yield stress model to small amplitude oscillatory shear data. Morphological analyses revealed that the clay was intercalated, that its addition resulted in a decrease in the size of the dispersed phase and that it was preferentially located at the interface, except in the case of saturated interfaces, in which case the remaining clay was dispersed in PMMA. By applying the simplified Palierne model to Small Amplitude Oscillatory Shear (SAOS) experiments, the interfacial tension between the polymers forming the blend was inferred and shown to decrease upon addition of clay. The relaxation spectra inferred from the SAOS data, using the Honerkamp and Weese method, revealed four relaxation times: relaxation of PMMA and PS chains, relaxation of the droplet shape, as well as an additional relaxation phenomenon attributed to the Marangoni stress. Although, Marangoni stresses have already been studied in the case of blends

compatibilized by block copolymers, this is the first time that it has been evidenced in the case of a clay as compatibilizer.

### A.    Introduction

Polymer blends have been extensively used in industry due to the interesting properties they present. Most polymers are thermodynamically immiscible, resulting in a multiphase material whose engineering properties can be controlled by their morphology. The blends' morphology is controlled during processing, but at the same time, the processability of polymer blends is influenced by the microstructure. The interplay between flow, morphology, and rheology is therefore a key point in tailoring the final material properties.

The immiscibility between the polymers forming the blends can however lead to a coarse morphology or even to phase separation, which is not interesting, as it leads to poor physical properties. The addition of a so-called compatibilizer is a way to control the morphology over time [6], [24]. Premade block copolymers are commonly used for this purpose, and have been shown to be very efficient. However, their use involves significant drawbacks, including the fact that each chosen blend type needs to have a block copolymer with a tailored chemistry adapted to it, which in turn results in an expensive block copolymer design. At the industrial level, it is more common to create a compatibilizer during processing thanks to an interfacial reaction, followed by the use of a so-called reactive compatibilization [11]. Although this has been shown to be efficient in stabilizing the blend morphology, when it is employed, it becomes difficult to quantify and adjust the amount of compatibilizer created, as well as its exact structure. In the case of a droplet dispersion, as the compatibilizers settle at the interface, the addition leads to a reduction in the dispersed phase size [13]; a stabilization of morphology, inhibiting the dispersed phase coalescence [7]; a decrease in interfacial tension [13], [14], and the presence of an additional relaxation phenomenon [15], [16], [48]. All this leads to an improvement of the blend properties.

Recently, some studies have shown that the addition of nanoparticles could have a similar effect as adding compatibilizer, as in some cases, the former can result in a reduction in the dispersed phase size [29], morphology stabilization [19], as well as a decrease in interfacial tension [26], [29], when the nanoparticles are located at the interface. However, if the nanoparticles are located in a single phase other possible mechanisms can be

considered: change in the viscosity of the phases, immobilization of the dispersed drops by the creation of a physical network of particles in the matrix (possible when concentration of solid above the percolation threshold) or the strong interaction of polymer chains onto the solid particles inducing steric hindrance [27], [88]. Therefore, the localization of the nanoparticles is key to understanding the compatibilization mechanism. This localization is a function of the nature of the nanoparticles, and thus depends on the size, shape and chemical surface of the nanoparticles. That is why most often, nanoparticles are organomodified either by chemical grafting [35], [89], [90] or by ionic exchange [37], [91]–[93] in order to be more compatible with blend components. However, while some studies have shown that adding organoparticles could be similar to adding block copolymers, when the latter are located at the interface, no additional relaxation phenomenon has as yet been observed.

The linear viscoelastic rheological behavior of a blend can provide information on the morphology and the interfacial tension of the blended component: small amplitude oscillatory shear experiments show an increase in elasticity at low frequencies, resulting in a shoulder on the storage modulus curve. This increase is associated with the relaxation of the shape of the droplets ($\tau_F$), which were previously deformed by the stress applied [55]. In the case of compatibilized blends, an additional relaxation time ($\tau_\beta$) may be observed, as already mentioned. Van Hemelrjick et al. showed that $\tau_F$ depends mainly on the concentration of the dispersed phase, whereas $\tau_\beta$ strongly depends on the concentration of compatibilizer [54]. Therefore, the latter relaxation time is believed to be due to the presence of copolymer at the interface, and especially to the Marangoni stress illustrated in FIG. 3.1 [15], [16], [51]. This Marangoni stress occurs when the compatibilizer is not distributed equally around the droplet. When two droplets approach, the matrix in between them will flow elsewhere and drag the compatibilizer with it. It results in a gradient in compatibilizer concentration on the surface of the droplets. Because of that, an opposite force will cause the compatibilizer to come back equally distributed on the surface, thereby preventing coalescence. This is called the Marangoni stress. In this regard, Jeon and Macosko [21] showed gradients in block copolymer concentration during flow by visualizing a fluorescent PS-PMMA copolymer at the surface of a PMMA droplet in a PS matrix. On those matters, rheology can provide information on the morphology and compatibilization mechanism in a blend.
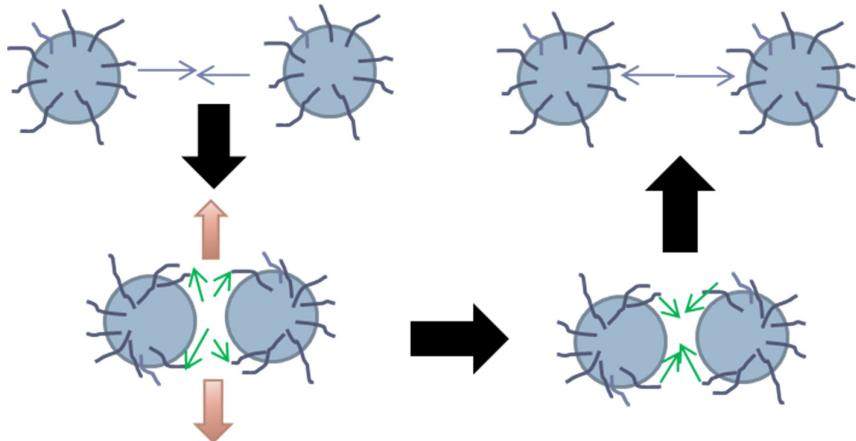
**FIG. 3.1 Illustration of the Marangoni stress**

In order to better study the Marangoni stress relaxation, relaxation spectra can be recovered from classical small amplitude oscillatory shear measurements by the method of Honerkamp and Weese [50]. Usually, on a relaxation spectrum, the two relaxation times, each corresponding to a phase, can be seen, followed by a longer relaxation time induced by the relaxation of the shape of the droplets $\tau_F$. Upon the addition of block copolymer, a fourth relaxation time $\tau_\beta$ can be observed between 10 to 100 s in some cases. However, this last relaxation phenomenon can be observed at even longer times that are hard to reach with only SAOS measurements. One possibility for avoiding this problem is to use creep experiments for complementary data over longer times [94].

Several models have been developed to link the rheological behavior of polymer blends to their morphology, composition, and interfacial tension between components. One such model is the Palierne model, which predicts the rheological behavior of a blend formed by two viscoelastic polymers [52]. The polymers should be viscous enough to render bulk forces such as gravitation and inertia negligible, and the emulsion should be monodispersed and diluted. This model is made to predict the behavior of blends in the linear viscoelastic regime so at small and slow deformations. As such, the constitutive equations which relate stress to deformations are linear.

Palierne developed a constitutive equation to describe the complex modulus $G(\omega)_b^*$ of the blend as a function of the modulus of the matrix $G(\omega)_M^*$ and the dispersed phase $G(\omega)_I^*$ as written below:

$$G_b^* = G_M^* \left[ \frac{1 + \frac{3}{2}\Sigma_I \frac{\Phi_I E_I}{D_I}}{1 - \Sigma_I \frac{\Phi_I E_I}{D_I}} \right] \tag{3.1}$$

$$E_I = 2(G_I^* - G_M^*)(19G_I^* + 16G_M^*) + \frac{48\beta'\alpha^0}{R} + \frac{32\beta''(\alpha^0 + \beta')}{R^2}$$
$$+ \frac{8\alpha^0}{R}(5G_I^* + 2G_M^*) + \frac{2\beta'}{R}(23G_I^* - 16G_M^*) \tag{3.2}$$
$$+ \frac{4\beta''}{R}(13G_I^* + 8G_M^*$$

$$D_I = 2(G_I^* - G_M^*)(19G_I^* + 16G_M^*) + \frac{48\beta'\alpha^0}{R} + \frac{32\beta''(\alpha^0 + \beta')}{R^2}$$
$$+ \frac{40\alpha^0}{R}(G_I^* + G_M^*) + \frac{2\beta'}{R}(23G_I^* + 32G_M^*) \tag{3.3}$$
$$+ \frac{4\beta''}{R}(13G_I^* + 12G_M^*)$$

where $\alpha^0$ is the interfacial tension, $R$ the radius of the droplets, $\Phi$ the dispersed phase volume concentration, $\beta'$ the interfacial dilatation modulus relative to the area varation and $\beta''$ the interfacial shear modulus relative to shear without change of area [52].

To simplify the model in the case of polydispersed blends, Graebling et al. showed that an average radius $R_v$ can be used up to a polydispersity of 2.3 [55].

A second simplification often used is to take $\beta' = \beta'' = 0$, which corresponds to a constant interfacial tension despite the addition of interfacial agents. This version of Palierne is the most simple, and the most used [22, 30]. The expression has often been used to fit the storage modulus in order to find the interfacial tension or the average radius of droplets because these two parameters are the only unknowns. These expressions allow the following relaxation time to be found:

$$\tau_F = \frac{\left(\frac{R_v \eta_M}{4\alpha}\right)(19p + 16)(2p + 3 - 2\Phi(p - 1))}{10(p + 1) - 2\Phi(5p + 2)} \tag{3.4}$$

where $R_v$ is the average droplet radius, $\alpha$ the constant interfacial tension, and p the viscosity ratio.

This time corresponds to the relaxation of the droplets' shape. The original Palierne model was also modified by Jacobs et al., who noticed that the two interfacial parameters β' and β" of the original version had symmetrical roles in the equations [49]. In that regard,

they decided to consider one of them constant, and set the other to zero. This approach requires the existence of an additional shape relaxation time other than the drops' relaxation time. In this work, the following expression was used for the relaxation times:

$$\tau_F = \frac{\lambda_{12}}{2}\left(1 - \left(1 - \frac{4\lambda_{11}}{\lambda_{12}}\right)^{0.5}\right) \tag{3.5}$$

$$\tau_\beta = \frac{\lambda_{12}}{2}\left(1 + \left(1 - \frac{4\lambda_{11}}{\lambda_{12}}\right)^{0.5}\right) \tag{3.6}$$

With

$$\lambda_{11} = \frac{R_v \eta_m}{4\alpha} \frac{(19p+16)(2p+3-2\Phi(p-1))}{10(p+1) + \frac{\beta_{20}}{\alpha}(13p+12) - 2\Phi\left((5p+2) + \frac{\beta_{20}}{2\alpha}(13p+8)\right)} \tag{3.7}$$

$$\lambda_{12} = \frac{R_v \eta_m}{8\beta_{20}} \frac{10(p+1) + \frac{\beta_{20}}{\alpha}(13p+12) - 2\Phi\left((5p+2) + \frac{\beta_{20}}{2\alpha}(13p+8)\right)}{(1-\Phi)} \tag{3.8}$$

In the next work, the rheological behavior of poly(methylmethacrylate)/polystyrene (PMMA/PS) blends compatibilized by a clay (Cloisite 20A) was studied. PMMA/PS blends are often used in research on compatibilization of polymer blends as it is a "model" blend with a relatively simple rheological behavior. The morphology, the dispersion state, and the localization of clay in the blends were assessed. The interfacial tension was found using the simplified Palierne model. Relaxation phenomena were also studied by using the relaxation spectra inferred from SAOS measurements.

B. **Materials and methods**

1. **Materials**

Poly(methylmethacrylate) (PMMA, DHAF grade) from Metacrill S.A. and polystyrene (PS, N1841 grade) from InNova S.A. were used in this study. The characteristics of the polymers are reported in TABLE 3.1. Cloisite 20A was purchased from Southern Clay.

**TABLE 3.1 Properties of the polymers**

| Polymer | $M_w$ (g/mol) | $M_n$ (g/mol) | $M_w/M_n$ | Viscosity ($\eta_0$) (Pa.s) at 200 °C | Viscosity ($\eta_0$) (Pa.s) at 220 °C |
|---------|---------------|---------------|-----------|------------------|------------------|
| PMMA | 65,000 | 31,000 | 2.1 | 24,000 | 4,300 |
| PS | 198,000 | 87,000 | 2.2 | 3,200 | 2,100 |

### 2.    Blending

Blends of PMMA/PS were prepared in 90/10 and 70/30 weight concentrations. For each concentration in PMMA and PS, several blends were prepared with different concentrations of Cloisite 20A ranging from 0 to 8 wt% with respect to the dispersed phase PS. All the percentages in this paper are weight percentage and clay weight percentage is always given with respect to PS.

The blends were prepared using a Haake PolyLab 900/Rheomix 600p batch mixer at 200 °C and 50 rpm after PMMA was dried at 60 °C for 12 hours. They were prepared in two steps: in the first step, the nanoclay was mixed with the minor phase (PS) for 5 minutes, and in the second, PS+nanoclay was mixed with the matrix (PMMA) for 7 minutes. The clay was added to the PS because of the affinity between the polymer and the clay (see part 3.C.2). In the case of the non-modified blends, the minor phase was processed twice in order to ensure it had the same thermal history.

### 3.    Characterizations

Samples for rheological and morphological analyses were obtained by compression molding. Discs with a 25 mm diameter and 1 mm thickness were molded at 200 °C under 18 MPa for 10 minutes.

The rheological characterization of pure phases, PMMA/PS blends to which clay was or was not added, was performed using a stress-controlled MCR 501 rheometer from Anton Paar. Measurements were carried out under dry nitrogen atmosphere. A parallel-plate geometry was used with a gap size of 0.9 mm and plate diameter of 25 mm. Time sweep tests were performed in order to check the thermal stability of the samples (see an example in FIG. 3.2).

Strain sweep tests were carried out for all blends and pure polymers to define the linear viscoelasticity region. Finally, dynamic frequency sweep tests were performed for all blends and pure polymers at 200 and 220 °C. The strain varied from 1.5 to 6 %. The measurements were performed from 300 to 0.01 Hz. The zero-shear viscosity of the individual phases necessary to calculate the interfacial tension between the components of the blend, using Palierne's model, was determined using the curve of complex viscosity (Pa.s) versus frequency (rad/s) obtained from dynamic frequency sweep tests. Rheological experiments were shown to be reproducible within 5 %.
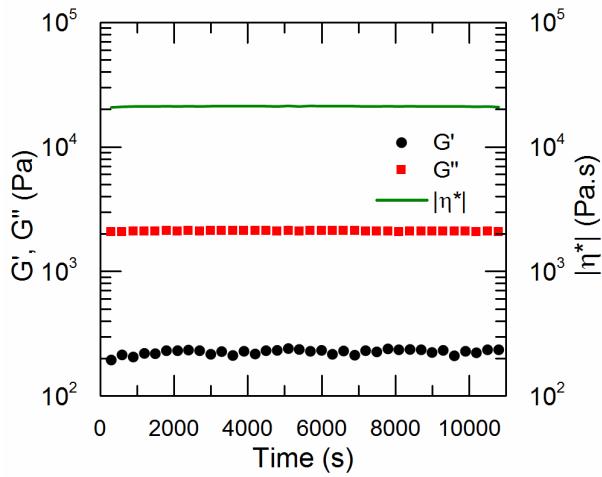
**FIG. 3.2. Variation of the complex viscosity, the storage modulus and the loss modulus over time of the 90/10 (PMMA/PS) blend at 200 °C and 0.1 rad/s**

The morphology was characterized by scanning electron microscopy (SEM) using a Philips model XL 30 microscope as described by Yee et al.[15], [95]. The samples were previously fractured in liquid nitrogen and covered with gold using a Balzers sputter coater, model SCD-050. The PS was extracted using cyclohexane at room temperature under continuous stirring for six hours in order to improve the contrast of pictures. The morphology was quantified using an image analysis software package (KS 300) after analysis of the SEM photomicrographs. About 1000 particles were considered for each sample. For the calculation of the average droplet radius, Saltikov's correction was used [96]. This correction takes into account the polydispersity of the morphology of the samples and the fact that the fracture in the samples does not always occur at the maximum diameter of the droplets of the dispersed phase.

SAXS experiments were carried out using the synchrotron source from the National Synchrotron Light Laboratory (LNLS), Campinas, Brazil, to evaluate the state of dispersion of the clays within the polymers. The wavelength of the X-Ray beam was 1.488 Å. The sample-to-detector distance was 950 or 1125 mm. Other samples were subsequently characterized using WAXS on a PANalytical diffractometer, model X'Pert Pro, with a CuKα radiation of wavelength 0.154 nm scattering at ambient temperature.

In order to obtain TEM pictures, samples were sectioned at room temperature, with a thickness of ~ 90 nm with a Leica Microsystems UCT ultramicrotome and transferred to 200-mesh Cu TEM grids with carbon support film. The images were collected on the FEI

Tecnai G2 F20 S/TEM equipped with a Gatan Ultrascan 4000 CCD Camera Model 895 at an accelerating voltage of 200 kV.

### C.   Results and discussion

#### 1.   Morphology

SEM observations were used to assess the morphology of the blends. FIG. 3.3 shows the morphology of 90/10 and 70/30 blends with and without the addition of 8 % of clay. A droplet dispersion morphology type is observed for all the blends. According to FIG. 3.3a and FIG. 3.3c, the size of the droplets increases as a function of the concentration of PS. The experimental values of the volume average droplet radius ($R_v$) and the polydispersity ($R_v/R_n$) are reported in TABLE 3.2, where the increase in the radius of the droplets is quantitatively confirmed. This expected behavior is generally due to an increase in the coalescence of the dispersed phase when its concentration increases[7], [96].
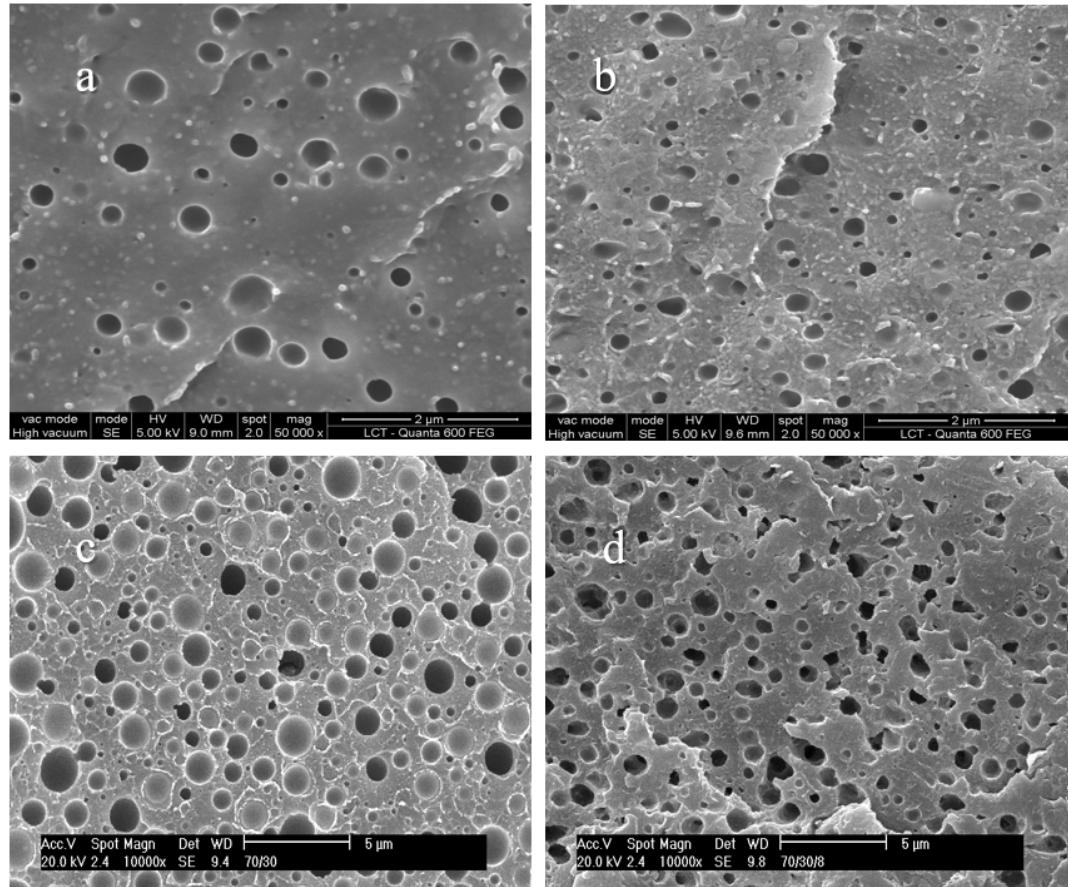


**FIG. 3.3. Morphology of blends for a 90/10 composition (a) with and (b) without the addition of 8 % Cloisite 20A, and for a 70/30 composition (c) without and (d) with addition of 8 % of Cloisite 20A**

Moreover, a decrease of $R_v$ of 34 % upon addition of clay can be seen, which illustrates a compatibilizing effect of the clay. However, this reduction in droplet diameter size is smaller than what we obtained previously when using a random copolymer [15]. This may be due to a different interface coverage due to the less adequate chemistry when compared to that of the copolymer.

TABLE 3.2. Volume average radius (Rv) and polydispersities (Rv/Rn) of the dispersed phase

| Composition | % Compatibilizer with respect to PS | % Compatibilizer with respect to the whole blend | Cloisite 20A | | PMMA-ran-PS* | |
|---|---|---|---|---|---|---|
| | | | $R_v$ (µm) | $\dfrac{R_v}{R_n}$ | $R_v$ (µm) | $\dfrac{R_v}{R_n}$ |
| 90/10 | 0 | 0 | 0.125 ± 0.015 | 1.8 | 0.125 ± 0.015 | 1.8 |
| | 1 | 0.1 | - | - | - | - |
| | 4 | 0.4 | 0.094 ± 0.005 | 2.0 | 0.060 ± 0.007 | 1.9 |
| | 8 | 0.8 | 0.083 ± 0.009 | 1.8 | 0.050 ± 0.007 | 1.8 |
| 70/30 | 0 | 0 | 0.620 ± 0.080 | 2.3 | - | - |
| | 1 | 0.3 | 0.580 ± 0.070 | 2.4 | - | - |
| | 4 | 1.2 | 0.482 ± 0.070 | 2.4 | - | - |
| | 8 | 2.4 | 0.437 ± 0.080 | 2.6 | - | - |

*Results extracted from [15]

As stated in the introduction, the compatibilization mechanism can have several explanations. To understand it, the dispersion and localization of clay in the blends must be known.

## 2. Dispersion state of clay

The basal spacing of Cloisite 20A alone and in the polymers was estimated from WAXS and SAXS patterns. The values of $d_{(001)}$ are reported in TABLE 3.3 and TABLE 3.4.

It can be seen that the basal spacing increases when clay is dispersed in blends or pure polymers, indicating that chains of polymer are intercalated between the clay platelets. Parts of the clay platelets might however be exfoliated within the polymer. It can be seen from TABLE 3.3 that the interlayer spacing between the clay platelets is larger for the

composites with 1 wt% clay than for that with 8 %. This could be due to the fact that at higher clay content, the formation of aggregates could occur more easily because of the interactions between particles. A similar behavior was observed by Amurin et al. [97].

TABLE 3.3. SAXS results for PMMA+(PS+C) blends

| Composition | % Cloisite 20A | q (Å-1) | $d_{(001)}$ (nm) | $\Delta d_{(001)}$ (nm) |
|---|---|---|---|---|
| Cloisite 20A | - | 2.57 | 2.44 | - |
| PS | 1 | 1.68 | 3.73 | 1.29 |
| | 8 | 1.76 | 3.56 | 1.12 |
| 70/30 | 1 | 1.71 | 3.67 | 1.22 |
| | 4 | 1.74 | 3.61 | 1.16 |
| | 8 | 1.73 | 3.63 | 1.18 |
| 90/10 | 1 | 1.74 | 3.61 | 1.16 |
| | 4 | 1.71 | 3.67 | 1.22 |
| | 8 | 1.74 | 3.61 | 1.16 |

TABLE 3.4. WAXS results

| Composition | % Cloisite 20A | $2\theta_2$ (°) | $d_{(100)}$ (nm) | $\Delta d_{(001)}$ (nm) |
|---|---|---|---|---|
| PS | 8 | 5.04 | 3.51 | 1.07 |
| PMMA | 1 | 5.07 | 3.49 | 1.05 |
| | 4 | 4.99 | 3.54 | 1.10 |

FIG. 3.4 shows the complex viscosities measured for pure PMMA and PS which clay was added. An increase in the complex viscosity at low frequencies can be observed with the addition of clay in the case of PMMA. This addition does not have a large influence on the rheological behavior of PS, except when 8 % is added. In this case, the viscosity of the material increases for the whole frequency range, indicating that it acts as a filler.
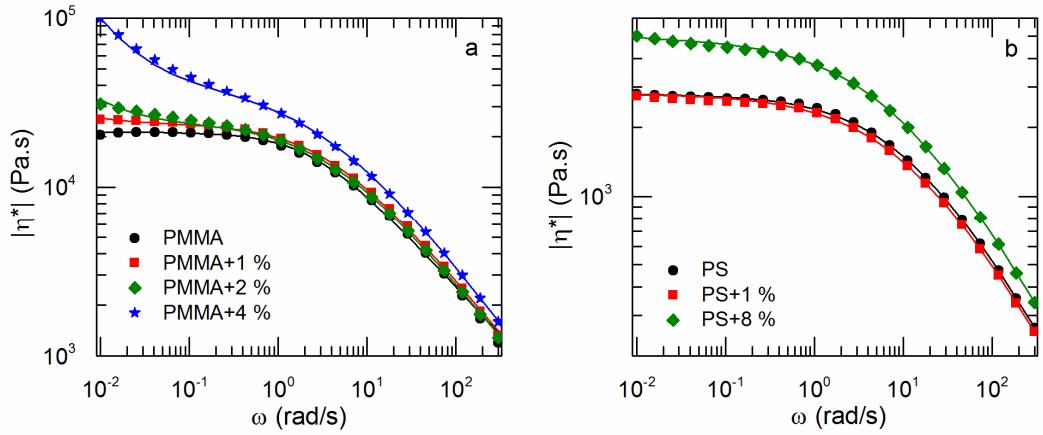
**FIG. 3.4. Complex viscosity of (a) pure PMMA and (b) pure PS with different levels of Cloisite 20A at 200 ºC. Lines represent the fit of Carreau-Yasuda with yield stress equation.**

The complex viscosities were fitted to the Carreau-Yasuda model to which a yield stress had been added, as described by Vergnes [98], in order to obtain further information on the dispersion state of clay. According to Vergnes, the complex viscosity of a material to which clay has been added can be written as follows:

$$\eta^*(\omega) = \frac{\sigma_0}{\omega} + \eta_0 (1 + (\lambda\omega)^a)^{\frac{n-1}{a}} \tag{3.9}$$

where $\sigma_0$ is the melt yield stress, $\eta_0$ the zero shear viscosity, $\lambda$ is the time constant, n is the power law index, and a is the Yasuda parameter.

This model contains five parameters that were adjusted to obtain the best fit with the experimental data. FIG. 3.4 shows that the fits (lines) correspond well to the experimental data (points) in the complex viscosity curves. The corresponding values for the parameters are reported in TABLE 3.5.

**TABLE 3.5. Values of parameters of Carreau-Yasuda with yield stress found by fitting with experimental values**

| Matrix | PMMA | | | | PS | | |
|---|---|---|---|---|---|---|---|
| % clay | 0 | 1 | 2 | 4 | 0 | 1 | 8 |
| $\sigma_0$ (Pa) | 0.00 | 21.0 | 93.4 | 610 | 0.00 | 0.00 | 0.96 |
| $\eta_0$ (Pa.s) | 21000 | 23740 | 23740 | 40000 | 2800 | 2800 | 4920 |
| $\lambda$ (s) | 0.24 | 0.29 | 0.29 | 0.31 | 0.09 | 0.09 | 0.12 |
| a | 0.91 | 0.92 | 0.85 | 0.68 | 0.72 | 0.66 | 0.63 |
| n | 0.34 | 0.37 | 0.36 | 0.30 | 0.31 | 0.30 | 0.29 |

The only parameters that vary significantly are the zero shear viscosity and the yield stress. This is in agreement with the work of Lertwimolnum and Vergnes, who noticed the same effect [99]. The increase in zero shear viscosity is particularly noticeable for high clay

contents (PMMA +4 % and PS+8 %), and seems to be linked to the combined effect of high clay levels and partly exfoliated clay. On the other hand, the yield stress is essentially affected by the exfoliation of clay [98]: for PS+8 %, the viscosity has doubled, but the yield stress had almost no increase. In the case of PMMA+4 %, the viscosity has doubled as well, but the yield stress dramatically increased compared to pure PMMA and PS+8 %. This indicates that clay has more affinity with PMMA, and as a result, if the clay were to disperse in one of the phases, it would be PMMA. In the blending method, the nanoparticles were dispersed in PS prior to mixing the whole blend. The goal was to locate clay at the interface between PMMA and PS, thanks to the migration of clay nanoparticles during blending. The localization of clay is confirmed below by TEM and rheological experiments.

### 3.      Localization of clay

TEM pictures showed that in a 70/30/8 blend, clay is located both at the interface and in PMMA (see FIG. 3.5a). For 90/10/8 blends, clay is located mainly at the interface (see FIG. 3.5b). These results indicate that while clay is located preferably at the interface, however, 8 % of clay in 70/30 blends leads to a saturated interface, and excess clay goes to PMMA.
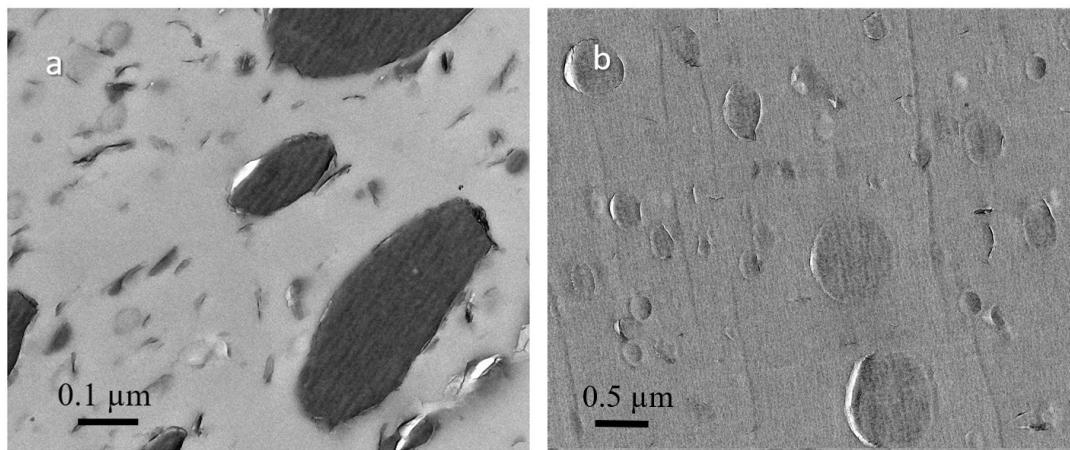


**FIG. 3.5. Typical TEM picture of 70/30/8 (a) and 90/10/8 (b) blends**

FIG. 3.6 shows the rheological behavior of pure blends. It can be seen that for low frequencies, the storage moduli of the 70/30 blends exhibit a shoulder corresponding to the presence of a dispersed phase. This shoulder cannot be well observed for lower dispersed phase concentrations, as expected in the work of Graebling et al. [55].
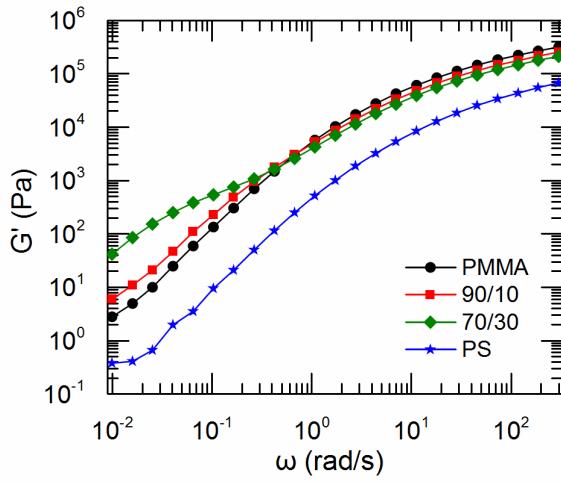
**FIG. 3.6. Storage moduli of PMMA and PS and of pure blends 90/10 and 70/30, in order to emphasis the effect of dispersed phase at 200 °C**

FIG. 3.7 shows the rheological results for blends with different amounts of clay. The rheological behavior of 90/10 blends does not seem to be affected by the presence of clay, most likely due to a too low concentration of both dispersed phase and clay. Conversely, a shoulder, typical to immiscible blend rheological curves, is clearly visible in the case of 70/30 blends, which also shows different behaviors depending on the amount of clay.
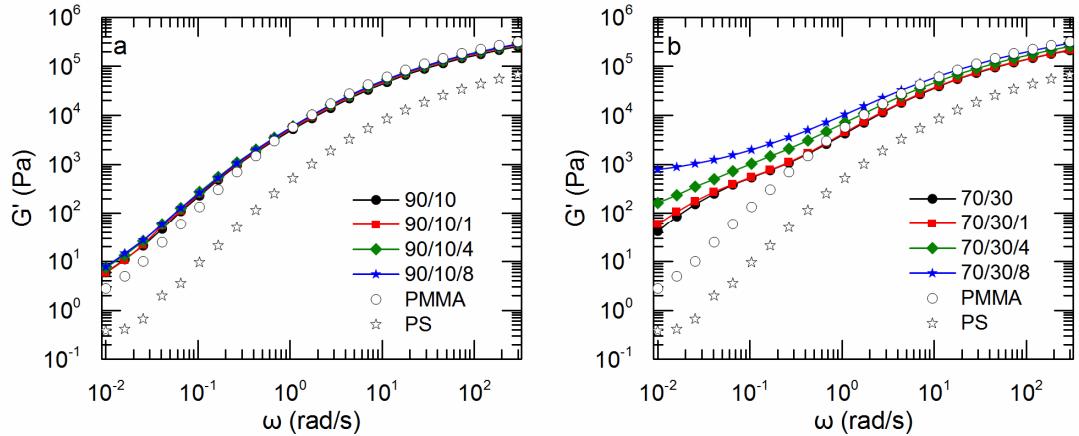


**FIG. 3.7. Storage moduli of PMMA/PS/Cloisite20A blends for 90/10 (a) and 70/30 (b) concentrations and different levels of clay at 200 °C**

FIG. 3.8 compares the rheological behavior of 70/30/8 blends with that of the pure polymers with clay. 8 % of clay with respect to PS corresponds to 3.4 % of clay with respect to PMMA, and as such, the 70/30/8 curve can be compared to PMMA+4 % if all the clay is dispersed in PMMA, and to PS+8 % if all the clay is dispersed in PS. In the 70/30/8 curve, the shoulder due to the presence of droplets disappears, and a plateau is observed at low frequencies, mimicking the behavior of PMMA+4 % of clay.
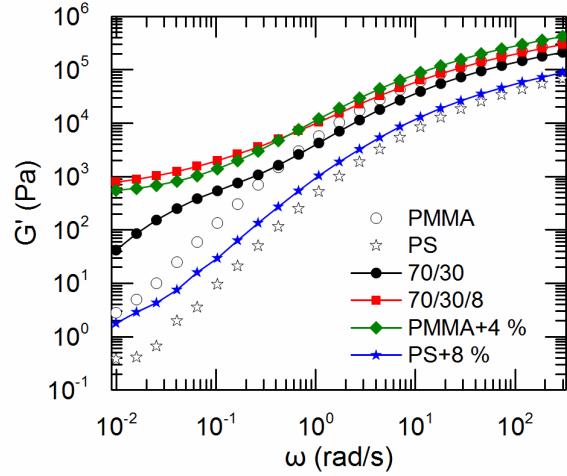
**FIG. 3.8. Storage moduli of PMMA+4 %, PS+8 %, 70/30/0 and 70/30/8 blends as a comparison**

There are several phenomena that can influence the evolution of the storage modulus at low frequencies: the droplet relaxation, the interface relaxation, and the presence of clay in one of the phases. In order to try to differentiate those phenomena, the simplified Palierne model with the approximation of Graebling et al. [55] was fitted to a 70/30 pure blend, leading to an interfacial tension of 0.89 mN/m. The fit is presented in FIG. 3.9a. The blends with clay were then compared to their predictions using the same Palierne model with $R_v$ extracted from TABLE 3.2 and the interfacial tension defined previously (0.89 mN/m). This model only considers the droplet shape relaxation.

If we compare the theoretical predictions of Palierne's model to the experimental curves (see FIG. 3.9), it can be seen that for 70/30/1, the fit corroborates the experimental data, and that a discrepancy between theoretical predictions and experimental data starts to surface for clay concentrations of 4 %. Palierne's model predicts a shoulder shifting slightly to a higher frequency, and hence to shorter relaxation times induced by the decrease in the dispersed phase size, upon addition of clay, whereas the experimental data show a gradual increase at low frequencies and the disappearance of the shoulder in favor of this increase, starting at 4 % of clay. The loss modulus is also increased as compared to predictions, indicating an effect on the viscosity of the blend.
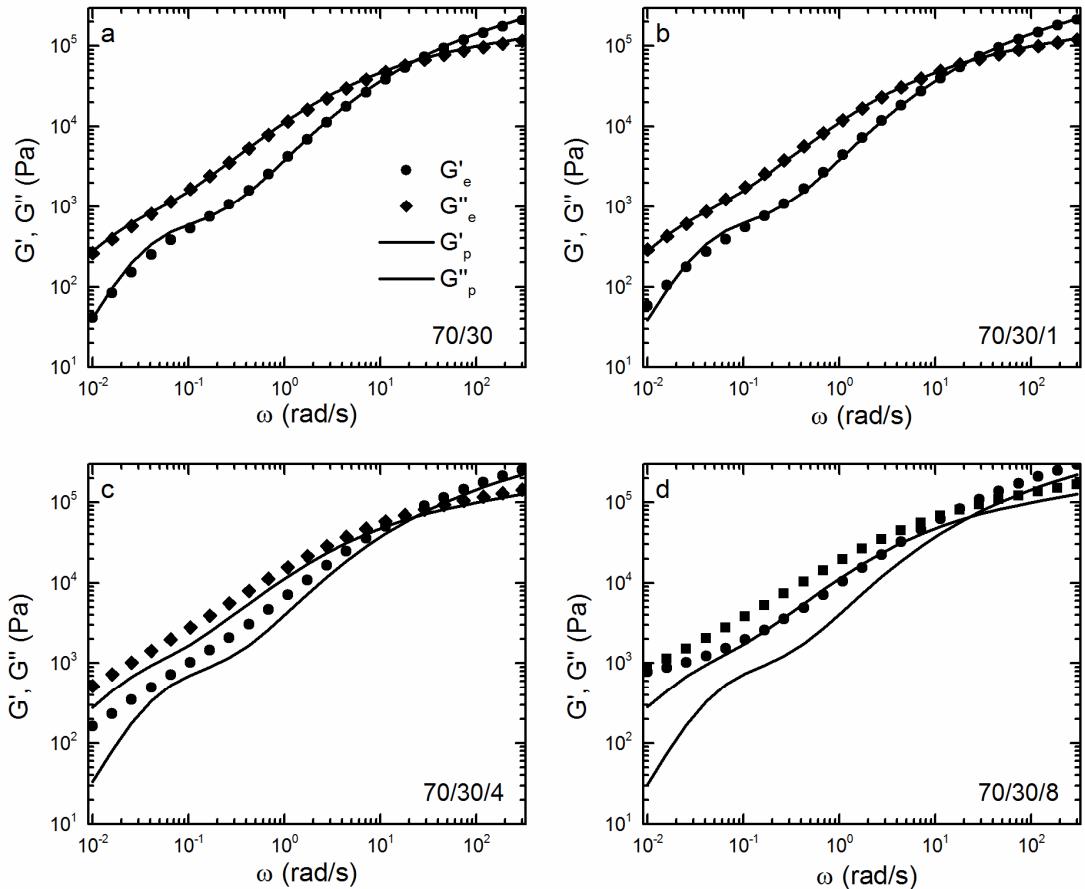
**FIG. 3.9.** Experimental storage moduli (G'$_e$) and loss moduli (G"$_e$) and their prediction by the Palierne model (G'$_p$ and G"$_p$) of (a) 70/30, (b) 70/30/1, (c) 70/30/4 and (d) 70/30/8 blends at 200 °C

To better visualize the difference with the theory, the experimental storage modulus (G'$_e$) was plotted as a function of the theoretical storage modulus (G'$_p$) (see FIG. 3.10). As expected, the pure blend and 70/30/1 had no noticeable deviation from the theory, whereas 70/30/4 and 70/30/8 showed a significant deviation at low frequencies. As the model takes into account the shape relaxation of the droplets, the deviation from the line could represent the effect of nanoparticles at the interface or in one of the phases. FIG. 3.5 shows that for a 70/30/8 blend, the clay was present at the interface as well as in the PMMA phase. For a 90/10/8 blend, clay was located only at the interface. The rheological behavior changes from a typical blend behavior to a behavior close to a PMMA filled with clay for 4 % and 8 % of clay in 70/30 blends. This have not been observed for 90/10 blends, therefore it is considered that the interface is saturated in 70/30/8 and 70/30/4 blends and the excess of clay disperse in the matrix.
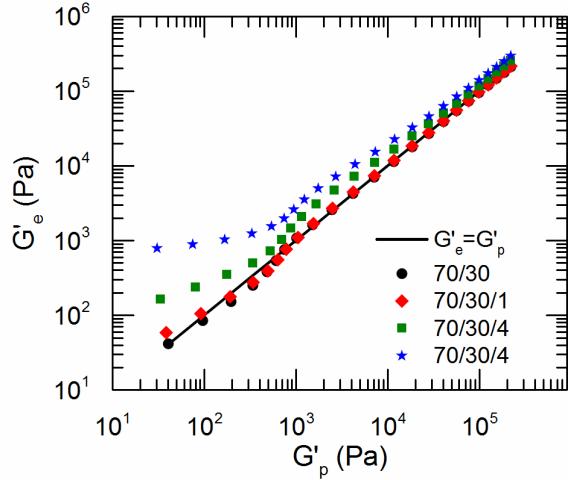
**FIG. 3.10. Experimental storage moduli (G'$_e$) as a function of theoretical storage moduli (G'$_p$)**

The concentration of clay at which the interface is saturated can be evaluated by the following equation used by Ray et al. [93]:

$$\%C_{sat} = \frac{3e}{R_v} \%PS \tag{3.10}$$

where e is the thickness of one clay platelet, $R_v$ is the PS average droplet radius, and %PS is the volume fraction of PS.

The authors primarily estimate that the clay is exfoliated, and thus use the thickness of a single clay platelet in their equations. In this study, since the clay may not be fully exfoliated, we considered that the clay could be held in tactoids containing 1, 2, 3 or 4 layers of clay. The results are reported in TABLE 3.6, while the thickness is calculated, adding successive layers of clay (1 nm thickness) and the basal spacing reported in TABLE 3.3. The percentage of clay needed to saturate the interface is smaller for 70/30 blends, which is normal because as the droplets are bigger, the total interfacial area is smaller than for 90/10 blends. If the clay saturates the interface for concentrations below 4 %, then the sheets are stacked together into 1 to 2 sheets tactoids on average (see also FIG. 3.11).

**TABLE 3.6. Weight percentage of clay with respect to PS needed to saturate the interface**

| Number of sheets | thickness (nm) | %C 70/30 | %C 90/10 |
|---|---|---|---|
| 1 | 1.0 | 0.8 | 4.0 |
| 2 | 5.6 | 4.5 | 22.5 |
| 3 | 10.2 | 8.3 | 40.9 |
| 4 | 14.8 | 12.0 | 59.4 |
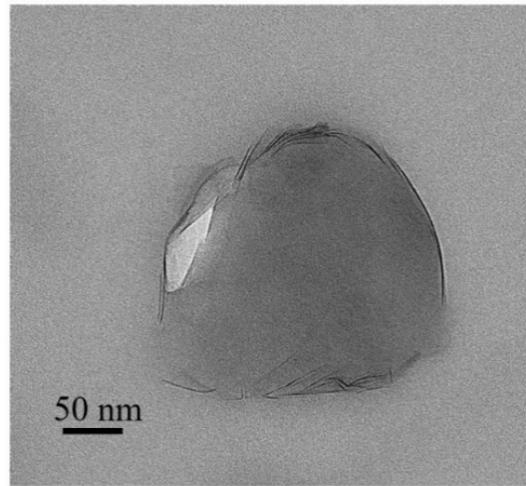
**FIG. 3.11. Typical TEM of a PMMA/PS/Cloisite 20A droplet**

Concerning the 90/10 blends, nothing could be inferred, as no noticeable difference could be seen directly on neat rheological results. In that case, TABLE 3.6 indicates that the interface was not saturated in those blends, and TEM pictures discussed previously showed that clay is located at the interface (FIG. 3.5).

This presence of clay at the interface limits the possible hypotheses for the compatibilization mechanism to the decrease in interfacial tension and/or the inhibition of coalescence by steric hindrance, solid barrier or Marangoni stress.

### 4. Interfacial tension

The interfacial tension was calculated by fitting the simplified Palierne model on SAOS experimental data. FIG. 3.12 show the fits of the Palierne model on 90/10 blends.

The values reported in TABLE 3.7 show that the interfacial tension decreases upon addition of clay. Our results corroborate those of Yee et al. [15], who found similar values of interfacial tension fitting Bousmina's model (see TABLE 3.7). The interfacial tension is lower for the 70/30 blend than for the 90/10 blend. This has already been shown by Calvão et al. [100] who found similar values (0.9 mN/m) for a 70/30 PMMA/PS blend.
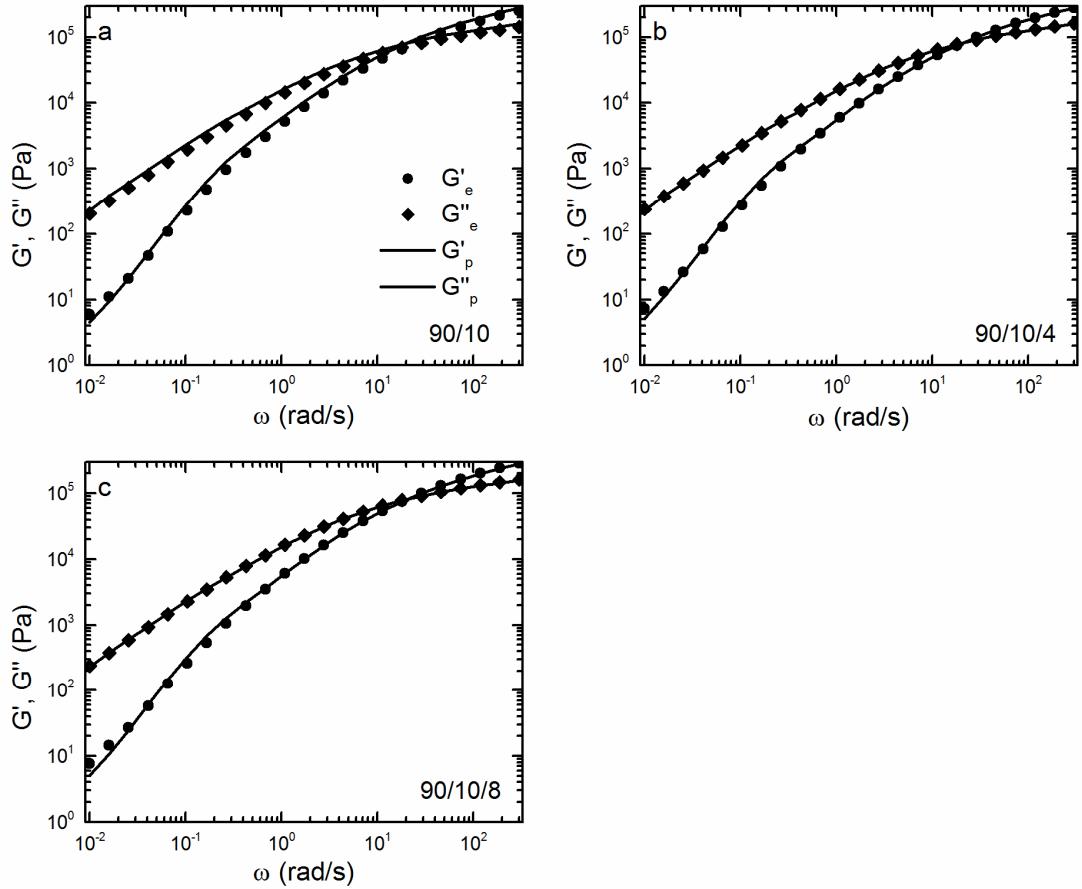
**FIG. 3.12. Experimental storage moduli (circles) and loss moduli (diamonds) and their fit of the Palierne model (lines) on the (a) 90/10, (b) 90/10/4 and (c) 90/10/8 blends at 200 °C**

**TABLE 3.7. Values of interfacial tension ($\alpha^P$) found by fitting the simplified Palierne model on SAOS experimental results and ($\alpha^Y$) values found by Yee et al. [15]**

| Composition | % Compatibilizer with respect to PS | % Compatibilizer with respect to the whole blend | $\alpha^P$ (mN/m) | $\alpha^Y$ (mN/m) |
|---|---|---|---|---|
| 90/10 | 0 | 0 | 1.35 ± 0.16 | 1.4 |
| | 1 | 0.1 | - | - |
| | 4 | 0.4 | 0.70 ± 0.04 | 0.97 |
| | 8 | 0.8 | 0.65 ± 0.08 | 0.85 |
| 70/30 | 0 | 0 | 0.89 ± 0.12 | - |

In the case of a block copolymer, a decrease in interfacial tension is often combined with Marangoni stresses to explain the compatibilization mechanism. As we showed that an interfacial tension decrease occurs upon the addition of clay, the relaxation phenomena were investigated.

### 5.    Relaxation phenomena

The relaxation phenomena were studied by using the relaxation spectra inferred from SAOS measurements. The NLREG technique was used to convert the dynamic results into continuous relaxation spectra [50]. FIG. 3.13 shows the corresponding weighted relaxation modulus $(H(\tau)*\tau)$ as a function of the time $\tau$ of PMMA, PS and pure blends. Two peaks can be identified for the blends; one related to the relaxation times of the blends phases (PS and PMMA) which are overlayed because they are very close to one another [15], and a second, which is associated with the form relaxation of the dispersed droplets. When the concentration of the dispersed phase is higher, the peaks have more amplitude, and the second peak, corresponding to the relaxation of the droplets, is longer because for 30 % of PS, the droplets are larger.
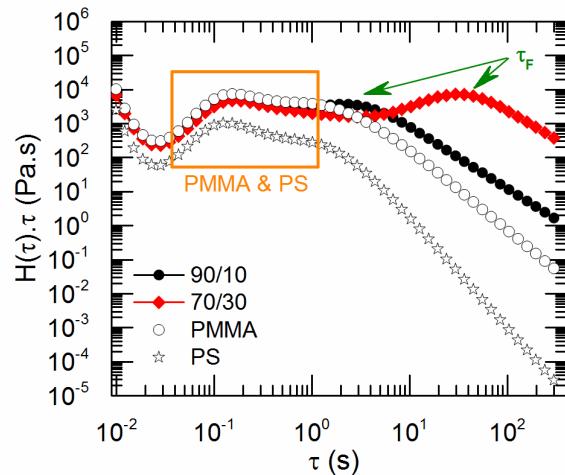


FIG. 3.13. Weighted relaxation spectra of pure blends and materials
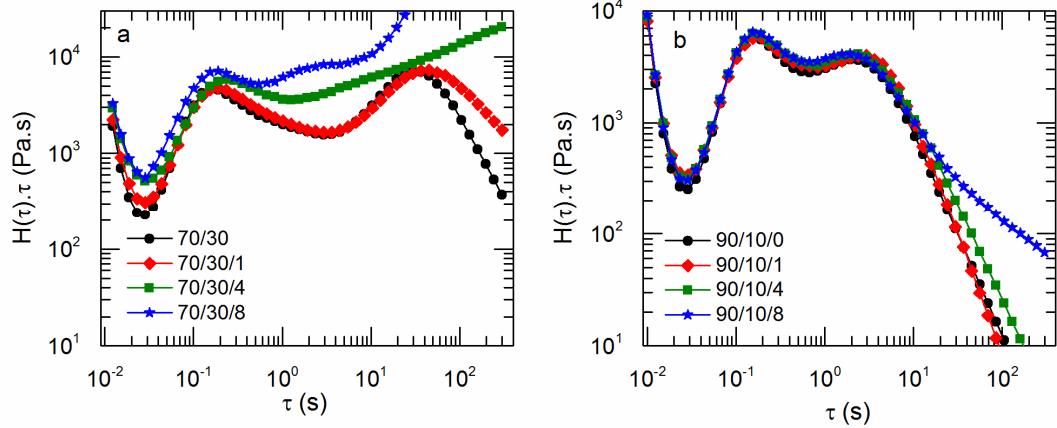
**FIG. 3.14. Weighted relaxation spectra of (a) 70/30 and (b) 90/10 blends with different levels of Cloisite 20A at 200 °C**

For both 90/10 blends and 70/30 blends (see FIG. 3.14), the rise of the relaxation modulus at long times with the addition of clay could suggest the presence of an additional relaxation phenomenon at longer times. One way to obtain data at those times is to use creep experiments as a complimentary technique [94]. In this case, another approach was used consisting of increasing the temperature as it decreases relaxation times. Therefore, additional measurements were carried out at 220 °C. FIG. 3.15a shows the results. As expected, the pure materials with clay exhibit only the relaxation of PMMA or PS chains. The increase at long times for PS+8 % is believed to be due to the relaxation of clay network or agglomerates. Concerning the 90/10 blends, a third relaxation time is revealed. This relaxation time is believed to be due to the Marangoni stress, as neither PMMA+1 % nor PS+8 % have a similar peak as the 90/10/8 blend (see FIG. 3.15b), and clay is located at the interface. This is the first time that this relaxation time has been observed in the case of nanoparticles. The Marangoni stress time decreases with increasing concentration of clay so even if the relaxation does not appear for 90/10/1 the increase at long time indicates a possible relaxation longer than 300 s. This trend is in accordance with the results obtained by several researchers in the case of block copolymer compatibilizers [23], [48], [49], [54], [99]. This means that Cloisite 20A behaves similarly to block copolymers.
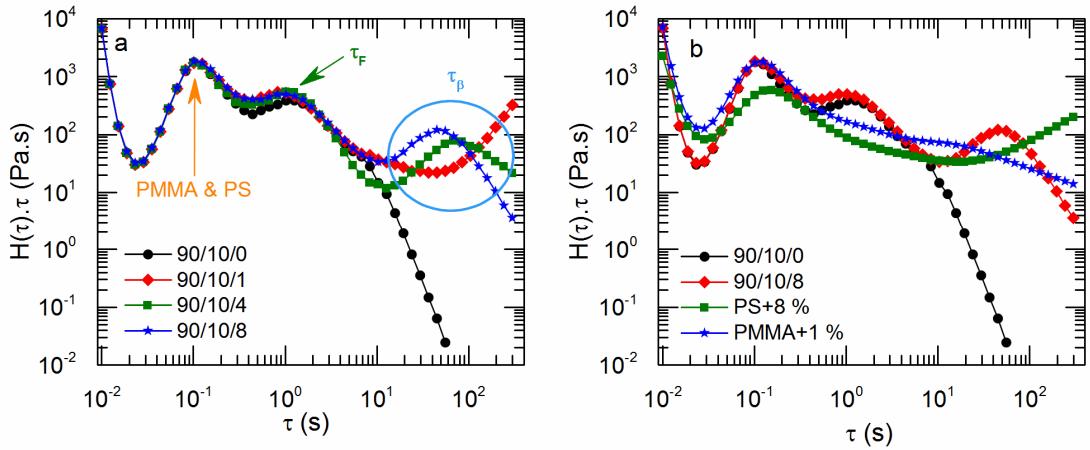
FIG. 3.15. Relaxation spectrum of PMMA+(PS+C) (90/10) (a) blends with different levels of Cloisite 20A at 220 °C, (b) comparison of 90/10/8 blends with PMMA+1 % and PS+8 %

The Palierne model described by Jacobs et al. takes into account a second relaxation phenomenon that has been shown to correspond to the Marangoni stress in previous studies [15], [48], [49]. In order to compare the values found experimentally using the relaxation spectra to the values predicted by the Palierne model, an estimation of the shear modulus of the interface is needed. Indeed, the shear modulus of the interface is likely to be influenced by the nature of the compatibilizer so block copolymers may correspond to a different interfacial shear modulus than nanoparticles. The literature provides values for block copolymers [15], [48], [49] as compatibilizer, but not for clay nanoparticles. By applying equations (3.5) and (3.6), corresponding to the version of the Palierne model given by Jacobs et al. [49], the results at 200 °C allow an estimation of the shear moduli of the interface $\beta_{20}$. The results show that $\beta_{20}$ is higher than for the block copolymer (see TABLE 3.8). However, the tendency is the same: $\beta_{20}$ increases with the addition of clay as well as with addition of block copolymers. These results are in accordance with the observations of Labaume et al. [101].

At 220 °C, a theoretical estimation of the relaxation times was carried out, considering the influence of temperature on the interfacial tension and the interfacial shear modulus to be negligible over 20 °C (i.e., from 200 to 220 °C). The interfacial tension was extracted from TABLE 3.7, $R_v$ was extracted from TABLE 3.2, and $\beta_{20}$ was the one calculated previously (reported in TABLE 3.8). The results show good agreement between the theoretical and experimental scenarios for droplet shape relaxation times, even though the model underestimates the results. Regarding the Marangoni stress relaxation, the values were much smaller than those given by experiments. According to the theoretical results,

the Marangoni stress relaxation should be around 1.5 s, which would likely be overlayed with the droplet shape relaxation at 0.5 s. This underestimation was also observed in the publication of Yee et al. [15]; however, it is significantly more dramatic in this case than in their case, which may be due to the fact that nanoparticles are used instead of copolymers, which would change the interface properties.

**TABLE 3.8. Experimental values of the relaxation times $\tau_F^E$ and $\tau_\beta^E$ extracted from the relaxation spectra; the theoretical values $\tau_F^T$ and $\tau_\beta^T$ were found using equations (3.5) and (3.6) and $\beta_{20}$ the shear moduli of the interface**

| | % Cloisite 20A | $\tau_F^E$ (s) | $\tau_\beta^E$ (s) | $\beta_{20}^1$ (mN/m) | $\beta_{20}^2$ (mN/m) | $\tau_F^E$ (s) | $\tau_\beta^E$ (s) | $\tau_F^T$ (s) | $\tau_\beta^T$ (s) |
|---|---|---|---|---|---|---|---|---|---|
| | | 200 °C | | | | 220 °C | | | |
| | 0 | 2.95 | - | - | - | 0.82 | - | 0.73 | - |
| 90/10 | 1 | 2.60 | * | 0.80 | 0.18 | 0.70 | * | 0.55 | 1.51 |
| | 4 | 2.15 | * | 1.15 | 0.22 | 0.50 | 74 | 0.46 | 1.58 |
| | 8 | 1.71 | * | 1.32 | 0.30 | 0.50 | 50 | 0.37 | 1.45 |

*Not observed, [1]Calculated using equation $(3.5)$ and $(3.6)$, [2]Extracted from [49]

In the case of 70/30 blends, the relaxation spectra at 220 °C are not displayed as no third relaxation time was observed. In the case of a saturated interface (70/30/4 and 70/30/8), no Marangoni stress may even be present, as the clay may not be able to move around the droplets enough. Here, the compatibilization could be due to a physical barrier created by clay around the droplets and/or an increase in matrix viscosity due to the presence of clay. Knowing that 8 % of clay with respect to PS corresponds to 1.7 % with respect to PMMA, and by recalling the results found on PMMA+clay complex viscosity (TABLE 3.5 and FIG. 3.4), we know that PMMA+2 % does not induce any noticeable increase in viscosity. Moreover, as clay is also present at the interface, the clay content in PMMA is strictly lower than 1.7 %. We can conclude that the presence of clay in PMMA for 70/30/8 blends does not influence the viscosity of the matrix. As such, for 70/30/4 and 70/30/8 blends, the compatibilization mechanism is believed to be due to a decrease in interfacial tension and physical barrier, what is also called a Pickering effect, around the droplets.

### D.    Conclusion

The aim of this work was to understand the compatibilization mechanism of PMMA/PS/ Cloisite 20A blends. First, the morphology was assessed, a decrease in the droplet radius upon addition of clay indicated a compatibilizing effect. The dispersion and localization of clay was then studied as it is a key element in understanding compatibilization mechanisms. The results on pure materials showed that clay was better dispersed in PMMA than in PS. In the blends, it was shown that clay localizes itself to the interface until saturation of the interfacial area, after which the remaining clay disperses in PMMA rather than in PS. By considering the blends with a saturated interface, it was possible to say that clay is dispersed in 1 to 2 sheets on average. Linear rheology results combined with the Palierne model showed the compatibilization mechanism to be due to a decrease in interfacial tension as well as Marangoni stresses in the case of an unsaturated interface. This is the first time that Marangoni stresses are shown in the case of nanoparticles. In other words, these results showed that Cloisite 20A behaves similarly to block copolymers Althought, small differences can be observed due to the inherent nature of the ceramic particles: 1) the interfacial shear modulus ($\beta_{20}$) from the Palierne model is higher than the ones observed for block copolymers, 2) the Marangoni stress time is longer in the case of nanoparticles as an increase in the temperature of the SAOS experiments was needed to be able to observe it. This indicates that the mobility of ceramic particles around the droplet is smaller than the one of block copolymers which have affinity with both phases.

# CHAPTER 4

# INFLUENCE OF THE MOLAR MASSES ON THE COMPATIBILIZATION MECHANISM INDUCED BY TWO BLOCK COPOLMERS IN PMMA/PS BLENDS

Julie GENOYER[1,2], Jérémie SOULESTIN [1], and Nicole R. DEMARQUETTE[2]

[1] *IMT Lille Douai, Department of Polymers and Composites Technology & Mechanical Engineering, Douai, France*
[2] *École de technologie supérieure, Department of Mechanical Engineering, Montreal, QC H3C 1K3, Canada*

## Abstract

The compatibilization mechanism of PMMA/PS blends induced by PMMA-b-PS block copolymers of different molar masses (30 and 104 kg/mol) was studied. The blend morphologies with and without copolymers were observed by scanning electron microscopy. The rheological behavior was studied performing small amplitude oscillatory shear experiments. The experimental results were compared to Palierne's model predictions. Shear induced coalescence tests were also conducted. Contrary to what was expected, adding block copolymers did not result in a refinement of the droplets size. However, it induced Marangoni stresses, a decrease in interfacial tension and an inhibition of coalescence of the dispersed phase. During coalescence tests a decrease of the relaxation time due to Marangoni stresses with time was revealed. This interesting behavior contradicts previous works on the subject and is believed to be due to a migration of block copolymers to the interface during the tests rather than droplets' coalescence. As such, the morphology was explained by the fact that block copolymers are not entirely at the interface initially. Also, the block copolymer with a higher molecular mass was shown more efficient at inhibiting coalescence, indicating that the compatibilization mechanism is a combination of Marangoni stresses and steric hindrance.

### A.    Introduction

The control of morphology of immiscible polymer blends is a common issue in polymer processing. When polymer blends are subjected to flow, their morphology is influenced by breakup and coalescence phenomena. Taylor [2] suggested that at low stress in a steady uniform shear flow, the deformation degree of a droplet is a function of :

- The capillary number Ca

$$Ca = \frac{F_{viscous}}{F_{interfacial}} = \frac{\eta_m \dot{\gamma} R_v}{\alpha} \tag{4.1}$$

- The viscosity ratio p

$$p = \frac{\eta_d}{\eta_m} \tag{4.2}$$

Where $\eta_m$ and $\eta_d$ are the viscosities of the matrix and the droplets respectively, $\dot{\gamma}$ is the shear rate, $R_v$ the radius of the droplets and $\alpha$ the interfacial tension.

Applying a flow can lead to droplet breakup when the interfacial tension forces cannot balance the viscous forces. That is what happens above a critical value of the capillary number $Ca_c$. Below this value the coalescence will be promoted. Grace [5] provided data about this phenomenon by experimentally plotting $Ca_c$ as a function of p for both simple shear and extensional flow (FIG. 4.1). The lowest $Ca_c$, in other words the range where breakup is the easiest, is found for $0.1 \leq p \leq 1.0$. This is the range where most blends will be chosen as a fine morphology is wanted for good final properties, however coalescence still often takes place during processing.
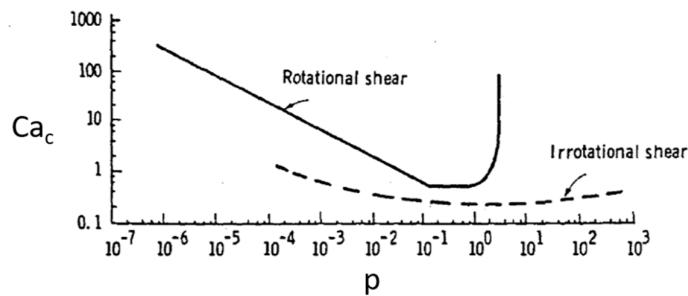


**FIG. 4.1 Effect of the viscosity ratio on critical capillary number in rotational shear and irrotational shear fields**
[5]

The addition of a so-called compatibilizer is a way to control the morphology over time [6], [24]. Premade block copolymers are generally used for this purpose, but at the industrial level it is more common to create a compatibilizer during processing thanks to

an interfacial reaction [11]. For both methods, in the case of a droplet dispersion, the compatibilizers settle at the interface because of their dual chemistry. Their addition leads to a reduction of the dispersed phase size [13]–[15], an inhibition of the droplet's coalescence [7], [17]–[20], a decrease of interfacial tension [7], [14]–[16], and the presence of an additional relaxation phenomenon [8], [16], [23], [25], [48], [49], [53], [100], [102] besides an improvement of the blend properties.

Coalescence suppression is generally believed to be induced by two phenomena. The first one is based on the appearance of Marangoni stresses. When two droplets approach each other, the matrix flows out from the gap between the approaching droplets and when it happens the compatibilizer is dragged along. This results in a gradient in compatibilizer concentration on the droplet surface, so in an interfacial tension gradient. Because of that, Marangoni stresses appear to make the compatibilizer come back homogeneously around the droplets and in doing so, prevents coalescence. Those Marangoni stresses are the source of the additional relaxation phenomenon mentioned previously. They were evidenced by Jeon and Macosko [21] who showed gradients in block copolymer concentration during flow by visualizing a fluorescent PS-PMMA copolymer at the surface of a PMMA droplet in a PS matrix. The minimum coverage of block copolymer necessary to completely suppress coalescence by considering Marangoni stresses can be estimated using equation **(4.3)** [22].

$$\sum_{min} = \frac{5}{32} \frac{2R_v \eta_m \dot{\gamma}}{kT} \tag{4.3}$$

The second mechanism, proposed by Sundararaj and Macosko [7], explains coalescence suppression by steric hindrance. When two droplets approach each other, the block copolymer is squeezed in between them. It leads to repulsion between the droplets because a change in the conformation of the copolymer chain leads to a gain in entropy. This hypothesis is consistent with the observations of Van Hemelrijck et al. [23], and Lyu et al. [20] that showed that the length of the diblock in the matrix influences coalescence in such a manner that the longer the block, the more coalescence is suppressed. This theory assumes that the block copolymer cannot move at the interface. By equating the Van der Waals force with the steric force, the minimum coverage of block copolymer can be estimated by the following expression [20]:

$$\sum_{c} = \frac{20}{27\pi <r_0^2>} \tag{4.4}$$

Where $< r_0^2 >$ is the square mean end-to-end distance of the chains of block copolymers. Originally, this steric hindrance theory was developed to explain suppression of static coalescence, thus it is independent of shear rate.

These two phenomena could also be present at the same time, but this is rarely dealt with in the literature. On this subject, Fortelny [25] assessed that steric hindrance can act only if the Marangoni effect is negligible, suggesting that Marangoni stresses usually dominates. All this is valid if the block copolymers settle only at the interface, however, some researchers evidenced that micelles can be present in the blends, decreasing the efficiency of the compatibilizers [22]. The efficiency is then linked to the quantity of block copolymer at the interface, thus to the surface coverage.

The rheological characterization of a blend in the linear regime can provide information on the morphology, interfacial tension between the polymers forming the blend and relaxation phenomena above mentioned. Indeed, small amplitude oscillatory shear experiments reveal an increase in elasticity at low frequencies, resulting in a shoulder on the storage modulus curve as a function of frequency. This increase is associated with the relaxation of the shape of the droplets ($\tau_F$), which were previously deformed by the stress applied [55]. In the case of compatibilized blends, an additional relaxation time ($\tau_\beta$) may be observed. Van Hemelrjick et al. [54] showed that $\tau_F$ depends mainly on the concentration of the dispersed phase, whereas $\tau_\beta$ strongly depends on the concentration of compatibilizer. Therefore, the latter relaxation time is believed to be due to the presence of copolymer at the interface, and especially to the presence of Marangoni stresses.

In order to evaluate clearly relaxation times, relaxation spectra can be recovered from classical small amplitude oscillatory shear measurements using Honerkamp and Weese method [50]. Those spectra allow a better visualization of the relaxation times originated from the relaxation of the droplet shape and Marangoni stresses. In the present work, these relaxation times will be called droplet's shape relaxation and Marangoni's relaxation.

Several models have been developed to link the rheological behavior of polymer blends to their morphology. One such model is Palierne's model, which predicts the rheological behavior of a blend formed by two viscoelastic polymers [52]. The polymers should be viscous enough to render bulk forces such as gravitation and inertia negligible,

and the emulsion should be monodispersed and diluted. This model is made to predict the behavior of blends in the linear viscoelastic regime in other words at small and slow deformations. As such, the constitutive equations which relate stress to deformations are linear. This model predicts the relaxations happening in a blend.

The simplified version commonly used gives the following expression for the droplet's shape relaxation time [56]:

$$\tau_F = \frac{\left(\frac{R_v \eta_M}{4\alpha}\right)(19p + 16)\big(2p + 3 - 2\Phi(p-1)\big)}{10(p+1) - 2\Phi(5p+2)} \tag{4.5}$$

where $R_v$ is the average droplet radius, $\alpha$ the interfacial tension, and $\Phi$ the volume fraction of the dispersed phase.

The original Palierne model was modified by Jacobs et al.[49] (see equations (4.6)-(4.9)) to take into account Marangoni's relaxation ($\tau_\beta$) resulting in values for both the droplet shape and Marangoni stress relaxation times as follows:

$$\tau_F = \frac{\lambda_{12}}{2}\left(1 - \left(1 - \frac{4\lambda_{11}}{\lambda_{12}}\right)^{0.5}\right) \tag{4.6}$$

$$\tau_\beta = \frac{\lambda_{12}}{2}\left(1 + \left(1 - \frac{4\lambda_{11}}{\lambda_{12}}\right)^{0.5}\right) \tag{4.7}$$

With

$$\lambda_{11} = \frac{R_v \eta_m}{4\alpha} \frac{(19p + 16)(2p + 3 - 2\Phi(p-1))}{10(p+1) + \frac{\beta_{20}}{\alpha}(13p+12) - 2\Phi\left((5p+2) + \frac{\beta_{20}}{2\alpha}(13p+8)\right)} \tag{4.8}$$

$$\lambda_{12} = \frac{R_v \eta_m}{8\beta_{20}} \frac{10(p+1) + \frac{\beta_{20}}{\alpha}(13p+12) - 2\Phi\left((5p+2) + \frac{\beta_{20}}{2\alpha}(13p+8)\right)}{(1-\Phi)} \tag{4.9}$$

Where $\beta_{20}$ is the interfacial shear modulus, an interfacial parameter.

In the present work, PMMA/PS blends with addition of PS-b-PMMA block copolymers of different molar masses were studied. PMMA/PS blends are often used as "model" blends for research as their rheological behavior is well known and not too much sensitive to side effects like degradation. The morphology and rheological behavior were assessed. The interfacial tension was calculated using Palierne's model. The compatibilization mechanism was studied using rheology: Marangoni stresses were evidenced using the relaxation spectra inferred from SAOS measurements, and shear induced coalescence tests were performed.

### B.    Materials and methods

#### 1.    Materials

In this study, poly(methylmethacrylate) (PMMA) from PLEXIGLAS, grade 6N, and polystyrene (PS) from INEOS Styrenics, grade EMPERA 350N, were used. Two symmetric (ratio PMMA/PS 1:1) block copolymers (BC) with their molar mass being the only difference were added to the blends. The BCs were purchased from Sigma Aldrich. The characteristics of the materials are reported in TABLE 4.1.

**TABLE 4.1 Properties of the polymers**

| Polymer | $M_n$ (g/mol) | $M_w/M_n$ | Melt flow index (cm³/10 min) | Viscosity ($\eta_0$) (Pa.s) at 200 °C |
|---|---|---|---|---|
| PMMA | - | - | 12 (230 °C / 3.8 kg) | 12,000 |
| PS | - | - | 1.5 (200 °C / 5 g) | 9,800 |
| BC1 | 30,000 | ≤1.2 | | - |
| BC2 | 104,000 | ≤1.2 | | - |

#### 2.    Blending

Blends of PMMA/PS in 90/10 weight concentrations were prepared. To these were added different concentrations of BC ranging from 0 to 1 wt%. All the percentages in this paper are weight percentage.

The blends were prepared using a micro twin screw extruder HAAKE MiniLab II from Thermo Scientific. Components were blended at 200 °C and 50 rpm after PMMA was dried at 80 °C for at least 12 hours. Blends were prepared in two steps: First, the block copolymers were mixed with the minor phase (PS) in direct extrusion mode, and then, PS+BC was mixed with PMMA for 7 minutes in cycle extrusion mode. The aim was to follow a process similar to another work [103]. In the case of the uncompatibilized PMMA/PS blend (without BC, called pure in the rest of the paper), the minor phase was processed twice in order to ensure it had the same thermal history as the others.

#### 3.    Characterizations

Samples for rheological and morphological analyses, discs with a 25 mm diameter and 1 mm thickness, were molded at 200 °C under 18 MPa for 10 minutes using a compression molding press.

The rheological characterization was performed using two stress-controlled rheometers: MCR 501 and MCR 302 from Anton Paar. All measurements were carried out under dry nitrogen atmosphere. A parallel-plate geometry was used with a gap size of 0.9 mm and plate diameter of 25 mm. Time sweep tests were performed in order to check the thermal stability of the samples and showed that the samples were stable at 200 °C for 2 hours. Strain sweep tests were carried out for blends and pure polymers to define the linear viscoelasticity region. The strain was fixed at 4 % in the linear region. Finally, dynamic frequency sweep tests were performed from 300 to 0.01 Hz for all blends and pure polymers at 200 °C and some at 180 °C. The zero-shear viscosity of the individual phases necessary for further analyses and calculation was determined using the curve of complex viscosity (Pa.s) versus frequency (rad/s) from dynamic frequency sweep tests. Rheological experiments were shown to be reproducible within 5 % for both rheometers.

Coalescence tests were conducted on the MCR 302 at 200 °C under nitrogen. As the blend already has a fine morphology, a pre-shearing was not considered necessary. The shear rate was chosen low enough to favor coalescence: using $p = 0.82$, the experimental fit of Grace's curve by De Bruijin [6] (equation (4.10)) gives a critical capillary number of 0.47. Equation (4.1) gives a critical shear rate of 0.12 s$^{-1}$ (using $\eta_m$ from TABLE 4.1 and $R_v$ = 0.323 µm, $R_v$ of the pure blend measured by SEM). Thus, a shear rate of 0.05 s$^{-1}$ was chosen to ensure coalescence conditions. The coalescence tests were designed as described in FIG. 4.2 with a succession of steady shear (shear induced coalescence) and frequency sweeps to probe the evolution of morphology.

$$logCa_c = -0.506 - 0.0995logp + 0.124(logp)^2 - \frac{0.115}{logp - log4.08} \tag{4.10}$$
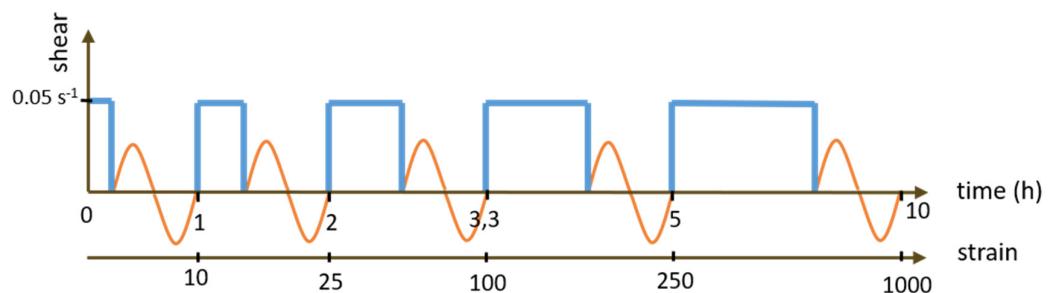


FIG. 4.2 Design of coalescence experiments

Those tests last 10 hours in total. The rheological behavior is then evaluated as a function of strain ((time length of steady shear)*(shear rate)). Neat polymers were characterized rheologically, TABLE 4.2 shows the evolution of the zero shear viscosity and the resulting viscosity ratio during the tests. During coalescence tests some thermal degradation occurs resulting in a decrease of PMMA and PS viscosity. These data were taken into account at each step of the test. Block copolymers probably also degrade during coalescence tests. This degradation is considered to be taken into account by considering PMMA and PS decrease of viscosity as their degradation will be similar and also because the amount of block copolymer is very low.

**TABLE 4.2 Evolution of complex viscosities of PMMA and PS and of the resulting viscosity ratio p during coalescence tests at 200 °C**

| strain | 0 | 10 | 25 | 100 | 250 | 1000 |
|---|---|---|---|---|---|---|
| $\eta_0$(PMMA) | 11,900 | 11,800 | 11,500 | 11,100 | 10,700 | 9,800 |
| $\eta_0$(PS) | 9,800 | 7,100 | 6,200 | 5,900 | 5,700 | 5,200 |
| p | 0.82 | 0.60 | 0.54 | 0.53 | 0.53 | 0.53 |

The morphology prior to coalescence was characterized by scanning electron microscopy using a HITACHI SU8230 FE-SEM. A JEOL JCM-600 plus was used for blends after coalescence. The samples were previously fractured at ambient temperature. For the use of JEOL JCM-600 plus, the samples were covered with gold. The morphology was quantified with ImageJ software considering at least 600 particles for each sample.

### C. Results and discussion

#### 1. Morphology

SEM observations were used to assess morphology. Small droplets were obtained but contrary to what has been observed in many other studies, the addition of BC did not result in a decrease in the droplets average volume radius (see FIG. 4.3 and FIG. 4.4). For PMMA/PS systems, Yee et al. [15] showed a decrease of $R_v$ with addition of random block copolymer.

An explanation could be that there are micelles in the blend which would limit the amount of BC at the interface, thus limiting the compatibilization mechanism. However, because of their dual chemistry it is expected that at least part of the BC is at the interface. In this case, the interfacial tension should be decreased [6], [23], [53] and Marangoni stresses should appear [48], [102].
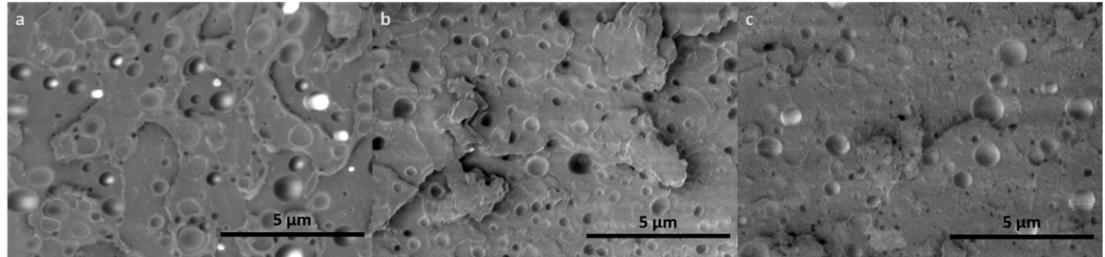
**FIG. 4.3 Morphology of (a) pure PMMA/PS blend, and blends with (b) 1% of BC1 and (c) 1% of BC2.**
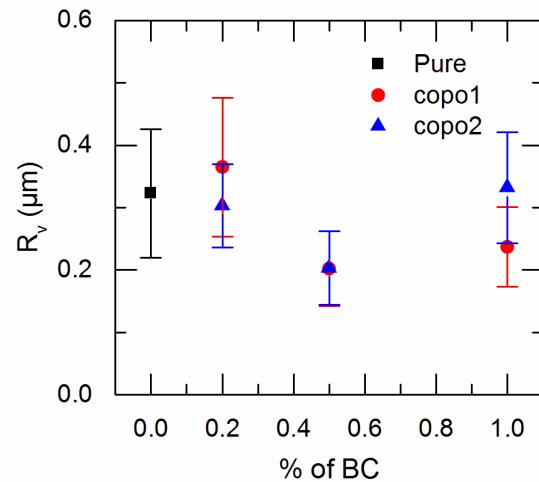


**FIG. 4.4 Evolution of the volume average droplet radius with addition of BC.**

## 2. Interfacial tension & Marangoni stresses

To verify if there is BCs at the interface, rheological experiments were conducted at 200 °C. FIG. 4.5a and FIG. 4.5b show the storage moduli of the blends as a function of frequency. It can be seen that the presence of BCs induces an increase in G' even at high frequencies. This could indicate the presence of BCs in one of the phases, however, this cannot be ensured here. As the concentration of dispersed phase and block copolymer is very low, the shoulder that should be present on the storage modulus, in the case of BC at the interface [53], is not apparent. In order to better visualize the relaxation phenomena, the relaxation spectra of the blends were calculated using the SAOS data reported in FIG. 4.5a. and FIG. 4.5b. The results are presented FIG. 4.5c and FIG. 4.5d. When the data are shown that way, the changes from one sample to another can be acknowledged more easily. The first relaxation observed in the blends spectra corresponds to mainly PMMA and minorly PS chains relaxation. The second relaxation phenomenon is due to the relaxation of the droplets shape ($\tau_F$). It can be noticed that this second relaxation is of the same order

than the second relaxation in neat PS' relaxation spectra. However, due to its very low concentration, PS' contribution to the relaxations of blends is considered negligible. The third relaxation observed only in the case of BC2 (FIG. 4.5d) is due to Marangoni stresses ($\tau_\beta$). As generally observed in the literature, FIG. 4.5d shows that this relaxation time decreases with addition of BC [48], [49]. This shows that BC2 is at least partially at the interface and a compatibilization mechanism should be observed.

The absence of these Marangoni stresses in the case of BC1 is probably due to the difference in molar mass as it is the only difference between BC1 and BC2. Knowing that Marangoni stresses relaxation is induced by movements of BC at the interface, BC1 should have a shorter Marangoni's relaxation: it has a smaller molar mass, so it should be able to move faster. As such, the relaxation of the droplets and Marangoni's relaxation may be overlapped or close enough to be not distinguishable in FIG. 4.5c.

To verify this assumption, other rheological measurements were conducted at lower temperature: as already shown by Genoyer et al.[103], Marangoni's relaxation is influenced by temperature. By decreasing the temperature, the movements of BCs at the interface will be longer as the viscosity increases. As predicted, at 180 °C the third relaxation corresponding to Marangoni stresses appears (see FIG. 4.6) for BC1. The relaxation time corresponding to relaxation of Marangoni stresses is not seen for 0.2 % of BC1 as the amount of block copolymer might be too low or the relaxation time too long to be observed. This confirms that BC1 also is at least partially at the interface, that the two relaxations were at similar times at 200 °C, and that Marangoni stresses are more influenced by temperature than the droplet shape relaxation. For the next results, the relaxation at 200 °C for BC1 blends is considered to be representative of the droplets shape relaxation.
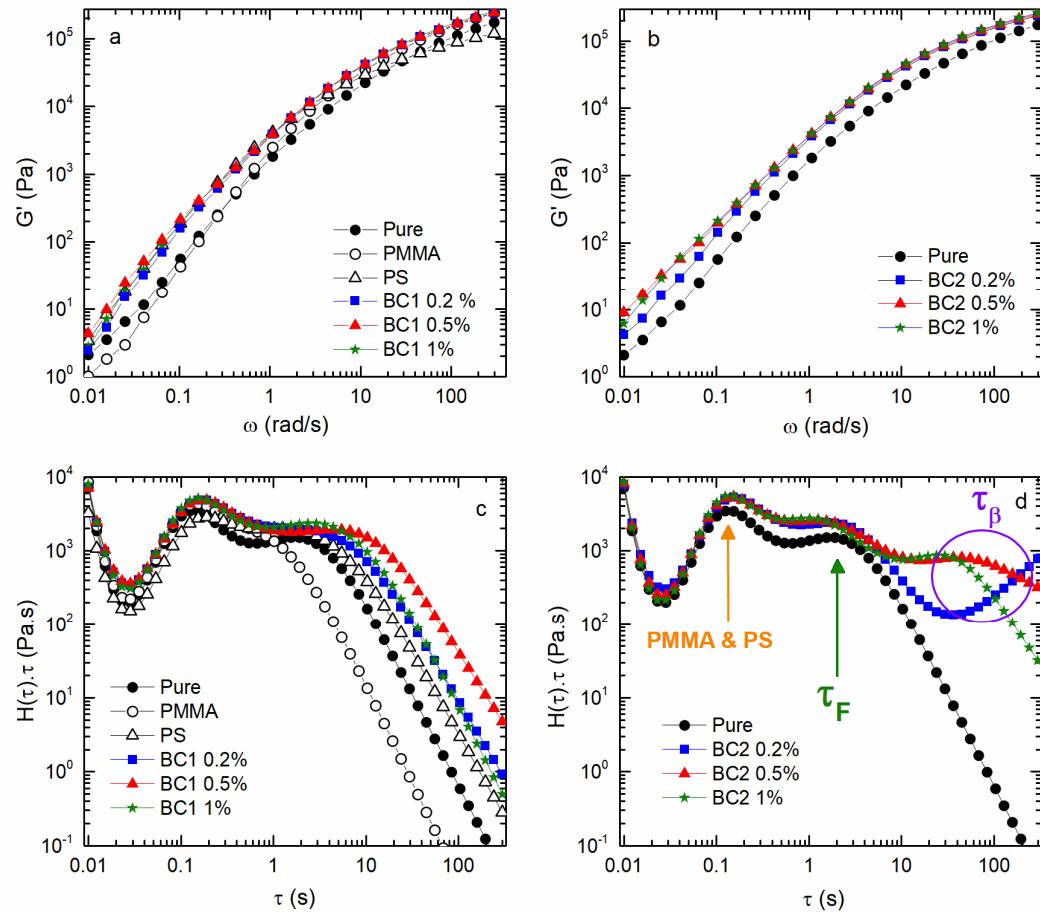
**FIG. 4.5 SAOS results at 200 °C : storage moduli of blends with (a) BC1, (b) BC2 and the relaxation spectra of (c) BC1 and (b) BC2**
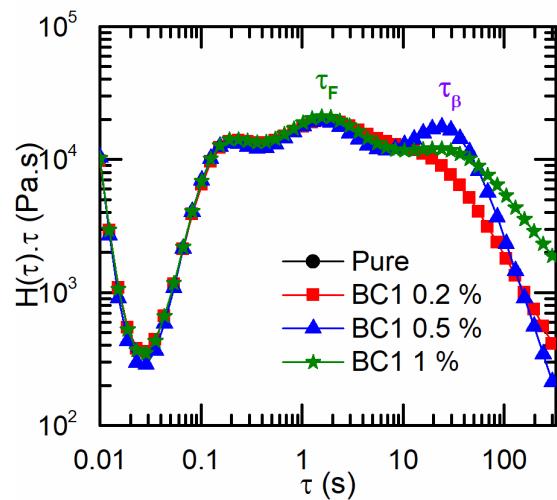


**FIG. 4.6 Relaxation spectra of BC1 at 180 °C**

By extracting the droplet shape relaxation time ($\tau_F$) and using equation (4.5) the interfacial tension of each blend can be calculated. The interfacial tension between PMMA and PS can be found in the literature to be between 1 to 3 mN/m [15], [49], [95], [103]. The values found here are of the same order of magnitude, decrease with addition of BC1 but increase with addition of BC2 (see TABLE 4.3).

TABLE 4.3 α the interfacial tension calculated using Rv from SEM observation and $\tau_F$ from the relaxation spectra of each blend

| Blend | Pure | BC1 | | | BC2 | | |
|---|---|---|---|---|---|---|---|
| %BC | | 0.2 | 0.5 | 1 | 0.2 | 0.5 | 1 |
| α (mN/m) | 4.29 ± 1.37 | 2.20 ± 0.67 | 0.60 ± 0.18 | 1.01 ± 0.28 | 2.96 ± 0.66 | 0.35 ± 0.10 | 0.67 ± 0.18 |

A decrease in interfacial tension and the presence of Marangoni stresses clearly attest the presence of block copolymers interface and that there should be a compatibilization effect. As generally Marangoni stresses are associated with coalescence suppression, coalescence tests were conducted to ensure the results reported here.

### 3.   Coalescence

Coalescence tests were carried out following the shear history described previously. The results for BC1 are shown in FIG. 4.7. An evolution of the storage modulus at low frequencies can be witnessed. To understand better this evolution, 3 storage moduli predicted by the simplified Palierne model [56] were plotted in FIG. 4.8. P0.37 is the actual fit of the simplified Palierne model to experimental data for BC1 0.2 % at strain = 0, with $R_v$ = 0.37 μm (determined previously by SEM). P0.037 and P3.7 curves are the model predictions with the parameters determined previously except $R_v$ that is changed to 0.037 μm and 3.7 μm respectively. The aim is to understand the evolution of the storage modulus when the droplets size changes. FIG. 4.8 shows that the shoulder for which the droplets relaxation is responsible, indicated by arrows, shifts to lower frequencies when $R_v$ increases and is more pronounced while doing so. This is the same type of evolution as observed in FIG. 4.7 during coalescence experiments. This increase in $R_v$ is the evidence that coalescence occurred during the tests.

To analyze the coalescence phenomenon, the relaxation spectra for the different blends were inferred from the SAOS data reported FIG. 4.7. In the case of BC1 (FIG. 4.9), the evolution of the droplets' relaxation time (second relaxation) is very clear and shifts to greater values during the experiment. Indeed, the bigger the droplets, the more they will be

deformed during shearing, therefore the longer the relaxation time of the shape after deformation. In the case of BC2, the results are slightly different because of Marangoni's relaxation: the relaxation of the droplets disappears starting at a strain of 100 for BC2 0.5 % and 1 %. This is most likely due to the fact that the shape and Marangoni's relaxation times are overlapped.
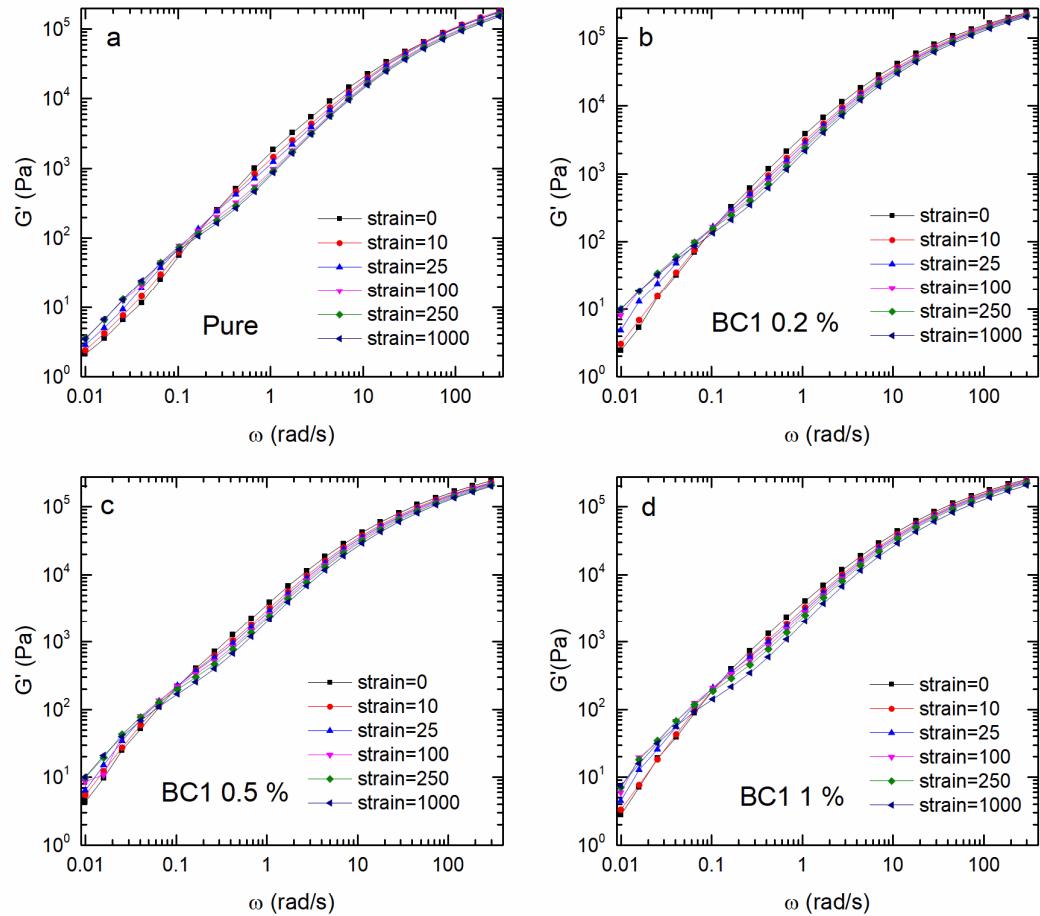


**FIG. 4.7 SAOS measurements from the coalescence tests of blends containing BC1**

**TABLE 4.4 Experimental values of relaxations times $\tau_F^E$ and $\tau_\beta^E$, $\beta_{20}$ the interface parameter calculated, $\tau_F^T$ the theoretical relaxation time of the droplets calculated after determining $\beta_{20}$**

| %BC2 | $\beta_{20}$ (mN/m) | $\tau_\beta^E$ (s) | $\tau_F^E$ (s) | $\tau_F^T$ (s) |
|---|---|---|---|---|
| 0.5 | 0.11 | 53.4 | 1.52 | 1.51 |
| 1 | 0.43 | 22.5 | 1.30 | 1.27 |

The evolution of the volume average radius was then calculated using $\tau_F$ extracted from the relaxation spectra (FIG. 4.9 and FIG. 4.10) for all the blends except BC2 0.5 % and 1 % where $\tau_F$ was used only until strain = 100. To do so, equation (4.5) was used and the interfacial tension was taken as calculated previously for strain = 0 and its variation during coalescence test was assumed negligible. Because of the disappearance of $\tau_F$ for 0.5 % and 1 % of BC2, $\tau_\beta$ was used to determine $R_v$. First, equation (4.7), (4.8) and (4.9) were used to determine the interface parameter $\beta_{20}$ at strain = 0 necessary for further calculation. $\beta_{20}$ was shown to increase when the amount of compatibilizer increases (see TABLE 4.4) which was already shown in other works [16], [48]. It is also shown in TABLE 4.4 that adjusting the $\beta_{20}$ parameter with the value of $\tau_\beta^E$ and then calculating the theoretical $\tau_F^T$ leads to a very good agreement with the $\tau_F^E$ extracted directly from the relaxation spectra. This very good agreement confirms the fact that the second relaxation corresponds to the droplet relaxation time ($\tau_F$) and the third to Marangoni's relaxation ($\tau_\beta$).
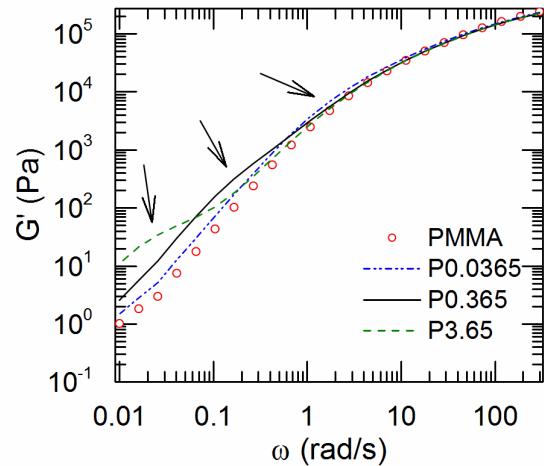


FIG. 4.8 Evolution of storage modulus predicted by Palierne's model when $R_v$ varies
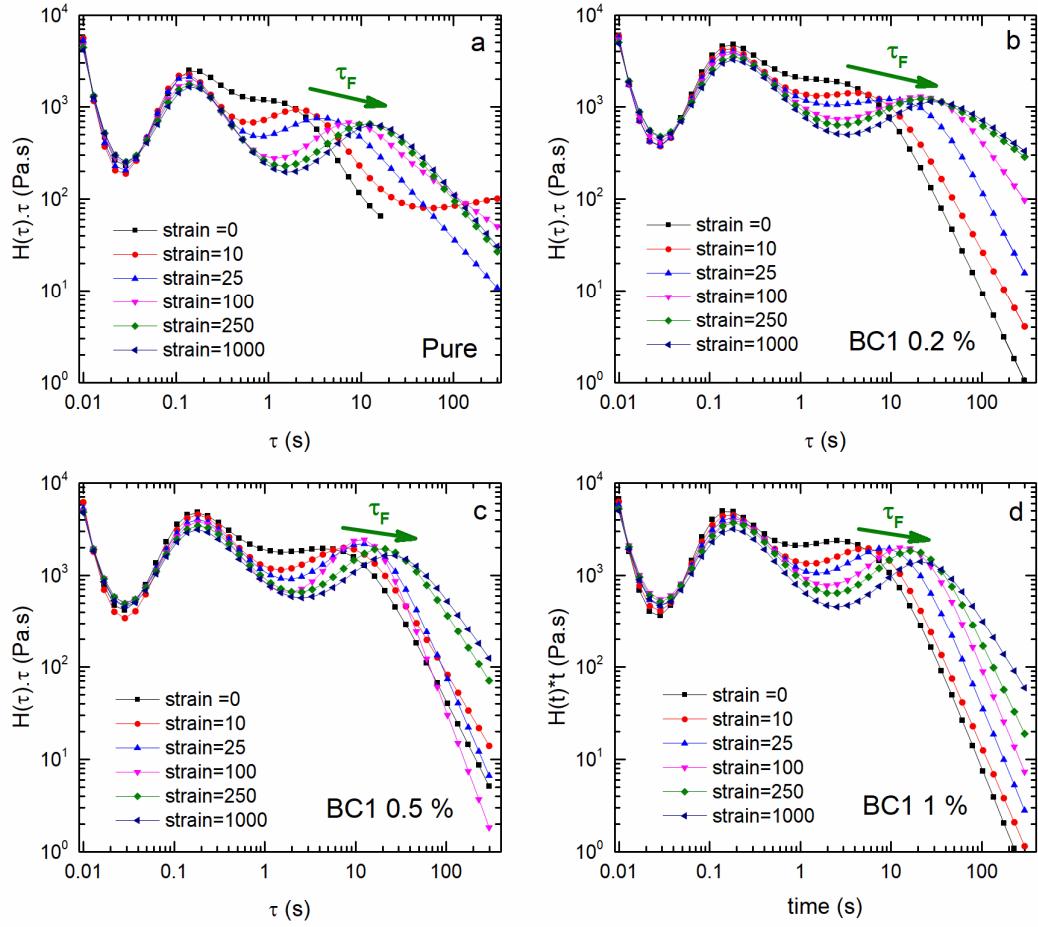
**FIG. 4.9 Relaxation spectra of the blends containing BC1 during coalescence test**

For more clarity on the evolution of Marangoni's relaxation during the test, the values of $\tau_\beta$ were extracted from the relaxation spectra and plotted in FIG. 4.11. Two regimes can be observed: a decrease until strain = 100 and then a minor increase. As $\tau_\beta$ decreases with time, the calculated $R_v$ decreases because Palierne's model predicts that $\tau_\beta$ varies with $R_v$ (see equation (4.7), (4.8) and (4.9)). It is the first time that such results were found: our results differ completely from Van Hemelrijck et al.'s observations [23] who found that $\tau_\beta$ increased during coalescence tests such as predicted in Palierne's model because the larger the droplets, the longer the distance required for the block copolymer to relax back to a uniform concentration. Because of the unusual evolution of $\tau_\beta$, it was preferred to fit Palierne's model [56] on the storage modulus directly for blends with 0.5 and 1 % of BC2 and for strain = 100, 250 and 1000. This way the exact value of $\tau_F$ is not

required. The results show a slight increase of $R_v$ and are reported in FIG. 4.14 along the results extracted from the relaxation spectra.
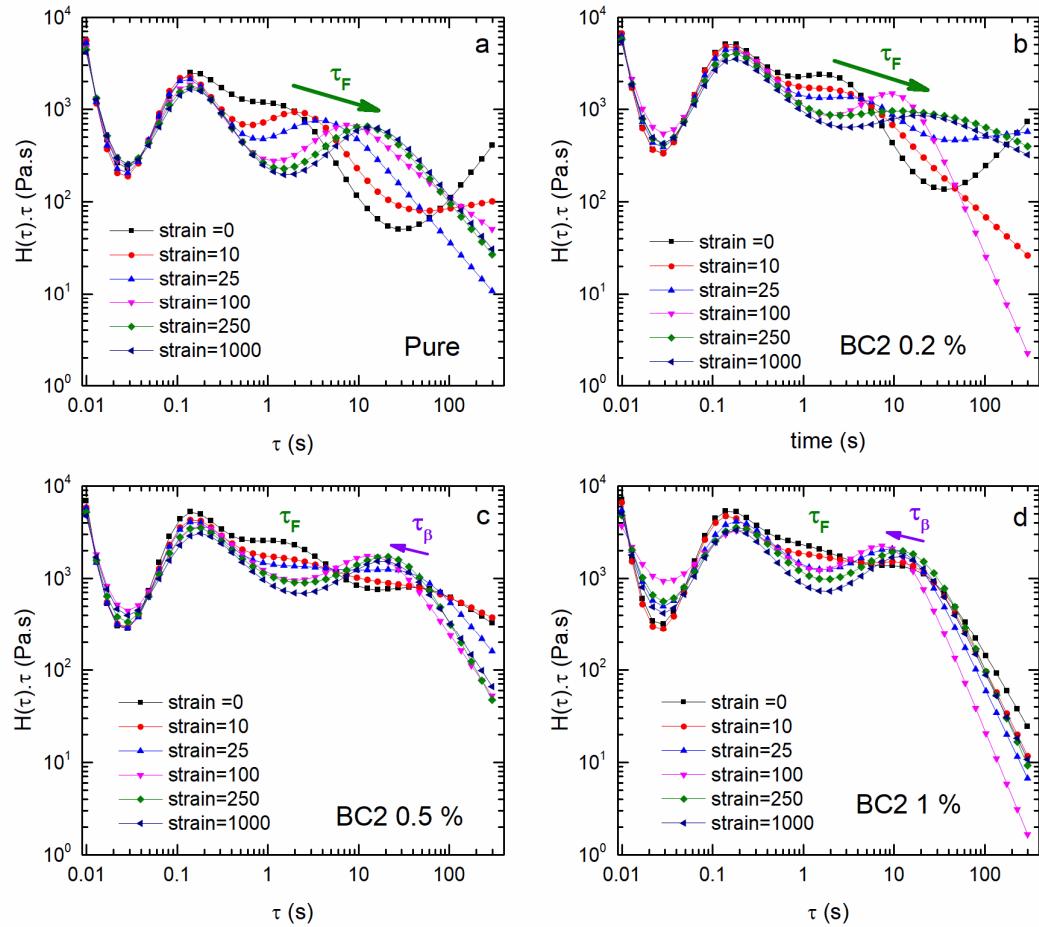


**FIG. 4.10 Relaxation spectra of the blends containing BC2 during coalescence test**

One explanation for $\tau_\beta$'s evolution previously reported in FIG. 4.11 could be that 7 min of mixing was not enough for the block copolymer to migrate entirely to the interface, so the decrease of $\tau_\beta$ would be due to an increase of BC concentration at the interface rather than coalescence. This would explain the evolution of $\tau_\beta$: it would decrease over time when BC are still migrating to the interface, and it would increase when all the BC are at the interface (starting around strain=100). To verify this assumption, the blend with 0.5 % of BC2 was prepared again using a longer mixing time (20 min).
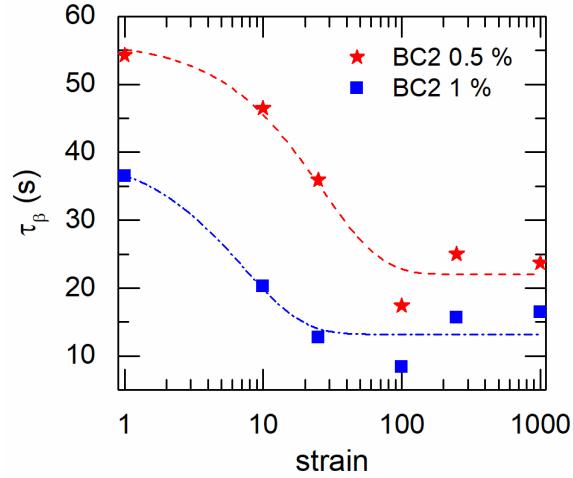
**FIG. 4.11 Evolution of Marangoni's relaxation ($\tau_\beta$) during coalescence tests, dotted lines are here to better visualize the tendencies**

The same experiments were conducted on this blend, named here BC2 0.5%-20 min. FIG. 4.12 shows the evolution of the relaxation spectra of the new blend at strain = 0, and compares it to the previous blends with BC2. In FIG. 4.12b, the droplets relaxation seems slightly shorter for BC2 0.5 %-20 min, which means that the droplets are slightly smaller. It also shows that Marangoni's relaxation is shorter when the blend is mixed 20 min (BC2 0.5 % - 20 min) than 7 min (BC2 0.5 %) and the relaxation peak is sharper. The evolution of $\tau_\beta$ during coalescence experiments is reported in FIG. 4.13. It can be clearly seen that the relaxation times are smaller for BC2 0.5 % - 20 min during the whole experiment. However, the same previously observed evolution was found: a decrease until strain = 100. This evolution is clearly less pronounced than for both BC2 0.5 and 1 %: the magnitude of the decrease in $\tau_\beta$ is smaller than the two previous blends. It seems to us that this indicates that initially there is more block copolymer at the interface and therefore less important migration. These results explain the evolution of morphology observed previously: there is no refinements as compatibilizer is added because there is not enough BC at the interface initially.
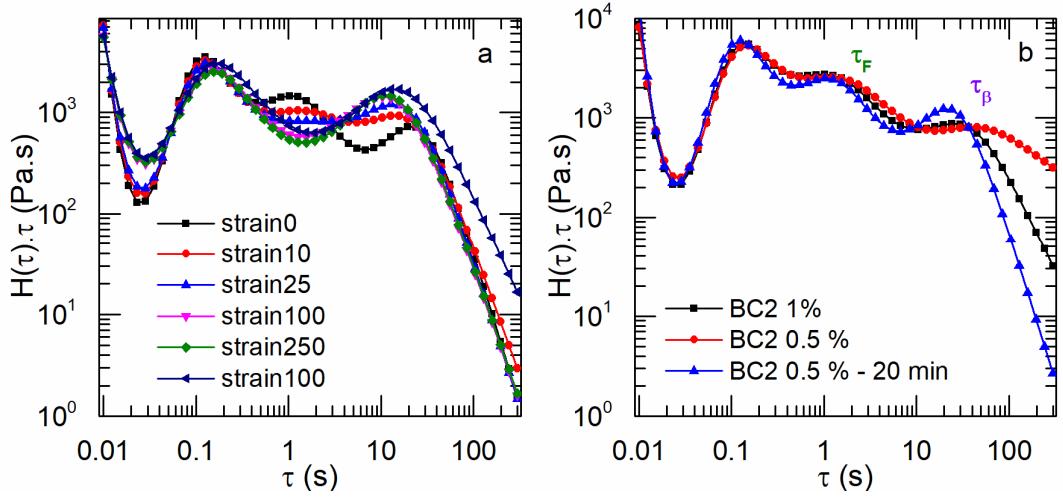
**FIG. 4.12 (a) evolution of BC2 0.5 % - 20 min during coalescence tests, (b) comparison of the relaxation spectra of blends containing 0.5 and 1 % of BC2**
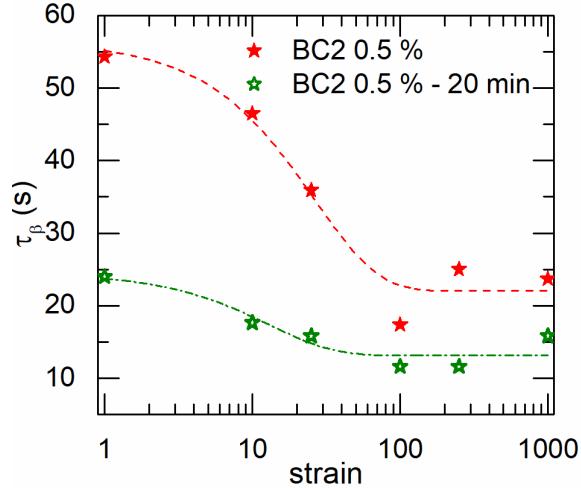


**FIG. 4.13 Evolution of $\tau_\beta$ for blends with 0.5 % of BC2 with 7 min (BC2 0.5 %) and 20 min of mixing (BC2 0.5% - 20 min)**

The evolution of $R_v$ can be seen in FIG. 4.14. 0.2 % of BC does not influence the coalescence process as no difference with the pure blend is observed. At higher BC content, 0.5 and 1 %, a decrease of coalescence is observed. In addition, it seems that BC2 has a stronger influence compared to BC1 and therefore is more efficient. Surprisingly it also seems that 0.5 % is slightly better than 1 %.
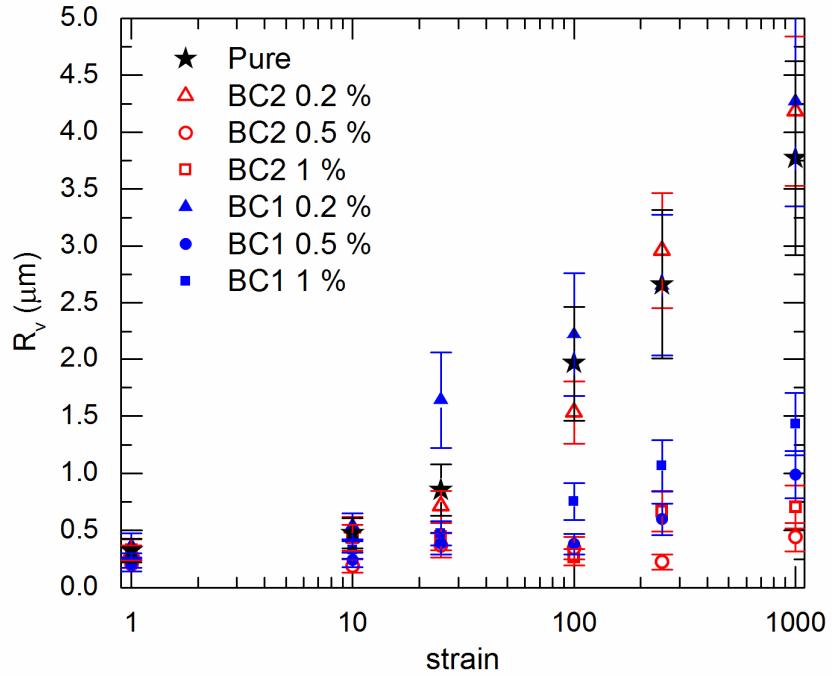
**FIG. 4.14 Evolution of R$_v$ during coalescence tests calculated using the Palierne model.**

All the samples after coalescence were observed with SEM to confirm results obtained by rheology. FIG. 4.15 shows the volume average radii after coalescence found with both rheology and SEM. Relatively good agreements were found for blends with 0.5 and 1 % of BC. However, blends with 0.2 % of BC show a huge disagreement between rheology results and SEM observations. We do not have an explanation for that important difference. However, those results confirm that BC2 is slightly more efficient than BC1.

To understand why BC2 is more efficient, the theoretical surface coverage was calculated using equation (4.11) extracted from Lyu et al.'s work [20]. Here the block copolymer is supposed to be at the interface only. The results reported in TABLE 4.5 show very low values compared to Adedeji et al. [22] who found values around 0.1 to 0.2 chain/nm². This is mainly because we use less block copolymers: they used 5 to 30 % of BC whereas our highest concentration is 1 %. According to those results, BC1 blends have a more important quantity of copolymer chains at the interface. This is not surprising as BC1 has a smaller molar mass so for a same mass there is more BC1 macromolecules than in the case of BC2. By multiplying the surface coverage by the area one chain of block copolymer can cover at the interface, the percentage of covered interface can be recovered (see TABLE 4.5). It can be noted that due to its bigger size, BC2 covers more interface

than BC for a weight concentration of 1 %. However, for 0.5 % of BC, the percentage of covered interface is similar but BC2 is more efficient.
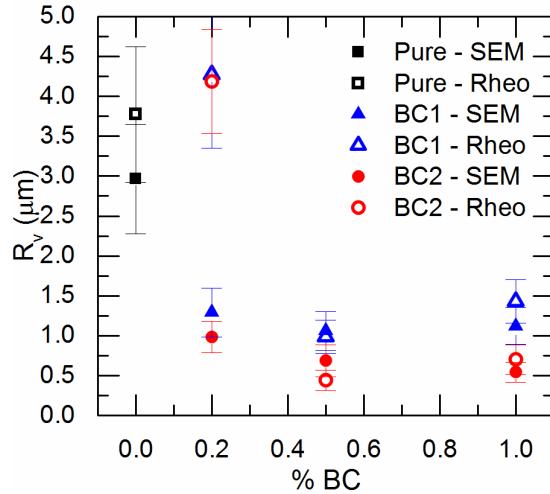


**FIG. 4.15 Comparison of the $R_v$ found by SAOS measurements and by SEM after coalescence tests**

**TABLE 4.5 Surface coverage**

|  | %BC | $\Sigma$ (chain/nm²) | Covered interface (%) |
|---|---|---|---|
|  | 0.2 | 0.0023 | 13 |
| BC1 | 0.5 | 0.0032 | 18 |
|  | 1 | 0.0075 | 43 |
|  | 0.2 | 0.0006 | 11 |
| BC2 | 0.5 | 0.0009 | 19 |
|  | 1 | 0.0030 | 60 |

Using equation (4.12) from Milner et Xi's work defining the minimum surface coverage needed to suppress coalescence and equation (4.11), the minimum percentage of BC needed can be found [104]. The results are 0.05 % for BC1 and 0.16 % for BC2. It shows that both block copolymers should suppress coalescence even with 0.2 %. This would indicate again that BC are not completely at the interface initially. The theory shows again that BC1 should be more efficient than BC2 as a smaller percentage should be required to suppress coalescence. However, both SEM and rheological results agree on the fact that BC2 is more efficient. As Milner and Xi based their equation on Marangoni stresses, it seems logical that BC1 should be more efficient as it can move more easily

around the interface due to its small molecular mass. As such, the efficiency of BC2 may not be due to Marangoni stresses but to a better steric hindrance.

$$\sum = \frac{\Phi_{BC}}{\Phi_{PS}} \frac{R_v \rho_{BC} N_A}{6 M_{wBC}}$$

(4.11)

$$\sum_{min} = \frac{5}{32} \frac{2 R_v \eta_m \dot{\gamma}}{kT}$$

(4.12)

On this matter, Macosko et al. [105] assumed that coalescence inhibition arises from the steric repulsive forces from block copolymers at the surface of two approaching droplets. They estimated the minimum surface coverage for coalescence suppression to be as following:

$$\sum_c = \frac{20}{27\pi <r_0^2>}$$

(4.13)

Where $<r_0^2>$ is the square mean end-to-end distance of the chains of block copolymer.

This minimum surface coverage is reported in TABLE 4.6. Contrary to Milner and Xi's work, the concentration of BC1 added to the blend needs to be 3 times larger than the one of BC2 to be efficient. By comparing $\sum_c$ to $\sum$, the theoretical surface coverage of the droplets of each blend, it can be noticed that both BC1 and BC2 should start to be efficient at 0.5 %. BC2 is indeed efficient at 0.5 % and 1 %, but even if BC1 shows some improvement it is still less efficient than BC2. Macosko et al. [105] had a similar result with a block copolymer with a low molecular mass of 55 000 g/mol, suggesting that BC1 simply has a molecular mass too low to induce any steric hindrance.

TABLE 4.6  $<r_0^2>$ the square mean end-to end distance of the BC chains and $\sum_c$ the minimum surface coverage for coalescence suppression according to the steric hindrance theory

|  | $<r_0^2>$ (nm) | $\sum_c$ (chain/nm²) |
|---|---|---|
| BC1 | 65.8 | 0.0036 |
| BC2 | 227.9 | 0.0010 |

This study leads us to think that steric hindrance and Marangoni stresses are both needed to be able to suppress coalescence as illustrated in FIG. 4.16. Indeed, Marangoni stresses are needed because if the block copolymer is not distributed equally around the droplet, coalescence can happen easily (see FIG. 4.16a). On the contrary, if there are

Marangoni stresses but the block copolymer is not big enough to induce steric hindrance, coalescence can be diminished but not completely suppressed as in the case of BC1 (see FIG. 4.16c). Finally, Marangoni stress combined with a good steric hindrance can suppress coalescence as in the case of BC2 (FIG. 4.16b). As such, an efficient coalescence suppression can be obtained at low concentration of block copolymers as the interface does not need to be saturated provided that the chosen compatibilizer induce enough steric hindrance.
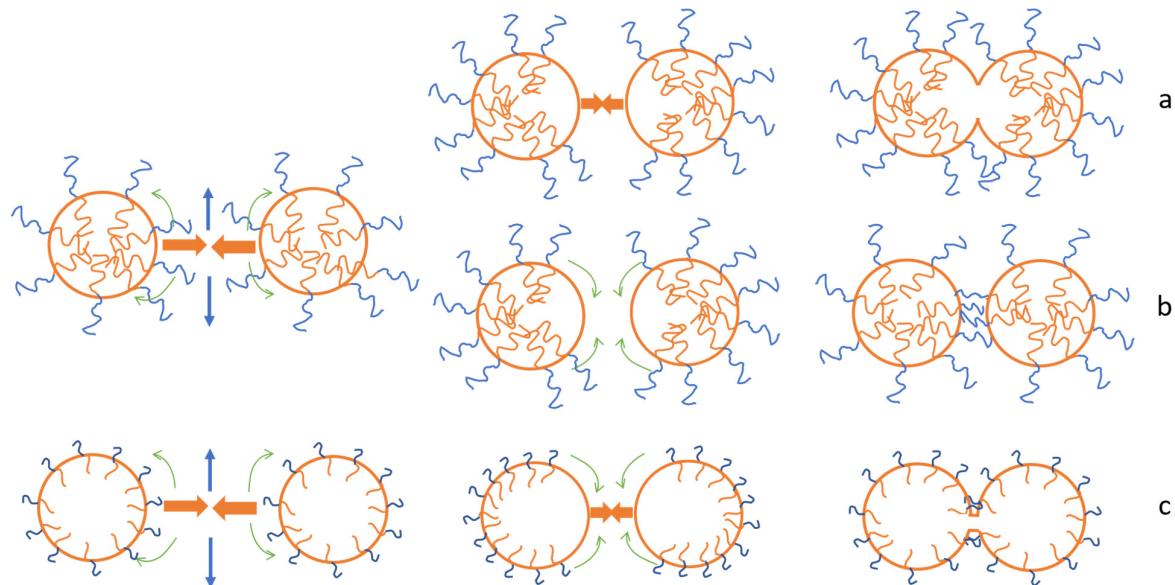


**FIG. 4.16 Illustration of the compatibilization mechanism: (a) Steric hindrance without Marangoni stresses leads to coalescence, (b) Marangoni stresses combined with steric hindrance prevent coalescence, (c) Marangoni stresses without steric hindrance does not suppress coalescence**

D.     **Conclusion**

The aim of this work was to understand the compatibilization effect induced by two block copolymers with different molar masses. The morphology was assessed by SEM and evidenced no refinement of the droplets's size contrary to what is expected. For further analysis, the rheological behavior was characterized.

The interfacial tension between the blend components for each blend was calculated using Palierne's model and relaxation spectra were inferred from SAOS results. A decrease of interfacial tension and the presence of Marangoni stresses were evidenced for blends containing the shorter block copolymer, indicating that at least part of block copolymers are at the interface and act as compatibilizers. To evidence these Marangoni stresses, lowering the temperature was necessary in the case of addition of block copolymer with a

low molar mass. Indeed, Marangoni's relaxation was too short and was not distinguishable from the droplet's shape relaxation. As lowering the temperature allowed to differentiate them, it proves that Marangoni stresses are very influenced by temperature, more than droplets' shape relaxation. In the case of blends with addition of the block copolymer with a higher molar mass, no decrease of interfacial tension was evidenced, however, Marangoni stresses were evidenced by relaxation spectra.

Knowing that Marangoni stresses helps inhibiting coalescence, shear induced coalescence tests were performed. Those tests resulted in the confirmation that the presence of block copolymers induce an inhibition of coalescence for both block copolymers. However, coalescence tests evidenced a decrease in Marangoni's relaxation during coalescence tests. This behavior was attributed to the fact that block copolymers were not fully at the interface after processing. Their migration to the interface during coalescence is an explanation for the decrease in $\tau_\beta$ and would also explain why there is no refinement of the morphology upon addition of copolymers: initially there is not enough block copolymer at the interface. Finally, the block copolymer with the higher molar mass was shown to be more efficient at inhibiting coalescence. However, if only Marangoni stresses were involved in the mechanism, the smaller block copolymer should be more efficient as it can move faster around the interface. These results evidenced the importance of steric hindrance in the compatibilization mechanism. Higher molar mass of the block copolymer results in more efficient repulsion between the droplets and thus decreased coalescence.

To conclude, the compatibilization mechanism in these systems was shown to be a combination of decrease of interfacial tension, Marangoni stresses and steric hindrance.

# CHAPTER 5

## COMPARISON OF MONTMORILLONITE, LAPONITE AND HALLOYSITE AS COMPATIBILIZERS IN PMMA/PS BLENDS

Julie GENOYER[1,2], Nicole R. DEMARQUETTE[2], and Jérémie SOULESTIN [1][*]

[1] *IMT Lille Douai, Department of Polymers and Composites Technology & Mechanical Engineering, Douai, France*
[2] *École de technologie supérieure, Department of Mechanical Engineering, Montreal, QC H3C 1K3, Canada*

**Abstract**

The addition of 3 types of clays (Laponite, Montmorillonite and Halloysite) to poly(methyl methacrylate), polystyrene and their blends was studied. Clays were organo-modified by ionic exchange. Infrared spectroscopy, thermogravimetric analysis and X-ray diffraction (XRD) were used to characterize the modified clays. PMMA and PS nanocomposites were characterized by XRD and small angle oscillatory shear (SAOS) tests. Modified montmorillonite and laponite were shown to have a larger interlayer d-spacing and to disperse better than their non-modified counterpart. It was also shown that organoclays dispersed better in PMMA than in PS. The morphologies of PMMA/PS blend with and without clays were observed by scanning electron microscopy. While calculating the wetting parameter allows to know where the non-modified clays are located, transmission electron microscopy was preferred to observe the localization of modified clays. SAOS experiments as well as shear induced coalescence tests were carried out. A refinement of the dispersed phase of the blend was generally evidenced upon addition of clay. Modified montmorillonite was shown to be located at the interface, modified laponite was dispersed in the whole blend whereas the other clays were dispersed in PMMA. A decrease in interfacial tension was shown upon addition of clay. Using the relaxation spectra inferred from SAOS results, it was possible to evidence Marangoni stresses in the case of clay located at the interface. Coalescence tests showed that modified montmorillonite was the most efficient at inhibiting coalescence thanks to its localization at the interface.

A.     **Introduction**

Currently, most of the commercial plastics products are made of immiscible polymer blends. Blending immiscible polymers is interesting as the final properties strongly depend on the morphology that can be controlled during processing. The control of morphology is usually achieved adding so-called compatibilizers. A classic compatibilizer can be a premade block copolymer or a copolymer created in-situ thanks to an interfacial reaction [6], [24]. Recently, nanoparticles were shown to be efficient compatibilizers as well, however they need to be organo-modified previously by either by chemical grafting [35], [89], [90] or ionic exchange [37], [91]–[93] to be efficient enough. Their modification enables a better dispersion and a better compatibility with the polymers involved. Especially, montmorillonite has already been used as a compatibilizer for polymer blends. Montmorillonite is a layered silicate composed of two siloxane tetrahedral sheets sandwiching an aluminum octahedral sheet. The silicate layers are negatively charged, which is counterbalanced by exchangeable cations such as $Na^+$ and $Ca^{2+}$ placed in the interlayer. When associated with polymers, the interlayer cations are usually exchanged with quaternary ammonium salts which increases the basal spacing [36], [37]. Because of its popularity, several modified montmorillonites are already commercially available.

There exist others type of clays which are less known and less used. One such clay is laponite. It is a synthetic clay shaped in discs of around 30 nm of diameter [38] which has the same chemical structure than montmorillonite. As such, the same organic modification can be done. The only difference is that laponite has a smaller Cation exchange capacity (CEC) than montmorillonite. Laponite CEC can be found in the literature between 47 and 75 meq/100 g [39]–[41] whereas montmorillonite CEC is 92.5 meq/100g. Contrary to montmorillonite, laponite was not extensively used for polymer blend compatibilization, however, laponite and montmorillonite's effect on phase-separation was studied by Yurekli et al. [34] showing that both clays slowed down the kinectic of the phenomenon. As such, laponite may be a suitable compatibilizer.

Halloysites are natural rod nanoparticles of 50 to 5000 nm length and 20 to 200 nm of outer diameter that have started to get some interest in nanocomposite recently [42]. Halloysite's chemistry is similar to the other clays mentioned as it is a silicate bi layer which is rolled into a cylinder, however, they have a very different size and shape. The outside layer of the nanotubes, made of $SiO_2$, is negatively charged whereas the $Al(OH)_3$ inner lumen is positively charged. Thanks to this difference in the external and internal

chemical composition, a selective modification is possible: cations can adsorb around the nanoparticles whereas anions can place itself inside the tube [47]. Halloysite has attracted attention as possible natural nanocontainers for loading and sustained release of chemical agents [47]. However, very few articles deal with the compatibilization of blends using Halloysites. On that matter, Pal et al. [45] studied the influence of adding Halloysites in a blend of polyoxymethylene/PP. They found out that the Halloysite induced a reduction in the average droplet radius. They also were able to show that modified Halloysites had more effect than the pure unmodified ones.

Generally, upon addition of a compatibilizer and irrespective of its chemical nature, one or several of the following phenomena can be observed in the case of a blend with a droplet dispersion type morphology: reduction of the dispersed phase size [13], [32], inhibition of the droplet's coalescence [7], [17]–[20], decrease in interfacial tension [16], [26], [29], and presence of an additional relaxation phenomenon [8], [23], [25], [48], [49], [54], [102], [103]. The additional relaxation phenomenon observed upon addition of compatibilizers is known to correspond to Marangoni stresses induced by a non-homogeneous concentration of the compatibilizers at the interface [8], [21], [54], [103]. Indeed, when two droplets approach, the matrix film in between them is evacuated, dragging some of the compatibilizers with it around the interface. A gradient in compatibilizer concentration on the surface of the droplets results from this, causing Marangoni stresses to appear. Those stresses make the compatibilizer comes back equally distributed on the surface, thereby preventing coalescence and creating the relaxation described previously. This was elegantly proven in the case of block copolymer by Jeon and Macosko [21] who showed gradients in block copolymer concentration during flow by visualizing a fluorescent PS-PMMA copolymer at the surface of a PMMA droplet in a PS matrix.

The morphology, the interfacial tension and the relaxation phenomenon of the blends can be inferred from rheological characterization in the linear viscoelastic regime. Small amplitude oscillatory shear (SAOS) experiments reveal an increase in elasticity at low frequencies, resulting in a shoulder on the storage modulus curve as a function of frequency. The relaxation of the shape of the droplets ($\tau_F$) is responsible for this increase [55]. In the case of compatibilized blends, an additional relaxation time ($\tau_\beta$) may be observed, corresponding to Marangoni stresses [54]. However, in the case of dilute systems those relaxations are very subtle if observed solely on the storage modulus. Obtaining the relaxation spectra by the method of Honerkamp and Weese [50] from SAOS data can help

with identifying the relaxation. Indeed, those spectra can display clearly the polymer chain relaxation, the droplet's shape relaxation, and the relaxation due to Marangoni stresses.

Relaxations can also be studied using existing rheological models which link the rheological behavior of polymer blends to their morphology. One such model is the Palierne model, which is made to predict the rheological behavior of a blend formed by two viscoelastic polymers in the linear viscoelastic regime [52]. The approximations needed include that the polymers should be viscous enough to render bulk forces such as gravitation and inertia negligible, and the emulsion should be monodispersed and diluted.

Several authors used and simplified the model to obtain the simple expression of droplet's shape relaxation time as follow [56]:

$$\tau_F = \frac{\left(\frac{R_v \eta_M}{4\alpha}\right)(19p + 16)(2p + 3 - 2\Phi(p - 1))}{10(p + 1) - 2\Phi(5p + 2)} \tag{5.1}$$

where $R_v$ is the average droplet radius, $\alpha$ the constant interfacial tension, $p$ the viscosity ratio, $\Phi$ the volume fraction of dispersed phase and $\eta_M$ the viscosity of the matrix.

In the following study, the effect of shape and size of the nanoparticles on the compatibilization mechanism was studied. To do so, 3 clays (montmorillonite, laponite and halloysite) were chosen because of their similar chemistry but different sizes and shapes. They were first organo-modified by ionic exchange and then added to the blends. PMMA/PS blends were used as they have a very well-known rheological behavior and allow to identify clearly additional phenomenon induced by the addition of a compatibilizer. The morphology of the blends and the localization of clay were assessed. The linear rheology results combined with Palierne's model were used to find the interfacial tension, relaxations induced by Marangoni stresses and study coalescence phenomena.

### B. **Materials and methods**

#### 1. **Materials**

Poly(methylmethacrylate) (PMMA) PLEXIGLAS, grade 6N from Evonik, and polystyrene (PS) from INEOS Styrenics, grade EMPERA 350N, were used for this study. 3 different clays were used: Cloisite $Na^+$ from Southern Clay Products (named here MMT), Laponite RD (L) from BYK Additives, and Halloysite (H) from Gelest Inc. Clays were organically modified using di(hydrogenated tallow)dimethylammonium chloride, Arquad 2HT-75, purchased from Sigma Aldrich.

The characteristics of the materials are reported in TABLE 5.1 and TABLE 5.2.

**TABLE 5.1 Properties of the polymers**

| Polymer | Density (g/cm$^3$) | Viscosity ($\eta_0$) (Pa.s) at 200 °C |
|---|---|---|
| PMMA | 1.19 | 12,000 |
| PS | 1.04 | 9,800 |

**TABLE 5.2 Properties of clays**

| Clay | Shape | Size | Surface area (m²/g) | Cation exchange capacity (meq/100 g) |
|---|---|---|---|---|
| MMT | platelets | 150-250 nm* | 750 | 92.6 |
| L | discs | 25-30 nm D* | 370 | 55 |
| H | tubular | 0.1-1.5 μm length, 10-200 nm OD** | 64 | 8 |

*from the supplier

**measured using TEM pictures

## 2.     Modification of clays

An amount of ammonium salt equivalent to the CEC was dissolved in water. 5 g of clay (MMT, L or H) were added to the solution and left for 48 hours under stirring at room temperature. The solution was then filtered under vacuum and washed two times with water. The solid obtained was dried at 85 °C for several days until the weight percentage of water was less than or equal to 5% (verified by TGA). Before each use, the clays were re-dried at 85 °C for at least 12 hours.

## 3.     Blending

A concentration of 10 % of dispersed phase was chosen as droplet like morphology happens at low concentration and because the Palierne model, frequently used in this work, can be used only for dilute systems. As such, 90/10 Blends of PMMA/PS to which were added 0 to 1 % of clay were prepared. All the percentages in this paper are weight percentages.

A micro twin screw extruder HAAKE MiniLab II from Thermo Scientific was used to prepare the blends. The extrusion was carried out at 200 °C and 50 rpm. Prior mixing, PMMA was dried at 85 °C for at least 12 hours. The processing took part in two steps: first, the clays were mixed with the minor phase (PS) in direct extrusion mode, and then, PS+clay was mixed with PMMA for 7 minutes in cycle extrusion mode. The aim was to follow the same procedure as a previous study [103]. In the case of the PMMA/PS blend without clay,

the minor phase was processed twice to have the same thermal and shearing history as the others. This blend is called "Pure" in the rest of the paper.

Nanocomposites of PMMA and PS were also extruded. PMMA nanocomposites, to which 0 to 5 % of clays were added, were extruded for 7 min in cycle extrusion mode. PS nanocomposites were first extruded in direct extrusion mode and then for 7 min in cycle mode in order to undergo the same thermomechanical treatment as the dispersed phase in the blend. 0 to 10 % of clay were added to PS.

## 4. Characterizations

Infrared spectra (FTIR) were obtained using a Nicolet 6700 FT-IR spectrometer from Thermo Scientific at room temperature in transmission mode. Spectra were taken from 4000 to 400 cm$^{-1}$. Pellets were made from mixture of powder sample and KBr.

Thermogravimetric analysis (TGA) was investigated using a Diamond TG-DTA from PerkinElmer, from 50 °C to 900 °C at a heating rate of 10 °C /min.

X-ray diffraction patterns were obtained using an X-ray diffractometer (D8 Advance from Bruker) with a Co Kα cathode (λ=0.179 nm). The monochromator was used at a voltage of 40 kV and an intensity of 40 mA. The scattering angles (2θ) ranged from 4.6 to 40° with an interval of 0.02°. The interlayer spacing or d-spacing was estimated from XRD scans by using Bragg's law as follows:

$$d_{001} = \frac{\lambda}{2 sin\theta} \tag{5.2}$$

Samples for rheological and morphological analyzes were molded into discs with a 25 mm diameter and 1 mm thickness at 200 °C under 18 MPa for 10 minutes using a compression molding press.

The morphology was characterized by scanning electron microscopy (SEM) under high vacuum with a Hitachi S-4300SE/N SEM or a JEOL JCM-600 Plus. The samples were previously fractured at ambient temperature and covered with gold. The morphology was quantified with ImageJ software by considering at least 600 particles for each sample.

Samples for transmission electron microscopy were sectioned at room temperature at a thickness of ≈ 70 nm using a LEICA EM UC7 ultramicrotome and transferred to TEM grids with carbon supported film. The images were taken using a FEI TECNAI G² LAB6 at an accelerating voltage of 200 kV.

Linear rheology experiments were performed using two stress-controlled rheometers: MCR 501 and MCR 302 from Anton Paar under dry nitrogen atmosphere. A parallel-plate geometry was used with a gap size of 0.9 mm and plate diameter of 25 mm. Thermal stability of the sample was check by performing time sweep tests. It was shown that PMMA/PS blends were stable under nitrogen atmosphere for at least 2 hours at 200 °C.

The linear viscoelastic region was defined by carrying out strain sweep tests. Finally, dynamic frequency sweep tests were performed for all blends and pure polymers at 200 °C and 220 °C at 4 % of strain. The frequency range was chosen to be from 300 to 0.01 Hz. The zero-shear viscosities of the neat polymers were determined using the curve of complex viscosity (Pa.s) versus frequency (rad/s) obtained from dynamic frequency sweep tests. Rheological experiments were shown to be reproducible within 5 %.

Shear induced coalescence tests were conducted on the MCR 302 at 200 °C under nitrogen atmosphere. The design of those tests is described in a previous paper [106]. A constant shear rate of 0.05 $s^{-1}$ was chosen to ensure coalescence conditions. The coalescence tests were designed as described in Genoyer et al's work [106] with a succession of steady shear (shear induced coalescence) and frequency sweeps to probe the evolution of morphology as first described in Vinckier et al.'s work [10]. Those tests last 10 hours in total. The rheological behavior is then evaluated as a function of strain ((time length of steady shear)*(shear rate)). Neat polymers were also characterized using this procedure, the resulting data were taken into account at each step of the test.

C.     **Results and discussion**

1.     **Clay modification**

**5.1.1.1     Characterization of modified clays**

The infrared spectra of each modified clay were obtained. TABLE 5.1 shows a part of the IR spectra focused on the frequencies corresponding to $CH_2$-stretching mode. Those

peaks are induced by the aliphatic chains of the surfactant. In the surfactant spectra, the bands at 2916 and 2850 cm$^{-1}$ are attributed to CH$_2$ antisymmetric stretching vibration $v_{as}$(CH$_2$) and symmetric stretching vibration $v_s$(CH$_2$) respectively. The frequency $v_{as}$(CH$_2$) shifts to higher frequency in the case of modified clays indicating a change in the environment of the surfactant. Those results are in accordance with other studies [36] and confirm that surfactants are in interaction with clay surface for mMMT, mL and mH.
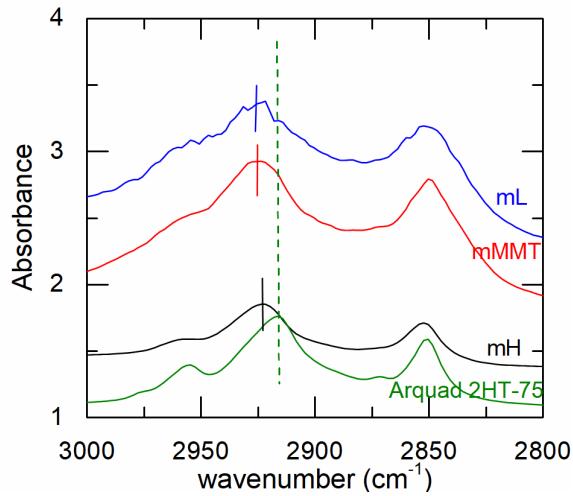


**FIG. 5.1 Asymmetric and symmetric stretching vibrations of CH$_2$ groups in modified clays and surfactant**

FIG. 5.2 shows the XRD patterns of clay before and after modification. After modification with the surfactant, the diffraction peaks shift slightly to smaller diffraction angles. It corresponds to a larger interlayer space which indicates that the surfactant is successfully intercalated in between the sheets of clay. The basal spacings (d$_{(001)}$) of clays calculated using equation (5.2) are reported in TABLE 5.3.

MMT has a basal spacing of 1.19 nm which corresponds well to the data of the supplier (1.17 nm). mMMT has a basal spacing of 1.24 nm which is larger than the one of MMT but smaller than the basal spacing of a commercial Cloisite 20A which is 2.24 nm (see Genoyer et al. [103]). This was expected as mMMT is modified with the same surfactant as Cloisite 20A but at a lower concentration (95 meq/100 g corresponding to 0.73 mg/m² for Cloisite 20A and 0.46 mg/m² for mMMT).

The basal spacing of laponite discs also increases when it is modified. Moreover, non-modified laponite's basal spacing of 1.30 nm corresponds to typical values found in the literature for Laponite RD which can range from 1.25 to 1.43 nm [38], [39], [41], [107].

Because of its tubular shape, Halloysite has a positively charged inner lumen and a negatively charged outer surface. The surfactant is positively charged so it is believed to be located on the outer surface of the nanotubes [47]. The basal spacing of 0.74 nm found for

Halloysite corresponds to values found in the literature for dehydrated halloysite [108], [109]. As the surfactant is not supposed to intercalate, no further XRD experiments were conducted on halloysite or halloysite nanocomposites.
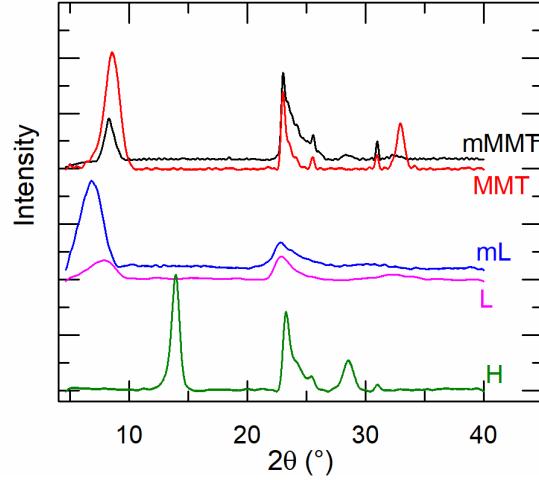


**FIG. 5.2 XRD pattern of clays before and after modification**

**TABLE 5.3 Basal spacing values of clays**

| Clay | $2\theta_1$ (°) | $d_{(001)}$ (nm) |
|------|-----------|------------------|
| MMT  | 8.6       | 1.19 |
| mMMT | 8.26      | 1.24 |
| L    | 7.88      | 1.30 |
| mL   | 6.85      | 1.50 |
| H    | 13.96     | 0.74 |

To determine the quantity of surfactant inserted, thermogravimetric analysis (TGA) was used. FIG. 5.3 shows the mass loss curves of neat and modified clays. There are 3 successive mass losses: the mass loss due to water (between 50 and 200 °C), the mass loss due to the thermal degradation of the surfactant for modified clays (between 200 and 500 °C) and the mass loss associated to the dihydroxylation of clay sheets starting around 400 °C. This is in good agreement with the work of Delbem et al. [37] who worked on the modification of smectite clays. The mass loss due to the surfactant only was calculated by subtracting the mass loss of non-modified clays due to dehydroxylation from the total mass loss of the modified clays. The results are reported in TABLE 5.4.

.
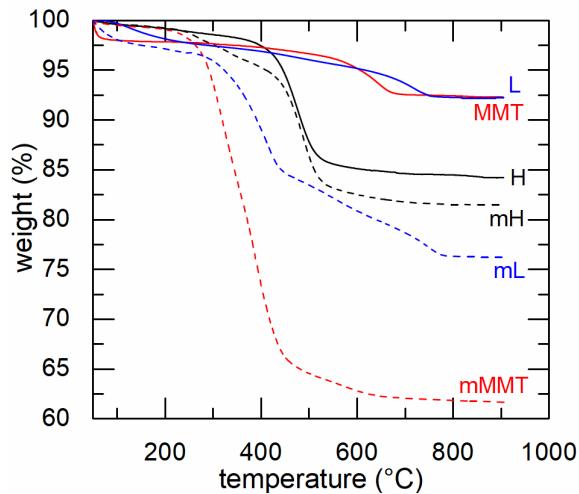
**FIG. 5.3 Mass loss curves of non-modified and modified clays**

A similar surface chemistry for each clay is necessary to observe only the influence of shape and size. As such, the same concentration of clay at the surface is necessary. Usually, when modified by ionic exchange, clays are modified at the concentration corresponding to their cation exchange capacity which is different for each clay (see TABLE 5.2). However, because they have a similar chemical structure, modifying montmorillonite, laponite and halloysite in the CEC quantities would lead to a similar weight concentration of surfactant per surface onto the nanoparticles: in the CEC conditions, the concentration of surfactant would be around 0.71-0.86 mg/m² (see TABLE 5.4). As such, the total amount of surfactant associated with the nanoparticles is greater for clays with larger surface area (halloysite < laponite < montmorillonite). The clays were put in presence of an amount of surfactant corresponding to CEC for ionic exchange. The amount of surfactant successfully intercalated, calculated using TGA, corresponds to a concentration of surfactant between 0.42 and 0.46 mg/m² so around 60 % of the CEC. To have a better percentage, working in excess of surfactant and playing with parameters such as pH and temperature could have made a difference. For this study, it is only necessary that the concentration of clay at the interface is similar for each clay. Those modified clays were then used in the following work and named mMMT, mL and mH.

**TABLE 5.4 Results extracted from TGA**

| Clay | Weight loss dehydroxylation of neat clay (%) | weight loss surfactant (%) | Weight of surfactant per surface obtained if at CEC (mg/m²) | Weight of surfactant per surface obtained experimentally (mg/m²) |
|------|------|------|------|------|
| mMMT | 5.66 | 34.23 | 0.71 | 0.46 |
| mL | 5.18 | 15.28 | 0.86 | 0.42 |
| mH | 14.95 | 2.73 | 0.71 | 0.43 |

### 5.1.1.2 Dispersion state of clays in pure polymers

The main expectation when modifying clays is to achieve a better dispersion state of clay platelet, discs or tubes in a polymer matrix. As such, clays were blended with pure polymers, PMMA and PS, and the resulting nanocomposites were characterized.

XRD was used to find the interlayer spacing of clays in the nanocomposite. The values are reported in TABLE 5.5. First, it is clear that the clays are all better dispersed in PMMA than PS as all the $\Delta d_{(001)}$, representing the difference in basal spacing with neat clays, are all superior to zero whereas in PS some clays have the same basal spacing as neat clays. It can also be noticed that mMMT is the clay with a higher $\Delta d_{(001)}$ so which disperse better in polymers. This can be surprising because laponite should be the more dispersible because of its very small size.

**TABLE 5.5 XRD results of nanocomposites**

| Matrix | Clay | %Clay | $2\theta_1$ (°) | $d_{(001)}$ (nm) | $\Delta d_{(001)}$ (nm) |
|------|------|------|------|------|------|
| PS | MMT | 5 | 8.70 | 1.18 | 0 |
| | mMMT | 5 | 6.25 | 1.64 | 0.40 |
| | L | 10 | 7.13 | 1.43 | 0.13 |
| | mL | 10 | 6.82 | 1.50 | 0 |
| | | 5 | 7.08 | 1.45 | 0 |
| PMMA | MMT | 2 | 6.73 | 1.52 | 0.33 |
| | mMMT | 2 | 5.78 | 1.78 | 0.52 |
| | L | 5 | 6.53 | 1.57 | 0.27 |
| | mL | 5 | 6.65 | 1.54 | 0.04 |

Small amplitude oscillatory shear experiments were also carried out on the nanocomposites at 200 °C. The storage moduli as a function of frequency of PMMA and PS with clays are reported in FIG. 5.4 and FIG. 5.5. The increase in the storage modulus at low frequencies, displayed for PMMA with 5 % of mMMT and PS with 10 % of mMMT

(FIG. 5.4a and FIG. 5.5a), can generally be associated with a better dispersion of the nanoparticles [99], [103]. It is the witness of a percolation of the nanoparticles which arises at low content when the dispersion is good. In the case of Laponite (FIG. 5.4b and FIG. 5.5b) and Halloysite (FIG. 5.4c and FIG. 5.5c), high contents of clay resulted in a slight increase in the whole frequency range but not a terminal behavior similar to mMMT.
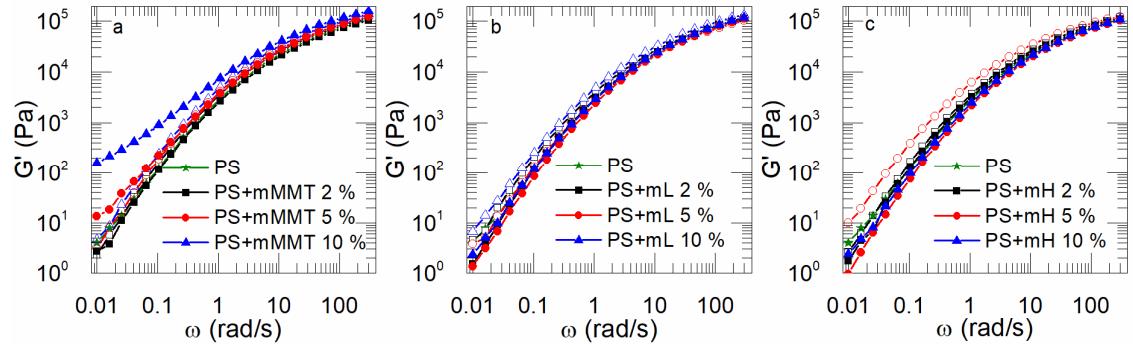


**FIG. 5.4 Storage moduli as a function of frequency at 200 °C of PS with (a) MMT and mMMT, (b) L and mL and (c) H and mH. Filled symbols correspond to the modified clays and open symbols to non-modified clays**
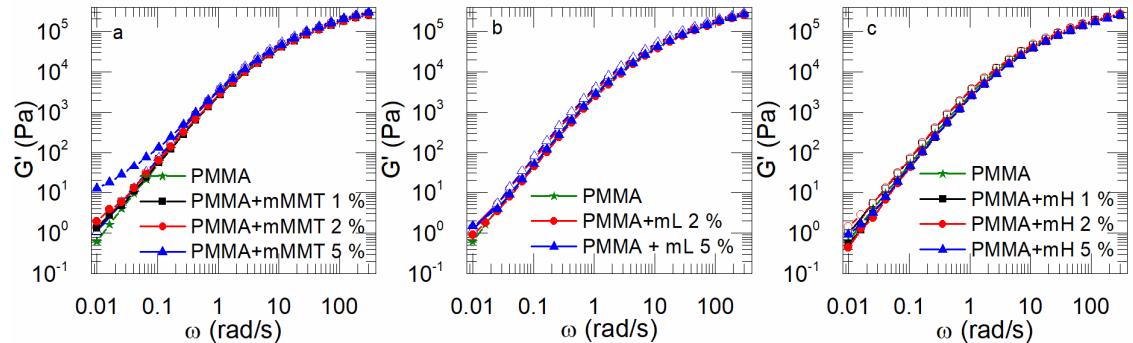


**FIG. 5.5 Storage moduli as a function of frequency at 200 °C of PMMA with (a) MMT and mMMT, (b) L and mL and (c) H and mH. Filled symbols correspond to the modified clays and open symbols to non-modified clays**

To obtain a more quantitative analysis of the dispersion state, the approach proposed by Ren et al.[110] was used. At percolation, the tactoids "touch" each other and induce the terminal behavior observed in rheological measurements. Ren et al. found the following expression to infer the number of nanoclay sheets per tactoids $n_{per}$ from rheology results considering the tactoids of nanoclay sheets as hydrodynamic spheres:

$$n_{per} = \frac{4}{3\Phi_{per}} \frac{\omega_{silper}\rho_{org}}{\omega_{silper}\rho_{org} + (1 - \omega_{silper})\rho_{sil}} \frac{R_h}{h_{sil}} \qquad (5.3)$$

Where $\Phi_{per}$ is 0.3, the volume fraction for percolation of random spheres, $\omega_{silper}$ is the weight fraction at rheological percolation, $\rho_{org}$ and $\rho_{sil}$ are the densities of the polymer and the nanoclay respectively, $R_h$ is the radius of the hydrodynamic spheres and $h_{sil}$ the thickness of the silicate sheets.

According to Vermant et al. [111], the value of the concentration at percolation necessary for the use of equation (5.3), can be determined by simply plotting value of the storage modulus at low frequency as a function of concentration of clay. As above the percolation threshold, G' increase linearly with clay concentration, the concentration at percolation can then be identified as the interception of the linear increase and the y = 0 axis.

In the case of the present study, the value of the storage modulus at 0.01 rad/s versus the concentration of mMMT is plotted in FIG. 5.6. For PS nanocomposite, as G' is supposed to increase linearly after percolation, the concentration at percolation was determined calculating a linear regression from the two last points (0.05 and 0.1 weight fraction). The value found was $\omega_{silper}$ = 0.045. In the case of PMMA composites, the evolution of the storage modulus is very similar to the one of PS nanocomposites, however, there is not enough data to apply the same procedure.
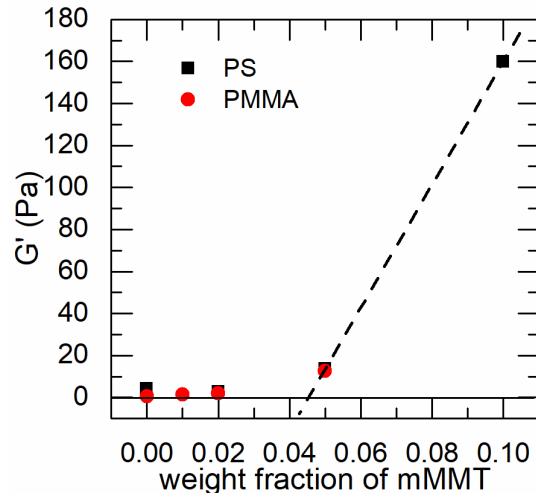


**FIG. 5.6 Storage modulus at low frequency (0.01 rad/s) as a function of weight fraction of mMMT**

Using equation (5.3), the number of nanoclay sheets in the tactoids was determined. The results indicated that mMMT is dispersed in tactoids composed of 7.8 sheets in average in PS. As a comparison, Genoyer et al. [103] showed that Cloisite 20A was dispersed in 1 to 2 sheets on average, showing that mMMT is not as well dispersed as Cloisite 20A in the same type of nanocomposite. This probably originates from the fact that Cloisite 20A is modified with a higher content of surfactant. As MMT does not display a percolation, it is clear that it has a number of sheets per tactoids superior to 8.

Due to its very small size, laponite nanocomposites do not display a terminal behavior in any of the nanocomposites. To understand this behavior, equation (5.3) was

used to calculate the theoretical concentration at percolation for several numbers of layers. The results are reported in TABLE 5.6. Knowing that the percolation threshold happens at more than 10 % of clay in PS, TABLE 5.6 indicates that L or mL discs are dispersed in group of 3 at least. However, it is not possible to infer the exact number of layers in tactoids such as for mMMT.

<p align="center">TABLE 5.6 Concentration at percolation of L or mL calculated for different number of discs $n_{per}$</p>

| $n_{per}$ | 1 | 2 | 3 | 4 |
|---|---|---|---|---|
| $\omega_{Lper}$ | 0.03 | 0.07 | 0.1 | 0.13 |

In the case of halloysite, due to its particular shape $R_h$ and $h_{sil}$ of equation (5.3) corresponds to half the average length of the tube (200 nm) and the average outer diameter (117 nm) respectively which were measured using TEM observation. If it is dispersed in single particles, the percolation should happen at 26 % of clay if dispersed individually. Despite its bigger size, halloysite would induce a terminal behavior at higher content than montmorillonite and laponite. It is because a single particle of halloysite have a smaller aspect ratio $f = \frac{2R_h}{h_{sil}}$ of 3.4 than montmorillonite which have an aspect ratio of 200 when individual. This shows that the rheological terminal behavior of clay nanocomposites is more influenced by the aspect ratio than the size of the droplets.

The non-modified and modified clays were added to a PMMA/PS blend in order to study a possible compatibilization mechanism.

## 2. Influence of clays in PMMA/PS blends

### 5.1.1.3 Morphology

The morphology of each PMMA/PS blend with clay was observed using SEM. The evolution of the droplet size upon addition of clay is represented in FIG. 5.7. There is a refinement of the droplets size of around 35 % when clay is added to the blend whether is it modified or not as well as a decrease in the standard deviation (see FIG. 5.7a). 0.2 % of mL induced a decrease of the radius of 20 %, however, at higher concentration, mL blends morphology size is similar to the one of the pure blend. mL might be too well dispersed and too small to have a significant influence on the morphology.

The refinement of morphology observed is in agreement with the results of Genoyer et al. [103] who showed a refinement of 34 % for 0.8 % of Cloisite 20A in PMMA/PS

blends. In their case, the refinement of morphology was explained by the presence of Cloisite 20 A at the interface which decreased the interfacial tension and stabilize the morphology. In order to understand the mechanism taking place in the refinement of morphology, knowing the localization of nanoparticles is essential.
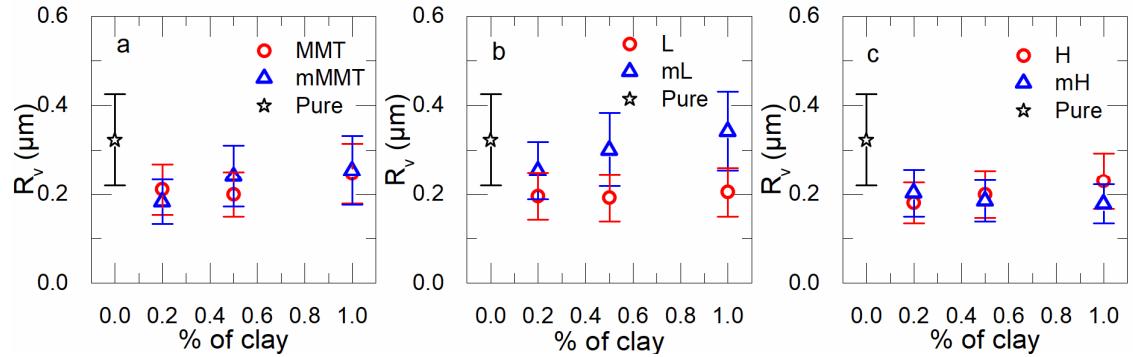


FIG. 5.7 Morphology of the blends with (a) MMT and mMMT, (b) L and mL and (d) H and mH

#### 5.1.1.4 Localization of NP

Inhibition of the droplet's coalescence, decrease in interfacial tension, relaxation phenomenon at the interface are some of the physical phenomena generally reported when nanoparticles are at the interface. Therefore, the localization of nanoparticles is of high interest for the discussion. This location can be predicted by theory as it depends strongly on the surface tension of each component (nanoparticles and two polymers)[26]. The localization at equilibrium can be defined by calculating the wetting parameter (see equation (5.4)) where $\gamma_{AB}$, $\gamma_{S-A}$ and $\gamma_{S-B}$ are the surface tension between polymer A and polymer B, between the solid nanoparticles and polymer A and between the solid nanoparticles and polymer B respectively.

$$\omega_{AB} = \frac{\gamma_{S-B} - \gamma_{S-A}}{\gamma_{AB}} \tag{5.4}$$

The wetting parameter expresses the most favorable position of the nanoparticles to minimize the free interfacial energy of the blend. If $\omega_{AB} > 1$, the particles are preferentially located in polymer A, if $\omega_{AB} < -1$, the particles are located in polymer B and if $-1 < \omega_{AB} < 1$, the particles are likely to locate at the interface between the polymers [27].

Even if most of the surface tension of typical polymer blends such as PMMA/PS is known, accessing experimentally the surface tension relative to solid nanoparticles is very difficult. They are usually calculated using theoretical models such as Owens-Wendt model as follow:

$$\gamma_{ij} = \gamma_i + \gamma_j - 2\sqrt{\gamma_i^d \gamma_j^d} - 2\sqrt{\gamma_i^p \gamma_j^p} \tag{5.5}$$

Where $\gamma_i^d$ and $\gamma_i^p$ corresponds to the dispersive and polar contribution to the surface tension $\gamma_i$. With this equation, the surface tension between two components can be found by knowing only the surface tension of one individual component.

However, the values of interfacial tension need to be measured at the same temperature than the temperature used for processing, in our case at 200 °C. Elias et al. [32] used Guggenheim's equation to calculate the surface tension at any temperature (see equation (5.6)).

$$\gamma(T) = \gamma_0 \left(1 - \frac{T}{T_c}\right) \tag{5.6}$$

Where $\gamma_0$ is the surface tension at 0 K and $T_c$ is the critical temperature.

The values of surface tension of each individual component used for the calculation of the wetting parameter are reported in TABLE 5.7TABLE 5.9 and used to calculate the surface tension between two components of the blends using equation (5.5). The resulting wetting parameter is calculated using equation (5.4) and reported in TABLE 5.8 for each type of blend.

**TABLE 5.7 Surface tension of each components of the blends**

| | Surface tension at 200 °C (mJ/m²) | | | References |
|---|---|---|---|---|
| | $\gamma$ | $\gamma^d$ | $\gamma^p$ | |
| PMMA | 27.4 | 19.6 | 7.7 | Calculated from [26] |
| PS | 27.8 | 21.9 | 3.9 | Calculated from [32] |
| Cloisite 20A | 24.4 | 22.8 | 1.6 | Directly extracted |
| MMT | 43.1 | 29.2 | 13.9 | from [112] |
| L | 45.0 | - | - | Calculated from [113] |
| H | 42.0 | - | - | Calculated from [91] |

**TABLE 5.8 Wetting parameters**

| Type of blend | $\omega_{PMMA/PS}$ |
|---|---|
| Cloisite 20A | 0.02 |
| MMT | 1.34 |

According to the theory, MMT is dispersed in PMMA. As the dispersive and polar components are not available for H and L, it is not possible to calculate the wetting parameter in this case. However, from the values of surface tensions reported in Table VII one can imagine easily that both L and H are also dispersed in PMMA. This can be

explained by the fact that MMT, L and H have a higher polar component compared to PS, as such they will have more affinity and will prefer to be dispersed in PMMA. Concerning modified clays, there is no data in the literature allowing us to do the calculations as they are home-made modified. Moreover, there are very few studies using modified Halloysite or Laponite. In the case of Montmorillonite, the wetting parameter was calculated for a PMMA/PS/Cloisite 20A blends (see TABLE 5.8). According to those results, modifying Montmorillonite with an organic compound modify the surface properties in such a way that modified montmorillonite is theoretically located at the interface. It is probably because modifying clay induce a decrease in the surface tension, especially the polar contribution, of the nanoparticle (see TABLE 5.7). In our case, Montmorillonite is modified by the same surfactant, but with a smaller quantity so an intermediate value of $\omega_{PMMA/PS}$ between the one with MMT and the one with Cloisite 20A is expected. As such, it is believed that mMMT will locate at the interface. However, one must keep in mind that the wetting parameter is valid only if the equilibrium state is reached. Knowing that PMMA and PS have close values of surface tension, the localization of clays might also be due to kinetic factors such as the migration from PS to PMMA or the viscosities.

As the wetting parameters of blends with modified clays could not be accessed, PMMA/PS blends with the highest content of modified clays (1 %) were observed with TEM. Pictures of those blends are displayed in FIG. 5.8. The droplets, darker than the matrix, can easily be identified and the black parts are the clays. FIG. 5.8a clearly confirms that mMMT is located at the interface. In FIG. 5.8c, it is clear that mH is too big to really locate itself at the interface, however, it seems always close to a PS droplet instead of dispersing clearly in PMMA. As such, mH might possibly locate at the interface if its size would allow it. In the case of mL, clays were difficult to visualize because of their very small size, it is believed the very small black points (not observed for other samples) of 20-30 nm of diameter are laponite discs (evidenced by arrows in FIG. 5.8b). Globally, modified Laponite seems to be dispersed in the whole blend with no preference.
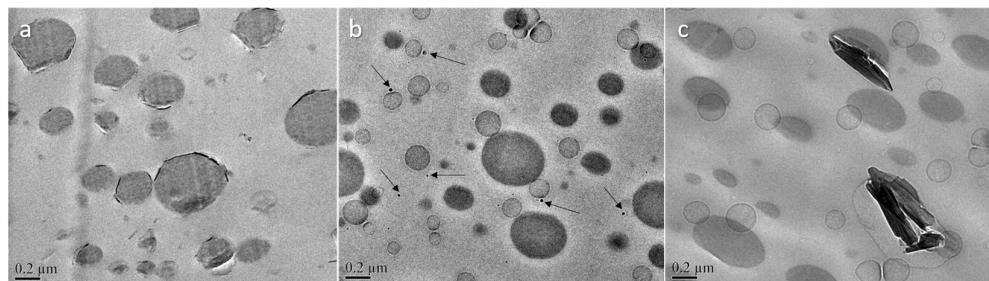


**FIG. 5.8 TEM pictures of PMMA/PS blends with 1 % of (a) mMMT, (b) mL and (c) mH**

### 5.1.1.5  Marangoni stresses & interfacial tension

SAOS experiments were conducted on the blends at 200 and 220 °C. The neat results are not displayed as the concentration in dispersed phase (10 %) and clay (0 to 1 %) are very low and no differences between the samples could be clearly identified on the storage moduli. The relaxation spectra were inferred to identify clearly the relaxation phenomena. At 200 °C, two relaxations were observed: the relaxation of PMMA and PS chains and the relaxation of the droplet after deformation ($\tau_F$). It is known from previous studies that these relaxation spectra can display a third relaxation induced by Marangoni stresses when the compatibilizers are at the interface [49], [53], [103] and it can be easily evidenced by increasing the temperature [103].
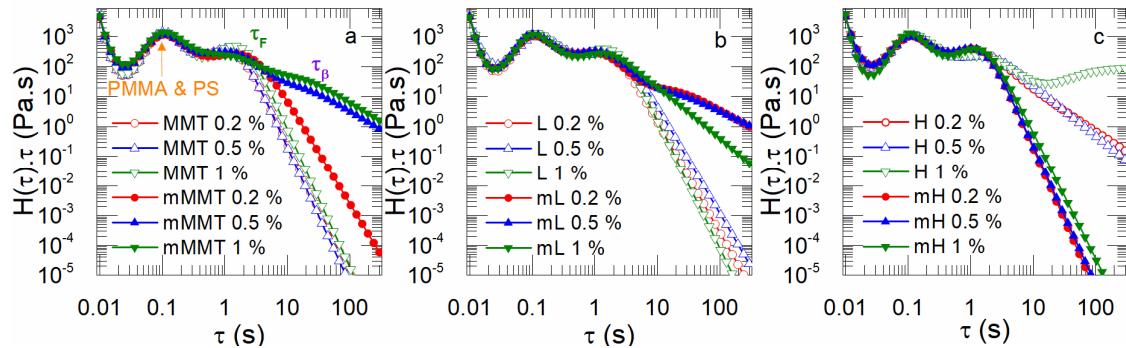


**FIG. 5.9 Relaxation spectra of blends at 220 °C with different concentration of (a) MMT and mMMT, (b) L and mL and (c) H and mH**

The relaxation spectra at 220 °C are displayed in FIG. 5.9FIG. 5.10. As expected, a third relaxation is evidenced for blends containing 0.5 and 1 % of mMMT (see FIG. 5.9a). 0.2 % of mMMT does not display a third relaxation time probably because the concentration of clay might be too low. mL also displays a Marangoni's relaxation (FIG. 5.9b). Even if TEM observations (FIG. 5.8b) showed that mL was dispersed, at least partly, in PMMA, the presence of Marangoni stresses indicates that enough quantity is located at the interface to induce this effect. No Marangoni's relaxation appears for blends with mH, possibly because they are not located at all at the interface (see FIG. 5.8b). In other words, by simply conducting a classic SAOS experiments and calculating the relaxation spectra, it is possible to determine if the nanoparticles are located at the interface or not. However, it does not exclude the presence of clay elsewhere in the blend as observed for mL. The blends with non-modified clays do not display a Marangoni's relaxation. It is believed that non-modified clays do not disperse well so they are probably in aggregates and in PMMA. As a result, no Marangoni's relaxation is possible.

Using Palierne's model (equation (4.5)), the value of the droplet shape relaxation time extracted from the relaxation spectra at 200 °C and $R_v$, the interfacial tension between components was calculated. The values are reported in TABLE 5.9. Usually, the literature reports values between 1 to 3 mN/m for PMMA/PS blends [15], [49], [95], [103]. In our case, the pure blend has a value of 4.29 mN/m, which is slightly higher than usual but still of the same order of magnitude. The addition of clay induces a lower interfacial tension than the pure blend. The interfacial tension decreases slightly upon addition of clay such as in a previous study with Cloisite 20A [103]. The modification seemed to have induced a smaller interfacial tension in the case of mMMT and mH. In the case of Laponite, the contrary is observed. This is in good agreement with the morphological results which showed that mL did not induce a decrease in the droplet size but L did. As a matter of fact, as the interfacial tension is calculated using the $R_v$ values discussed previously, it is directly linked to the evolution of morphology.

**TABLE 5.9 Interfacial tensions between the component of the blends determined using the Palierne model**

|  | Pure | MMT | | | L | | | H | | |
|---|---|---|---|---|---|---|---|---|---|---|
|  |  | 0.2 | 0.5 | 1 | 0.2 | 0.5 | 1 | 0.2 | 0.5 | 1 |
| α (mN/m) modified clay | 4.3 ±1.4 | 1.0 ±0.3 | 1.1 ±0.3 | 0.9 ±0.3 | 1.9 ±0.5 | 1.5 ±0.4 | 1.1 ±0.3 | 1.1 ±0.3 | 1.0 ±0.3 | 0.9 ±0.2 |
| α (mN/m) non-modified clay | | 1.6 ±0.4 | 1.2 ±0.3 | 1.2 ±0.3 | 1.0 ±0.3 | 1.3 ±0.4 | 1.0 ±0.3 | 1.2 ±0.3 | 1.2 ±0.3 | 1.4 ±0.4 |

### 5.1.1.6 Coalescence tests

Coalescence tests were carried out following the procedure described in a previous work [106]. The relaxation spectra from the SAOS were calculated for each blend at different strain during coalescence. FIG. 5.10 shows the relaxation spectra of mMMT blends. As expected, $\tau_F$ increases with strain, indicating that the size of the droplets increases so coalescence is happening. The same observations were made for all the blends. Also, mMMT 1% does not show clearly this increase in the droplets time relaxation, indicating that coalescence is stopped or at least decreased.

The volume average radius can be calculated using the relaxation time $\tau_F$ extracted from the relaxation spectra and Palierne's model (equation (4.5)). The results are reported in FIG. 5.11 for blends with non-modified clays and in

FIG. 5.12 for blends with modified clays. Non-modified clays induce a decrease in coalescence between 50 and 70 %. Coalescence is reduced in the presence of non-modified

clays but is not completely suppressed. Among the non-modified clays, L is the most efficient, it is probably due to the fact that L disperse better.
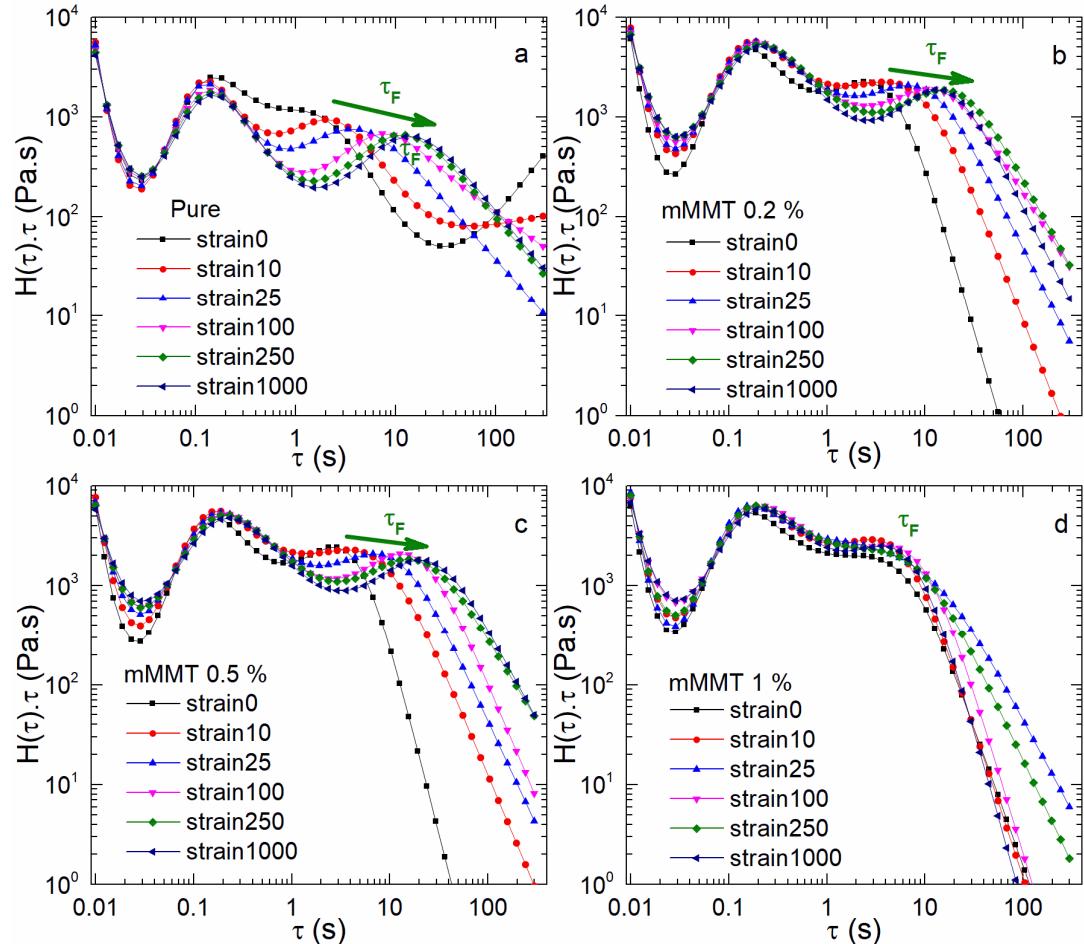


FIG. 5.10 Relaxation spectra of the blends containing (a) 0 %, (b) 0.2 %, (c) 0.5 % and (d) 1 % of mMMT during coalescence test
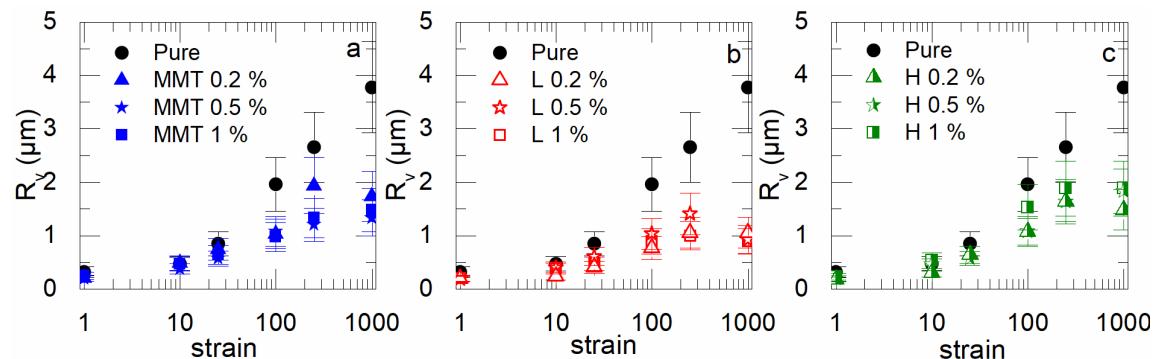


FIG. 5.11 Evolution of Rv during coalescence tests calculated using the Palierne model for blends containing (a) MMT, (b) L, (c) H

FIG. 5.12 shows that the modification of clay gave different results in terms of coalescence inhibition. mMMT is clearly the most efficient of the three types of clay as 1

% of mMMT completely suppress coalescence. mL and mH both decrease coalescence by around 70 % with 1 % of clay. However, the efficiency of mL increases with the concentration whereas mH blends have a similar effect regardless clay concentration.
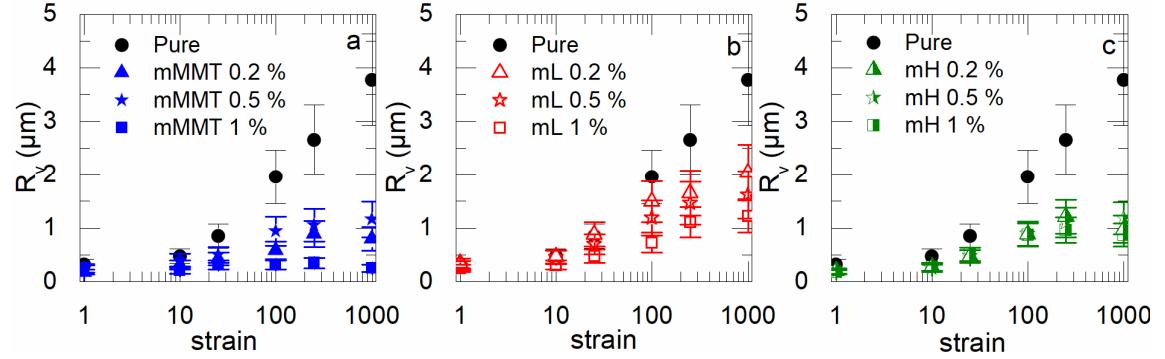


**FIG. 5.12 Evolution of Rv during coalescence tests calculated using the Palierne model for blends containing (a) mMMT, (b) mL, (c) mH**

To better understand the results in the case of clays located at the interface, the surface coverage of mMMT and mL nanoparticles was calculated using the following equation that was calculated by dividing the interfacial area with the number of nanoparticles:

$$\sum = \frac{\Phi_C}{\Phi_{PS}} \frac{R_v}{3\,V_{1C}}$$

(5.7)

Where $\Phi_c$ and $\Phi_{PS}$ are the volume fraction of clay and dispersed phase respectively, $R_v$ is the volume average radius and $V_{1C}$ is the volume of one clay nanoparticle.

The results are reported in TABLE 5.10. This calculation supposes that all clay is located at the interface. mMMT has a lower interfacial coverage because its size is larger than mL. The minimum surface coverage needed to suppress coalescence using equation (4.12) which takes into account an inhibition caused by Marangoni stresses was calculated [20]. mMMT is supposed to suppress coalescence starting at 6.06 % which is a value incredibly high. In the case of mL, it is supposed to suppress coalescence at 0.21 %. By considering only Marangoni stresses, mL should be significantly more efficient than mMMT and should suppress coalescence at 0.5 and 1 % which is not the case. This is mainly because the mL nanoparticles are only located partially interface (see FIG. 5.8b). Also, mMMT suppress coalescence at 1 %, so this theory is clearly not appropriate for this study. Coalescence inhibition is happening if clay is located at the interface, it is believed to be due partly to Marangoni stresses which allow to have an adequate distribution of clays

around the droplets, but mostly due to the barrier effect induced by nanoparticles such as in Pickering emulsions.

$$\sum_{min} = \frac{5}{32}\frac{2R_v\eta_m\dot{\gamma}}{kT}$$

(5.8)

**TABLE 5.10 Surface coverage calculated for mMMT and mL blends in the case of exfoliated clay (1 sheet) and intercalated clays (in tactoids of 8 sheets)**

| Clay | Clay concentration | surface coverage if exfoliated (particles/nm²) | surface coverage if tactoids (tactoids/nm²) |
|---|---|---|---|
| mMMT | 0.2 | 0.000016 | 0.000001 |
| | 0.5 | 0.000054 | 0.000003 |
| | 1 | 0.000114 | 0.000007 |
| mL | 0.2 | 0.000747 | - |
| | 0.5 | 0.002215 | - |
| | 1 | 0.005055 | - |

FIG. 5.13 shows $R_v$ as a function of strain during coalescence tests for blends containing 1 % of clay (non-modified and modified). It clearly shows that H is the least efficient clay to inhibit coalescence. MMT, mL and L have intermediate efficiencies. It can be noted that mL and L have comparable results, so the modification did not really have a significant role for Laponite. In comparison, mH is significantly more efficient than H. To understand why, the sample after coalescence was observed with TEM. FIG. 5.14 shows that during coalescence, modified halloysite particles placed itself at the interface. In doing so modified halloysites particles helped to prevent coalescence. According to FIG. 5.12, this seems to be the case starting at strain = 100 and $R_v$ = 1 µm.
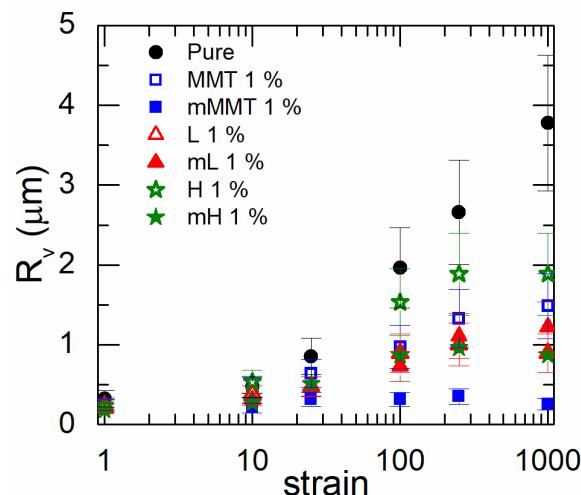


**FIG. 5.13 Evolution of Rv during coalescence tests for blends with 1 % of clay**
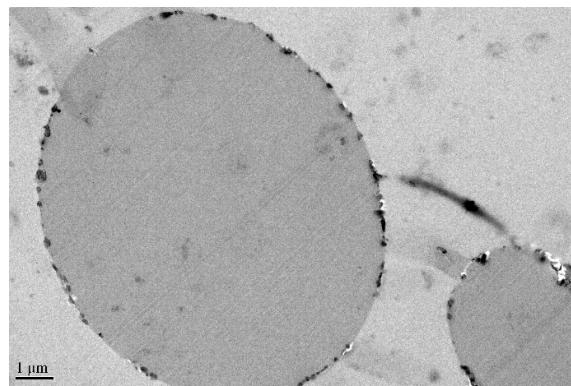
**FIG. 5.14 TEM of PMMA/PS blend with 1 % of mH after coalescence experiment**

### 5.1.1.7    Comparison with block copolymers

In a previous study [106], the same coalescence experiments were conducted on PMMA/PS blends with two block copolymers as compatibilizers. BC1 and BC2 have a molar mass of 30 000 g/mol and 104 000 g/mol respectively. It was shown that BC2 with a higher molar mass leads to better coalescence inhibition due to a combination of Marangoni stresses and steric hindrance. The results of their coalescence tests are compared to the results with modified clays in FIG. 5.15. Two tendencies arise from those results: mMMT and BC2 completely suppress coalescence whereas mL, mH and BC1 only decrease coalescence of 70 %. It can also be noticed mMMT needs to cover less interface to be as efficient as BC2 (see TABLE 5.11). This may be due to the very different chemistry and structure of the compatibilizers: BC2 inhibits coalescence using steric hindrance whereas mMMT induce a barrier effect. The barrier effect is then more efficient.
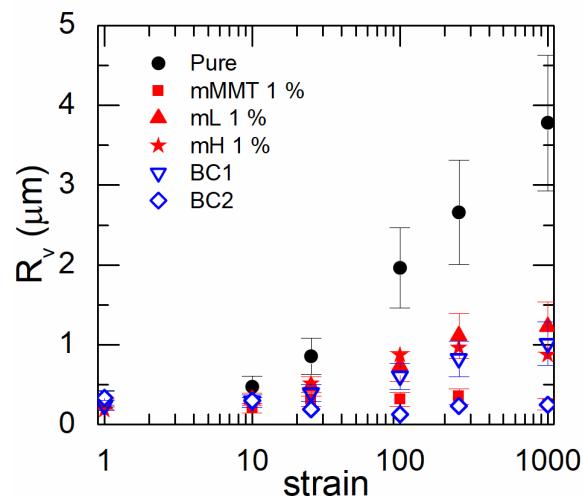


**FIG. 5.15 Comparison of results with modified clay and a similar study made with block copolymers as compatibilizers**

**TABLE 5.11 Comparison of the surface coverage of mMMT and BC2**

| | %Compatibilizer | $\sum$ (chain/nm²) | Covered interface (%) |
|---|---|---|---|
| | 0.2 | 0.00001 | 4 |
| mMMT | 0.5 | 0.00003 | 13 |
| | 1 | 0.00007 | 27 |
| | 0.2 | 0.00060 | 11 |
| BC2 | 0.5 | 0.00090 | 19 |
| | 1 | 0.00300 | 60 |

D.     **Conclusion**

The results reported in this paper indicated that it is possible to disperse montmorillonite (MMT) and laponite (L) clays within PS and PMMA polymers provided they are organically modified. However, no such conclusion could be done on the dispersion state of halloysite (H) and modified halloysite (mH) with our results.

The decrease of the dispersed size in the case of addition of modified montmorillonite (mMMT) originated most likely from the location of the clay at the interface between both polymers. mMMT was the most efficient clay in terms of coalescence inhibition, most likely thanks to the presence of Marangoni stresses and a certain Pickering effect.

In the case of H, mH, and MMT which were located in PMMA, the reduction of the size of the droplets might originate from the variation of viscosity of the matrix due to the presence of nanoparticles. This variation of the viscosity of the matrix is believed to be also the cause of a decrease in coalescence. The efficiency of mH at inhibiting coalescence, better than both MMT and H, originates from the fact that mH particles migrate to the interface during coalescence thus induce an effect similar to mMMT when enough mH have migrated.

L and mL were dispersed within the whole blend and we believe that their small sizes are the cause for a limited efficiency at inhibiting coalescence. The slight improvement in coalescence inhibition using mL is most likely due to a more important quantity of nanoparticles located at the interface as suggested by the presence of Marangoni

stresses. However, L induced a decrease in the droplet size whereas mL did not. No explanation could be found for that.

Finally, compared to block copolymers, mMMT is as efficient as a block copolymer with a high molecular mass (104 kg/mol) and mL, L and mH as a block copolymer with a lower molar mass (30 kg/mol). mMMT is as effective as BC2 even if it covers less interface, suggesting that a barrier effect is more efficient than steric hindrance. In regard to the very high price of block copolymers, replacing block copolymers by a clay such as mMMT, mL, L or mH is very cost effective.

# CHAPTER 6

## INFLUENCE OF ADDITION OF CLAY ON THE BEHAVIOR OF PMMA AND PS NANOCOMPOSITES AND ON THE MORPHOLOGY OF PMMA/PS BLENDS UNDER ELONGATIONAL FLOW

### A.    **Introduction**

Even if linear shear rheology is very useful to characterize polymer blends and study the compatibilization mechanisms by inferring the interfacial tension, the droplets' size, observing the relaxations after small deformations and study shear induced coalescence, it cannot describe what would happen at high deformations and under elongational flow. Furthermore, extensional flow is an important part of several processes such as, but not limited to, extrusion, blow molding and fiber spinning. The extensional properties of polymer melts have, therefore, been of great interest these past 40 years. Moreover, some polymers have shown a strain hardening behavior under elongational flow, a behavior which aroused the interest of many researchers [67]–[69]. Long-chain branching and broadness of molecular weight distribution are two main factors that are known to enhance strain hardening of polymers. Organoclays were also shown to enhance strain-hardening behavior of polymers too if well dispersed [72]–[74].

Studies reporting the behavior of polymer blends compatibilized or not, under elongational flow are still very rare in the literature. The pioneering works of Taylor [2], [3] can, however, help to understand the evolution of dispersed droplet blend morphology under elongational flows. Taylor pointed out the major influence of the capillary number on the deformation of drops. The capillary number Ca estimates the ratio of the viscous stress of the matrix to the interfacial stress. For a capillary number under a critical value (Ca < $Ca_c$), the interfacial stress dominates, and the the drop remains in a nearly spherical shape under flow, promoting thus coalescence phenomena. For a capillary number above the critical value (Ca > $Ca_c$), viscous stresses dominate, and the drop deforms affinely with the macroscopic strain and breakup is promoted. Grace [5] provided data about this phenomenon by experimentally plotting $Ca_c$ as a function of p, the viscosity ratio of the dispersed phase and the matrix, for both simple shear and extensional flow. In irrotational shear, such as extensional flow, the value of $Ca_c$ is very low and not significantly dependent

on the viscosity ratio implying that, in most cases, elongational flow is likely to induce breakup. After the work of Grace, very few experimental studies have been carried out to study the evolution of blend morphology when subjected to elongational flow. Delaby and al. [75], [76] showed that for large values of capillary number, the drops of the dispersed phase deform less than the sample if the viscosity of the dispersed phase is lower than the one of the matrix. Heindl et al. [77] studied the evolution of the extensional viscosity of PS/PE blends. They found that extensional viscosity is greatly influenced by the rheological properties of the matrix PS and that temperature plays a key role in the morphology developments.

If the evolution of morphology under elongational flow is interesting, it is also important to understand how it evolves after cessation of flow. On that matter, Gramespacher and Meissner [78] studied the elongational flow behavior as well as the recovery behavior of PMMA/PS blends. They showed that the elongational viscosity did not display notable differences between blends, but the recoverable elongational strains increased with the PS concentration. Mechbal and Bousmina [81] also studied the behavior after elongation and the following relaxation of PMMA/PS blends. They showed that the relaxation of the blend is slower than that of the pure components even with a small concentration of dispersed phase (5%). They compared experimental data with the model of Yu et al. [82] and found that the model described fairly the experimental results. Handge and Potschke [79] also studied elongational flow followed by a recovery behavior. They showed that the samples recover in two steps: first, the molecular recovery of each polymer dominates, then the interfacial tension is responsible for the recovery at long times. Stary et al. [83], [84] also worked on the relaxation and recovery of the samples after elongation. They showed that in a PS/LLDPE blend, elongation followed by a free recovery experiment can cause the fibrils to breakup due to Rayleigh disturbance or necking. Also, the lower the temperature, the finer the morphology obtained after recovery. They also showed that the relaxation experiments, where the sample length is kept constant after cessation of flow, leads to substantially higher frequency of droplet breakup resulting in a finer morphology than in the case of free recovery.

As said previously, adding what is called a compatibilizer is a way to control the morphology [6], [24]. Block copolymers or organo-modified nanoparticles can be used for this purpose. Among the few studies that have been reported in the literature on the effect of elongational flow on the evolution of morphology, very few evaluated the effect of

addition of compatibilizer. Stary et al. [85] showed that the presence of compatibilizer at the interface suppressed droplet breakup and promoted the shape recovery of the droplets. They explained it by the presence of Marangoni stresses at the interface. Mechbal and Bousmina [86] also explained their results by the presence of Marangoni stresses in PMMA/PS blends. In both cases, the blends were compatibilized by a premade block copolymer. No study concerning the behavior of polymer blends compatibilized by nanoparticles under elongation flow have been reported up to our knowledge.

In this work, the rheological behavior of PMMA and PS nanocomposites was studied under uniaxial elongation flow and compared to linear shear rheological results. In a second part, the deformation of the droplets under elongational flow as well as the following relaxation of PMMA/PS blends with and without clay was studied.

### B.    **Materials and methods**

PMMA, PS, montmorillonite (MMT), laponite (L), halloysite (H) and their modified counterpart mMMT, mL, mH respectively were the same as in CHAPTER 5. The characteristics of the materials are reminded in TABLE 6.1 and TABLE 6.2. The modification of the clays was explained in CHAPTER 5.

**TABLE 6.1 Properties of the polymers**

| Polymer | Grade | Melt volume rate (cm³/10 min) | Density (g/cm³) | Viscosity ($\eta_0$) (Pa.s) at 200 °C | Viscosity ($\eta_0$) (Pa.s) at 170 °C |
|---------|-------|-------------------------------|-----------------|----------------------------------------|----------------------------------------|
| PMMA | PLEXIGLASS 6N (Evonik) | 12 (230 °C / 3.8 kg) | 1.19 | 12,000 | 323,000 |
| PS | EMPERA 350N (INEOS Styrenics) | 1.5 (200 °C / 5 g) | 1.04 | 9,800 | 429,000 |

**TABLE 6.2 Properties of clays**

| Clay | Shape | Size | Surface area (m²/g) | Concentration of surfactant (mg/m²) |
|------|-------|------|---------------------|--------------------------------------|
| MMT mMMT | platelets | 150-250 nm | 750 | 0 0.46 |
| L mL | discs | 25-30 nm D | 370 | 0 0.42 |
| H mH | tubular | 1-15 μm L, 10-150 nm D | 64 | 0 0.43 |

All blends are in 90/10 weight concentrations of PMMA/PS. Concentrations of clay ranging from 0 to 1 wt% were added to the blends. All percentages are in weight percentages.

The blends were mixed using the same equipment and procedure as in CHAPTER 4 and CHAPTER 5.

Samples were molded at 200 °C under 18 MPa for 10 minutes using a compression molding press. Discs with a 25 mm diameter and 1 mm thickness were used for shear rheology. Rectangles of 20 mm long, 6 mm large and 0.7 mm of thickness were compression molded for elongational tests.

Shear rheology was performed using two stress-controlled rheometers: MCR 501 and MCR 302 from Anton Paar under nitrogen atmosphere exactly as described in CHAPTER 4 and CHAPTER 5.

Tests under elongation flow, specific to this chapter, were conducted on a MARS III rheometer from ThermoScientific using the Sentmanat Extensional Rheometer [66] device at 170 °C. This geometry consists of two drums rotating in opposite directions. Rectangular samples are fixed onto each drum and are stretched thanks to the roll motion.

During a uniaxial elongational test, a sample is stretched at a constant strain rate $\dot{\varepsilon}_0$, and the tensile force F is measured as a function of time. The magnitude of stretching is characterized by the Hencky strain $\varepsilon_0^H$. The relation between the constant strain rate and the Hencky strain is as follow:

$$\dot{\varepsilon}_0 = \frac{\partial \varepsilon_0^H}{\partial t} \qquad \text{(6.1)}$$

Usually, the tensile stress growth coefficient is studied and is defined as

$$\eta_E^+(t) = \frac{\sigma^+(t)}{\dot{\varepsilon}_0} \qquad \text{(6.2)}$$

After elongation or during relaxation, the morphology of the samples was observed using scanning electron microscopy (SEM) under high vacuum with a JEOL JCM-600 Plus. At the desired time during the experiment, the oven of the rheometer was opened, and the samples were cooled down using a compressed air jet. The time to cool down the sample

below $T_g$ was estimated experimentally to be less than 30 s. This will not influence the results as it is very short compared to the droplets relaxation (around 600 s) and because the same procedure was repeated for each sample. The samples were then cut parallel to the direction of the flow as indicated by a double arrow in FIG. 6.1, in order to visualize the deformation. They were then covered with gold or carbon. The morphology was quantified with ImageJ software by considering at least ≈ 200 particles for each sample.
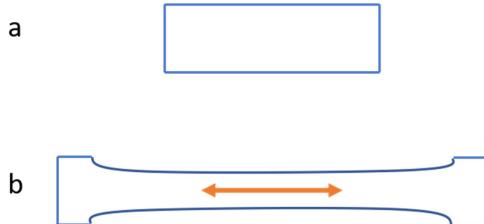


**FIG. 6.1 Scheme of the specimens (a) before and (b) after elongation. The double arrow represents the cut for SEM observations.**

### C.     **Results and discussion**

#### 1.     **PMMA and PS nanocomposites**

SAOS tests were conducted on PMMA and PS filled with clay at 200 °C. The complex viscosities of those blends are reported in FIG. 6.2 and FIG. 6.3. It can be seen that results from SAOS measurements are sensitive to the microstructural changes in the nanocomposites. At high frequencies, the rheological behavior of nanocomposites is dominated by the matrix, PMMA or PS. At lower frequencies 2 phenomena can take place: variation of the plateau value upon addition of clay and a strong increase at very low frequencies. The latter corresponds to a solid-like behavior and is generally associated with a good dispersion of clay. It is induced by a percolation which happens at low contents for exfoliated clays and would happen at higher content for clay that are not as well dispersed. As for a variation in the plateau value, an increase is generally noticed when nanoparticles are added whereas a decrease could be associated with some degradation.

The complex viscosities were fitted to the Carreau-Yasuda model with yield stress follows:

$$\eta^*(\omega) = \frac{\sigma_0}{\omega} + \eta_0(1 + (\lambda\omega)^a)^{\frac{n-1}{a}}$$

(6.3)

Where $\sigma_0$ is the yield stress sensitive to the dispersion state of clays and the resulting percolation, $\eta_0$ is the zero-shear viscosity characteristic to the material

corresponding to the value of the plateau, $\lambda$ is a time constant corresponding to the transition from the shear thinning behavior to the plateau, n is the power law index corresponding to the shear thinning behavior and a the Carreau-Yasuda parameter.
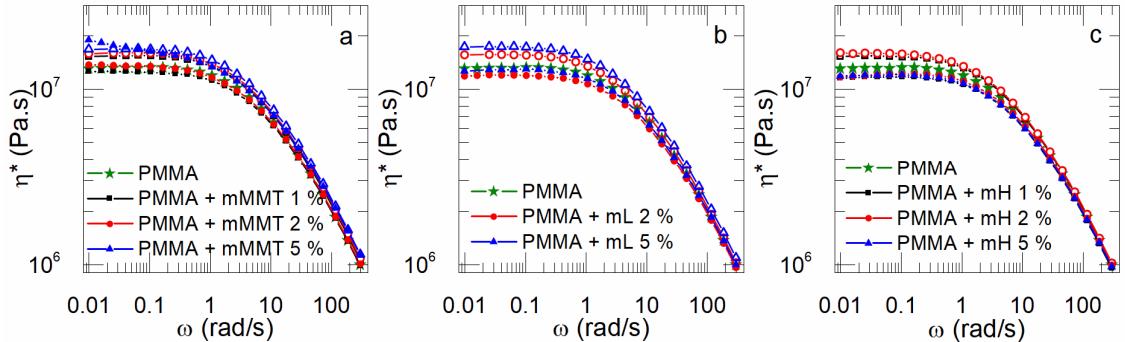


FIG. 6.2 Complex viscosities of PMMA with different concentration of (a) MMT and mMMT, (b) L and mL and (c) H and mH. Filled symbols correspond to the modified clays and open symbols to non-modified clays
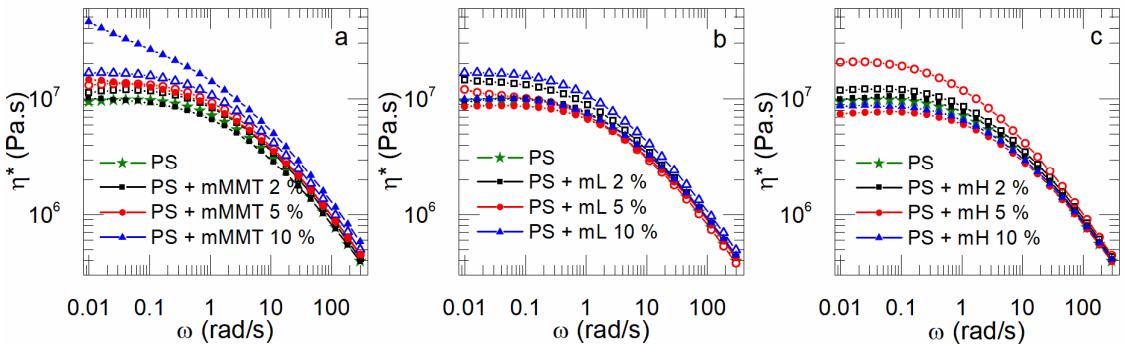


FIG. 6.3 Complex viscosities of PS with different concentration of (a) MMT and mMMT, (b) L and mL and (c) H and mH. Filled symbols correspond to the modified clays and open symbols to non-modified clays

Those five parameters were adjusted to fit the experimental data. Generally, $\lambda$, n and a are not really affected by the difference between the samples, their values remain close from one another for the same type of blend. On the contrary, the viscosity and the yield stress are very different from one sample to another. FIG. 6.4 and FIG. 6.5 shows $\eta_0$ and $\sigma_0$ as a function of concentration of clay respectively. To clearly visualize the influence of clay compared to the pure polymer, PS and PMMA's values of zero-shear viscosities are represented by a line. Non-modified clay (empty symbols) content increases systematically viscosity in both PS and PMMA. mL and mH (filled symbols), however, induce a decrease in the zero-shear viscosity which is most likely due to the degradation of part of the surfactant during processing as discussed in others studies [114]. On the contrary, mMMT induce a very strong increase in viscosity upon addition of nanoparticles. It is possible that

decrease of viscosity due to the degradation of surfactant is counterbalanced by the strong increase induced by the good dispersion of mMMT.
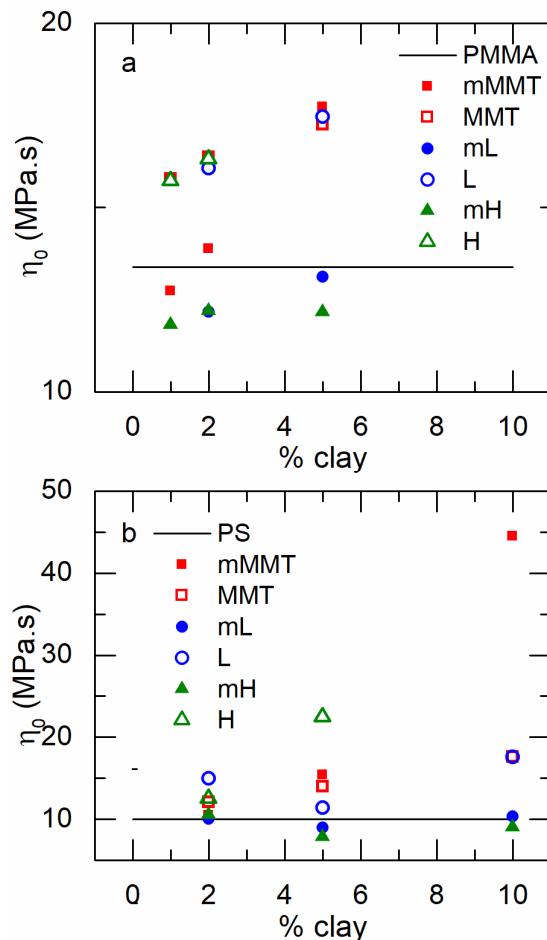


**FIG. 6.4 Zero-shear viscosities determined using Carreau-Yasuda model as a function of clay content for (a) PMMA nanocomposites and (b)**

To compare PS and PMMA nanocomposites, the variation of the zero-shear viscosity in PS and in PMMA for the same amount of nanoparticle is reported in TABLE 6.3. The presence of clay seems to have a stronger effect on the viscosity of PS than PMMA, especially in the case of mMMT and MMT. To characterize the dispersion of clays, XRD was conducted on some nanocomposites. The results were presented in CHAPTER 5 and reported in The main expectation when modifying clays is to achieve a better dispersion state of clay platelet, discs or tubes in a polymer matrix. As such, clays were blended with pure polymers, PMMA and PS, and the resulting nanocomposites were characterized.

XRD was used to find the interlayer spacing of clays in the nanocomposite. The values are reported in TABLE 5.5. First, it is clear that the clays are all better dispersed in

PMMA than PS as all the $\Delta d_{(001)}$, representing the difference in basal spacing with neat clays, are all superior to zero whereas in PS some clays have the same basal spacing as neat clays. It can also be noticed that mMMT is the clay with a higher $\Delta d_{(001)}$ so which disperse better in polymers. This can be surprising because laponite should be the more dispersible because of its very small size.

TABLE 5.5. Clearly, MMT and mMMT both have a smaller basal spacing in PS than in PMMA. This would mean that those clays are not as well dispersed in PS than in PMMA. However, this increase is more significant for mMMT than MMT. Knowing that mMMT is better dispersed, the increase in the zero-shear viscosity is probably associated with a good dispersion. It can be noticed the addition of L or H to the blend does not result in an increase of the zero-shear viscosity as much as MMT. This suggest that their dispersion is not as good. In the case of L it is also possible that its very small size is the reason its effect is limited.

In the case of the decrease due to the degradation of the surfactant (for mL and mH), the effect is also stronger on PS viscosity. This is probably caused by the fact that PS nanocomposites are processed twice in order to undergo the same thermal history than in the blends. As such, the surfactant would have more time to degrade in PS than in PMMA which is processed only once.

TABLE 6.3 Variation of the zero-shear viscosity induced by the presence of clay

| Clay | % of clay | Variation in the value of $\eta_0$ (%) | |
| --- | --- | --- | --- |
| | | in PS | in PMMA |
| MMT | 5 | +40 | +29 |
| L | 5 | +21 | +31 |
| H | 2 | +25 | +21 |
| mMMT | 5 | +54 | +32 |
| mL | 5 | -10 | -2 |
| mH | 5 | -21 | -9 |

FIG. 6.5 shows that the yield stress increases significantly starting at 5 % of mMMT in PMMA and PS. Consequently, the rheological percolation is exceeded at 5 %. The fact that MMT does not induce such a behavior confirms that it is not as well dispersed as mMMT. Laponite-based and Halloysite-based nanocomposites do not induce this kind of behavior as well, however, it does not mean that it is badly dispersed: the percolation strongly depends on the size and aspect ratio of clays. It was shown previously [115] that

Laponite would not induce any percolation at low content because of its very small size and Halloysite is also not likely to induce a percolation because of its low aspect ratio.
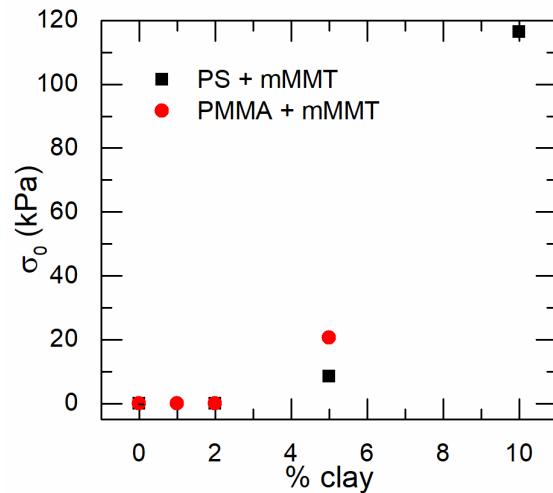


**FIG. 6.5 Yield stress from Carreau-Yasuda model as a function of clay concentration**

The tensile stress growth coefficients at different strain rates of PMMA and PS were measured at lower temperature (170 °C) so that the samples are viscous enough not to flow in the oven which would alter the measure. The results for pure PMMA and PS are represented in FIG. 6.6. At the beginning, the curves increase. After it reached a maximum, the tensile stress growth starts to decrease. This decrease is due to the necking of the sample followed by rupture. This behavior is totally normal for PS and PMMA which are not expected to show strain hardening. Instead of decreasing close to rupture, polymers exhibiting strain hardening would show a significant increase compared [67], [71], [116].
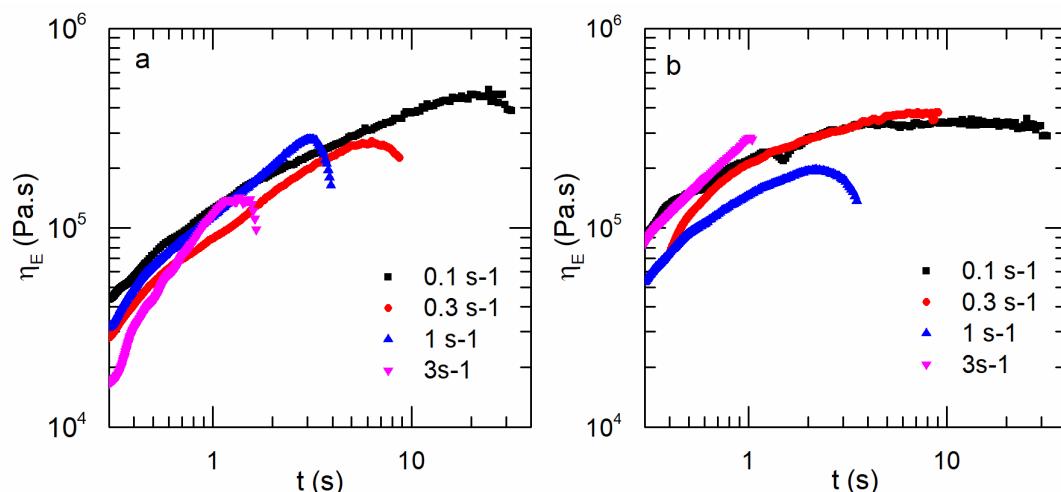


**FIG. 6.6 Tensile stress growth coefficients of (a) PS and (b) PMMA at 0.1, 0.3, 1 and 3 s$^{-1}$**

Tensile stress growth coefficients were also measured for PMMA and PS nanocomposites at 0.1 and 1 $s^{-1}$. FIG. 6.7 and FIG. 6.8 show the results for PS nanocomposites. It can be noticed that the increase in viscosity found for H with shear rheology can be confirmed in elongational experiments: the tensile stress growth coefficient curves increase with addition of H, which is linked to an increase in viscosity. This is not the case with addition of L and MMT which has lower or equal tensile stress growth coefficients of pure PS. Fornes et al. [117] evidenced a lower viscosity using capillary data than using shear flow. They suggested it to be caused by high clay platelet alignment, smaller particle sizes or matrix molecular weight degradation. It is true that MMT and L are smaller than H and may align better with the flow. In the case of modified clays (FIG. 6.8), all the nanocomposites have a lower or equal viscosity compared to PS caused by either degradation of surfactant discussed with shear data or better alignment.
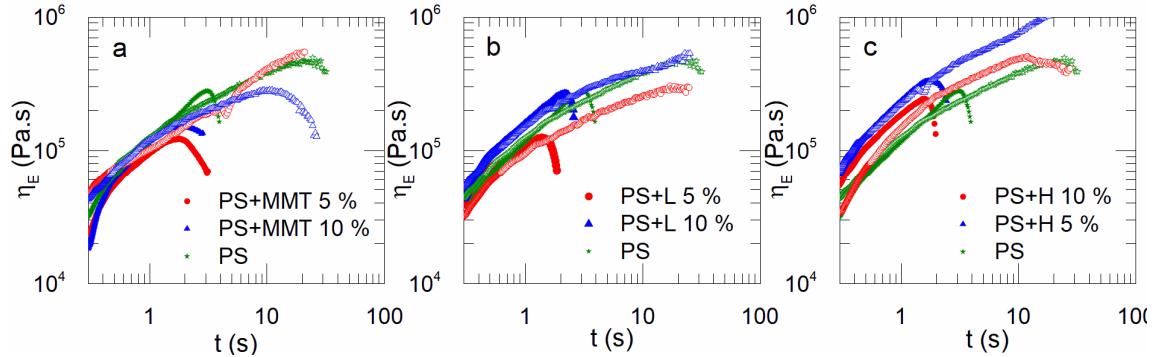


**FIG. 6.7 Tensile stress growth coefficients of PS at 0.1 (open symbols) and 1 $s^{-1}$ (filled symbols) with (a) MMT, (b) L and (c) H**
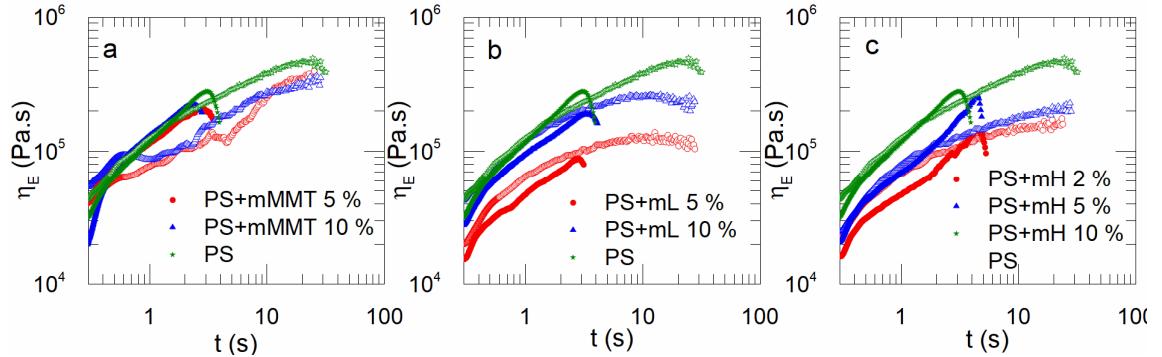


**FIG. 6.8 Tensile stress growth coefficients of PS at 0.1 (open symbols) and 1 $s^{-1}$ (filled symbols) with (a) mMMT, (b) mL and (c) mH**

The tensile stress growth coefficients for the PMMA samples are reported in FIG. 6.9 and FIG. 6.10. Contrary to PS nanocomposites, tensile stress growth coefficients did not increase with adding non-modified clays as the viscosities are equal or lower than that

of PMMA. As previously, it is probably because clay is better dispersed in PMMA so will more easily align under flow.
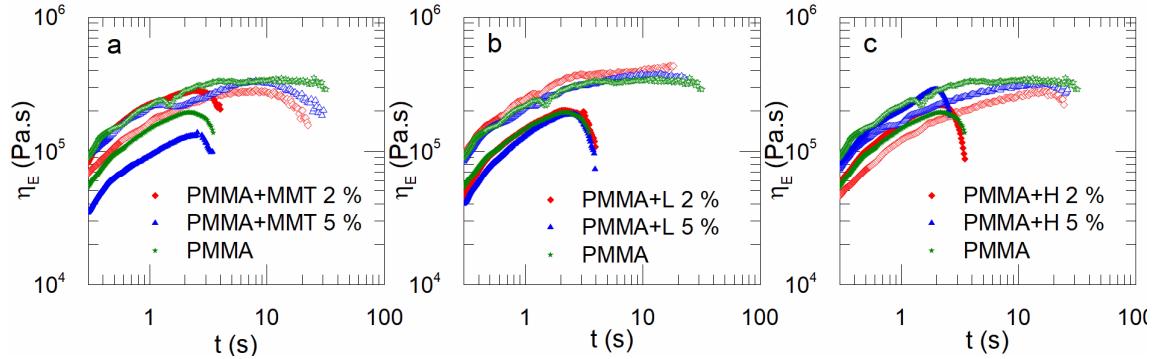


**FIG. 6.9 Tensile stress growth coefficients of PMMA at 0.1 (open symbols) and 1 s⁻¹ (filled symbols) with (a) MMT, (b) L and (c) H**
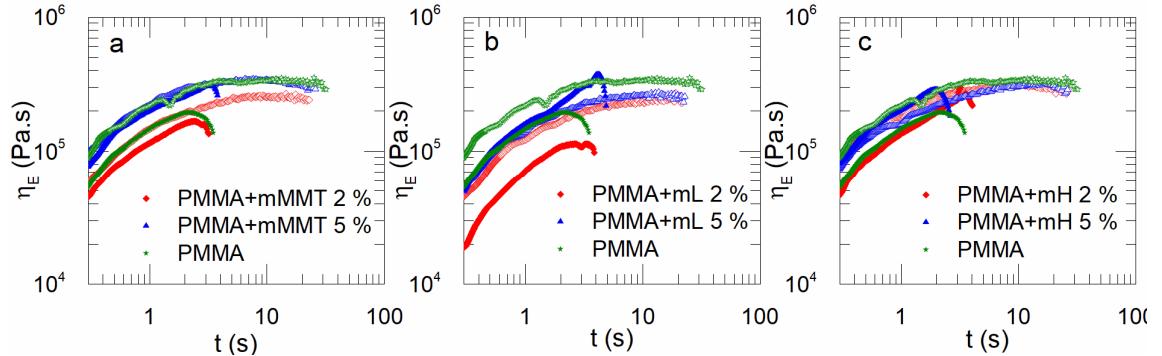


**FIG. 6.10 Tensile stress growth coefficients of PMMA at 0.1 (open symbols) and 1 s⁻¹ (filled symbols) with (a) mMMT, (b) mL and (c) mH**

Overall, it seems that the transient elongational viscosity at 1 s⁻¹ is often lower than the measure at 0.1 s⁻¹. This has already been observed, according to Tanoue et al. [118], this could be because the structure formed by the clay particles decreases in its complexity and strength when the deformation rate is increased.

No typical strong strain hardening could be evidenced. According to Park et al. [73] who worked with exfoliated structure, this confirms that the structure is intercalated as shown in CHAPTER 5. Li et al. [74], who worked on intercalated systems found a subtle strain hardening in the transient elongational viscosity curves. In our case, absolutely no strain hardening could be found in nanocomposites with non-modified clays because non-modified clays do not disperse well thus cannot create a structure which could induce strain hardening. However, nanocomposites with modified clays have a strain hardening behavior because they are better dispersed.

To better visualize this phenomenon, the tensile stress growth coefficients at 1s$^{-1}$ for nanocomposites with modified clays were plotted in FIG. 6.11. The transient viscosities first increase slowly, then the usual strain softening is followed by a strain hardening right before the sample breaks. This creates a sort of "bump" in the curve indicated by arrows in FIG. 6.11. This type of curves was already shown in the case of SEBS nanocomposites with a cylindrical morphology stretched in the direction transverse to cylinders orientation [97]. According to Okamoto et al. [72], strain hardening behavior in clay nanocomposites is caused by the silicate layers perpendicular to the flow. To do so, a good dispersion would have to be reached which is easier when the nanoparticles have more affinity with the polymer matrix so for modified clays. Also, if polymer chains are able to intercalate in-between clay sheets, interaction between polymer chains and clay particles and particle-particle interactions may be the cause of strain hardening [74]. The start of the increase is shown by arrows in  FIG. 6.11. This strain hardening decreases with increasing the concentration of clay. This probably originates by the fact that at low clay content the nanoparticles will disperse more easily whereas higher contents more aggregates are formed. Therefore, higher contents induce less stress.  As for the time at which the strain hardening occurs, no link between the concentration or type of clay could be evidenced.
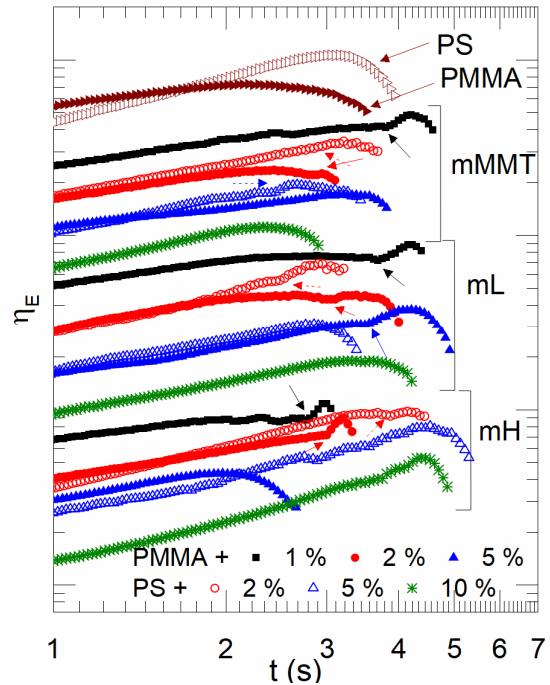


**FIG. 6.11 Transient elongational viscosities of PMMA and PS nanocomposites at 1 s$^{-1}$ with modified clays. The curves were shifted vertically to be able to compare them.**

It could have been interesting to study the evolution of the transient elongational viscosity of PMMA/PS blends, however previous studies showed that blends were so influenced by the matrix phase that no differences could be observed for a blend, especially with only 10 % of dispersed phase [77], [78]. As such, the work was focused on deformation and recovery of PMMA/PS blends under elongation flow.

### 2.    PMMA/PS blends

The initial morphologies were observed using SEM. The resulting volume average radius are reported in TABLE 6.4. There is a decrease of the droplet size (35 %) except for blends with mL. This is in good agreement with a previous work in which the volume average radius of blends of PMMA/PS decreased of 34 % with the addition of 0.8% of Cloisite 20A [103].

In the case of mL, 0.2 % seems to induce a decrease of 20 % of the Rv but 0.5 and 1 % do not influence the morphology significantly. No explanation for that is proposed at the moment.

TABLE 6.4 Volume average radius $R_v$ of the initial morphology

| Blend | Concentration of clay | Non-modified clays | | Modified clays | |
|---|---|---|---|---|---|
| | | $R_v$ (µm) | Standard deviation | $R_v$ (µm) | Standard deviation |
| Pure | 0 | 0.323 | 0.103 | - | - |
| MMT | 0.2 | 0.211 | 0.057 | 0.183 | 0.050 |
| | 0.5 | 0.200 | 0.051 | 0.241 | 0.069 |
| | 1 | 0.247 | 0.068 | 0.254 | 0.078 |
| L | 0.2 | 0.196 | 0.054 | 0.254 | 0.065 |
| | 0.5 | 0.192 | 0.053 | 0.301 | 0.082 |
| | 1 | 0.205 | 0.055 | 0.343 | 0.088 |
| H | 0.2 | 0.181 | 0.046 | 0.203 | 0.053 |
| | 0.5 | 0.200 | 0.053 | 0.185 | 0.047 |
| | 1 | 0.230 | 0.063 | 0.178 | 0.044 |

It was shown in CHAPTER 5 that non-modified clays (MMT, H and L) are dispersed in PMMA.  modified clays, mL is dispersed in the matrix and partly at the interface, mMMT is completely dispersed at the interface whereas most of mH could not disperse at the interface because of its size (see FIG. 5.8).

FIG. 6.12 shows pure PMMA/PS blend morphology before and after being submitted to an elongational flow at a strain rate of 0.1 s$^{-1}$ for various times. Initially, the droplets are spherical (see FIG. 6.12a). Upon elongation, the droplets are stretched into

ellipsoids oriented in the direction of the flow (FIG. 6.12b and c). As expected, the higher the Hencky strain, the more deformed the droplets. Elongational flow up to a Hencky strain of 2 (FIG. 6.12d) was not chosen because of experimental difficulties: the sample began to be too thin and difficult to prepare for observation. Moreover, it would be difficult to quantify the morphology with pictures such as FIG. 6.12d. As such, stretching up to 1.5 was chosen for further experiments.
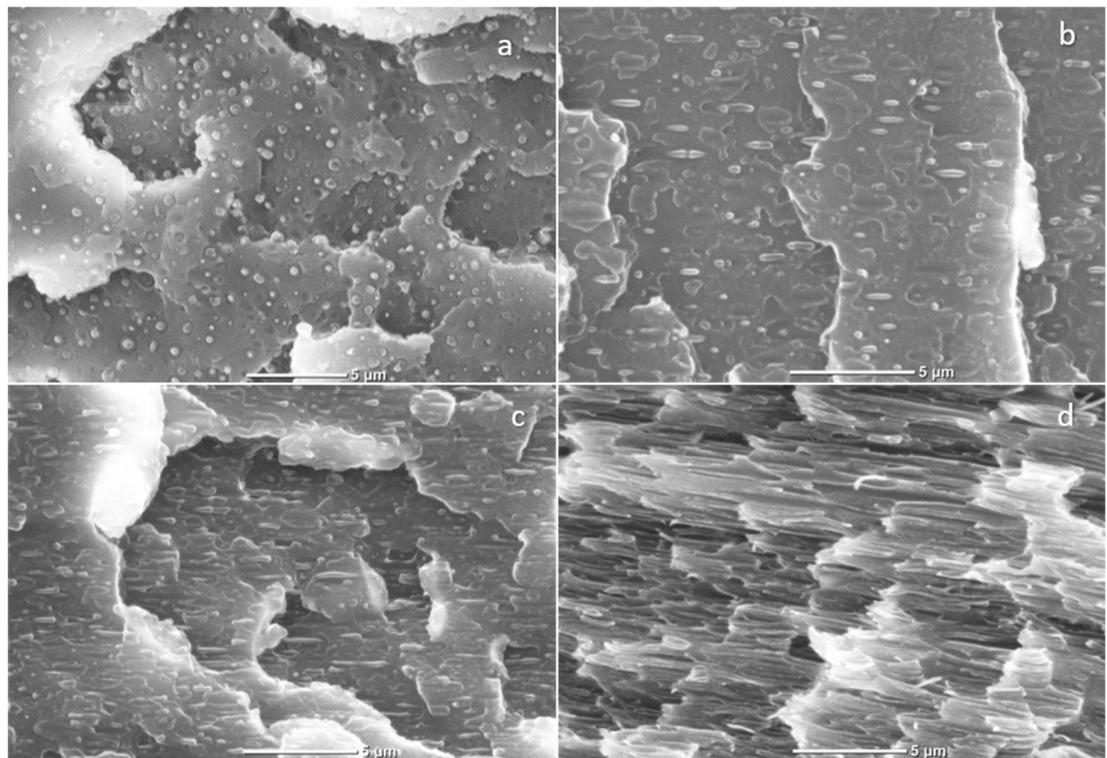


**FIG. 6.12. PMMA/PS blend morphology (a) before elongation, after elongation at 170 °C and 0.1 s-1 up to a Hencky**

**strain of (b) 1, (c) 1.5 and (d) 2.**

Stress as a function of time during elongation up to a Hencky strain of 1.5 followed by relaxation for Pure PMMA/PS blend is shown in FIG. 6.13. The length of the sample is kept constant during relaxation in order to hinder the shrinkage of the specimen and observe the relaxation of the droplets. To understand the relation between stress and morphology, sample were observed at different times in the process: right after elongation, during the relaxation process and after the relaxation process. When the elongational flow stops (FIG. 6.13a), the droplets are elongated and a sharp decrease in stress is observed. Then, the relaxation is driven by the relaxation of the droplets (FIG. 6.13b and c) due to interfacial tension until point d (t ≈ 600 s) when the stress decreases again, and the drops are relaxed

(FIG. 6.13d). It can be noted that the relaxation time in this experiment is much higher than in experiments conducted in linear shear rheology where the droplet relaxation was less than 2 s at 180 °C [106].
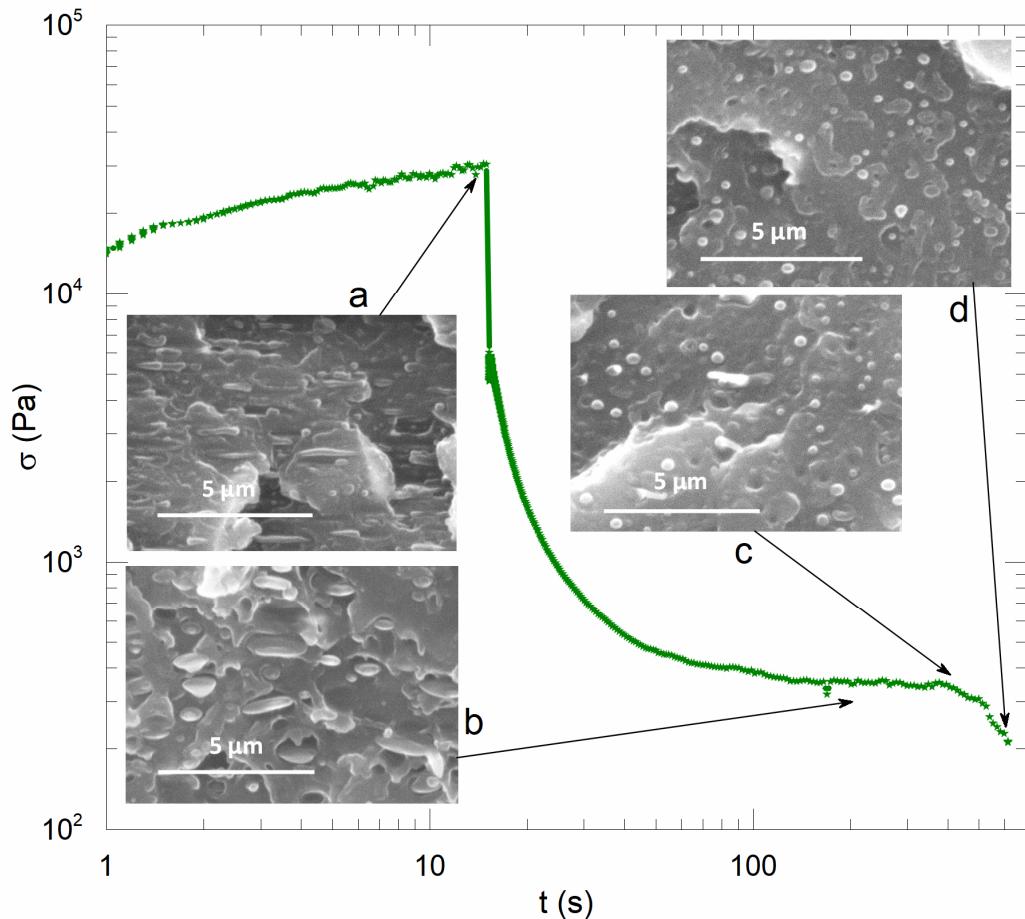


**FIG. 6.13 Stress as a function of time of Pure blend during elongation at 0.1 s-1 up to a Hencky strain of 1.5 followed by relaxation at 170 °C**

The deformation of the droplets was measured using SEM pictures and calculated using the following equation:

$$D = \frac{L^2 - B^2}{L^2 + B^2} \tag{6.4}$$

Where L is the major axis and B the minor axis of the ellipsoid.
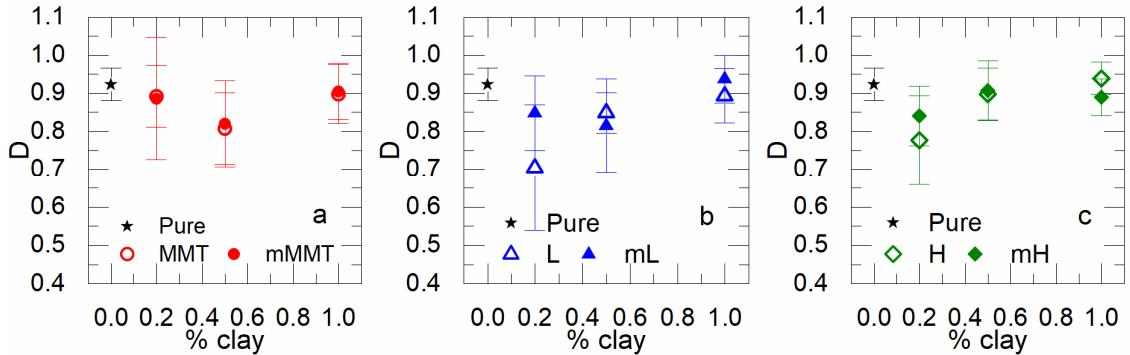
**FIG. 6.14 Drop deformation of blends as a function of concentration of (a) MMT and mMMT, (b) L and mL and (c) H and mH, after elongation at 0.1 s⁻¹ for 15 s. Bars corresponds to the standard deviation**

The deformations of each blend at t = 0 s (point a) is shown in FIG. 6.14. The deformations are between 0.7 and 0.9 so the droplets undergo high deformation in each case. Overall, adding nanoparticles seems to induce larger standard deviations (represented by bars in FIG. 6.14). It means that the droplets are not deformed as homogeneously as in the case of a pure blend. The presence of nanoparticles might hinder some of the droplets to properly deform with the matrix. Globally, the addition of clay also induces a decrease in the deformation for low content (0.2 % or up to 0.5% depending on the type of clay). It might be because the droplets are smaller than for the pure blend so it is more difficult to deform them. The fact that at high content the deformation of the droplets is similar to the one of pure blend suggests that high content of clay facilitate the deformation. This could be due to the increase of viscosity of the matrix phase for nanoparticles dispersed in PMMA. The modification of clays did not play a role in the deformation of the droplets.

The deformation of the droplets for each blend at each relaxation time is shown in FIG. 6.15. The deformation of the droplets was normalized in order to compare the samples more easily. The lines were drawn arbitrarily to guide the eye. A deformation of 0.2 is considered to correspond to relaxed droplets. For Pure PMMA/PS blend, the deformation gradually decreases with time [81], [84]. The time of the shape recovery driven by only interfacial tension can be calculated using the following equation:

$$\tau_{relax} = \frac{\eta_{0,b} d_0}{\varPhi \alpha} \tag{6.5}$$

Where $\eta_{0,b}$ is the zero-shear viscosity of the blend, $d_0$ the diameter of the droplets, $\varPhi$ the volume concentration of dispersed phase and $\alpha$ the interfacial tension. Gramespacher et al. used this expression to determine the interfacial tension between PMMA and PS and found good agreements with information extracted from linear shear rheology. In this

study, equation (6.5) is used to find the theoretical relaxation time of the droplets at 170 °C. The value of $R_v$ from TABLE 6.4, $\alpha = 4.29$ mN/m calculated in CHAPTER 4 and CHAPTER 5, $\eta_{0,b}$ measured by SAOS test and $\Phi = 0.11$ were used to calculate a relaxation time of 660 s. This is completely in agreement with the results shown in FIG. 6.15 where the droplets are almost completely relaxed at 600 s.
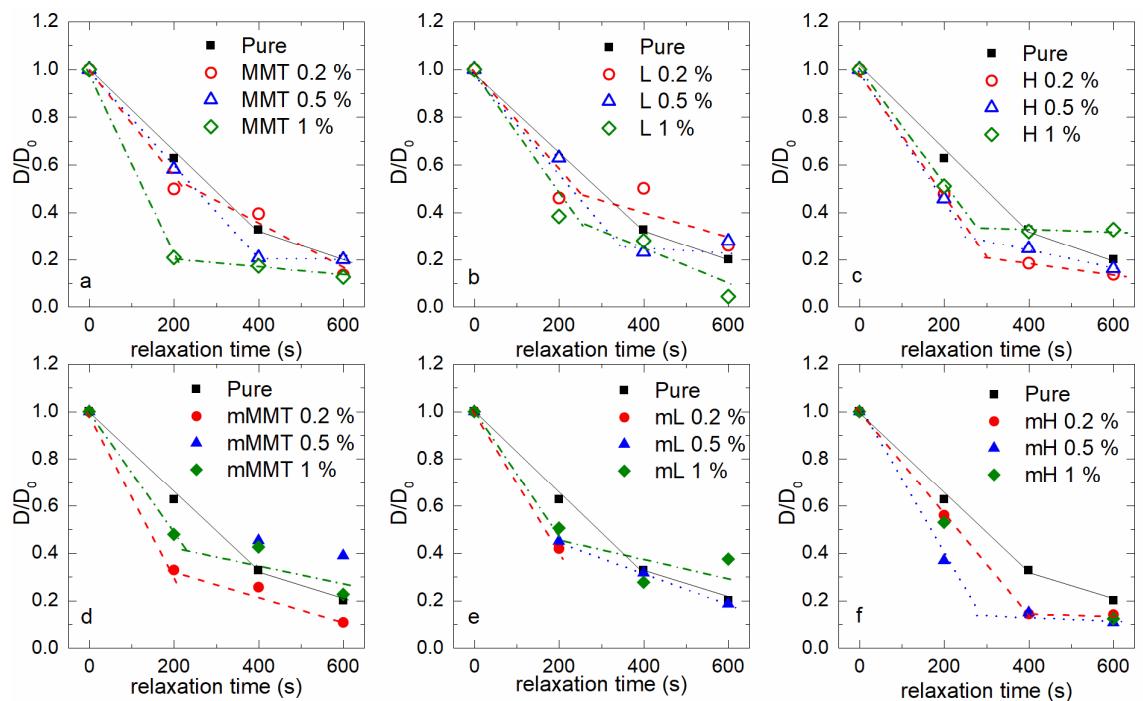


**FIG. 6.15 Normalized deformation of the droplets as a function of relaxation time for blends containing (a) MMT, (b) L, (c) H, (d) mMMT, (e) mL and (f) mH**

In the case of MMT, H and mH, the droplets relax clearly faster upon addition of clay: they reach a spherical state in-between 200 and 400 s instead of 600 s. Knowing that MMT, H and mH are dispersed in PMMA, this is probably due to a change in the viscosity ratio.

In the case of mMMT, mL and L, it seems that the presence of clay at the interface enhances the relaxation before 200 s but slows down the relaxation starting 200 s. A lower interfacial tension in the presence of compatibilizer at the interface would delay the shape recovery of the droplets. Consequently, it seems that relaxation process at long time is governed by the interfacial tension but at small time something else occurs. Stary et al. [85] evidenced a faster relaxation of the droplets and attributed it to the presence of Marangoni stresses. In our case, it might be possible that at small times, the gradient of concentration

of nanoparticle is so high that Marangoni stresses force the droplet to recover a less deformed shape to minimize concentration gradient for clays completely located at the interface (mMMT). For clays dispersed in the whole blends such as mL and L, the fast relaxation at small times may be caused by a combination of Marangoni stresses and viscosity effect. It would mean that at high deformations (so at small times), Marangoni stresses or variation in viscosity dominate the relaxation whereas at lower deformation (so longer times), the interfacial tension dominates.
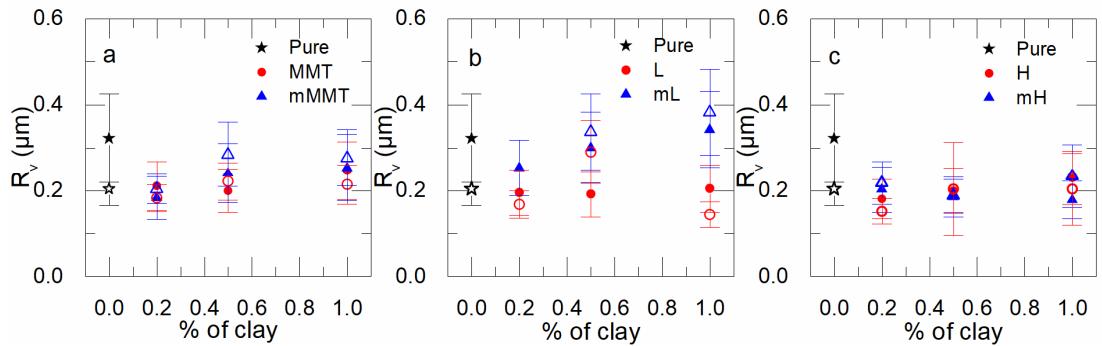


**FIG. 6.16 volume average radius of the dispersed phase before (filled symbols) and after elongation + relaxation (empty sympols) of blends containing (a) MMT and mMMT, (b) L and mL, (c) H and mH**

The morphology after the relaxation experiment is reported in FIG. 6.16 where the filled symbols represent the volume average radius before elongation and the empty symbols the resulting radius after relaxation experiments. Droplet breakup occurred in the pure blend during relaxation as the measured radius after elongation is smaller than initially. Also, the standard deviation is smaller after the experiment. Stone et al. [87] studied the breakup after elongation of a droplet. They found that the stretch ratio ($L_{fib}$ length of the ellipsoids divided by the initial diameter $d_0$) must be above a critical value for the droplet to break. They were able to plot experimentally $\frac{L_{fib}}{d_0}$ as a function of the viscosity ratio. In our case, for a viscosity ratio of 1.33, $\frac{L_{fib}}{d_0} \sim 3.4$ . All the stretch ratios were calculated and reported in TABLE 6.5. Pure PMMA/PS blends have a stretching ratio of 3.1 and was shown to undergo breakup. 3.1 is close to 3.4 so this is not surprising. However, according to the values found for blends containing clays, most of them should also undergo breakup as they are close or above 3.4.

**TABLE 6.5 Stretch ratio values for each blend**

| Blend | Concentration of clay | $\dfrac{L_{fib}}{d_0}$ non-modified clays | modified clays |
|---|---|---|---|
| Pure | 0 | 3.1 | |
| MMT | 0.2 | 3.6 | 4.6 |
| | 0.5 | 2.7 | 2.7 |
| | 1 | 6.7 | 5.0 |
| L | 0.2 | 2.6 | 3.1 |
| | 0.5 | 5.0 | 3.2 |
| | 1 | 4.5 | 3.7 |
| H | 0.2 | 3.2 | 2.8 |
| | 0.5 | 3.1 | 4.5 |
| | 1 | 2.5 | 3.7 |

Adding nanoparticles seems to have suppress droplet breakup. As it can be seen in FIG. 6.16, the droplet radii did not decrease, and the standard deviation seems to be as broad as initially. This was also shown in the case of addition of block copolymers by Stary et al [85]. They explained it by the presence of Marangoni stresses. In our case, the droplets are already very small, so it might be difficult to break them. As a matter of fact, the droplet radius of the pure blend after relaxation experiments is similar to the radii of blends with clay (around 0.200 µm). mL also suppressed droplet break up probably thanks to the part that is at the interface, by either Marangoni stresses or by preventing instabilities by their rigidity.

D.    **Conclusion**

The addition of clays (Montmorillonite, Laponite and Halloysite) to PMMA or PS nanocomposites induced a subtle strain hardening behavior under elongational flow whereas non-modified clays did not induce such a phenomenon. This suggests that the organic modification allowed a better dispersion of clays in both polymers.

The relaxation of the droplets after elongation at a strain rate of 0.1 s$^{-1}$ up to a Hencky strain of 1.5 was shown to be faster with addition of montmorillonite (MMT), halloysite (H) and modified halloysite (mH). As MMT, H and mH are dispersed in PMMA, it is most likely due to a variation in the viscosity of the matrix. In the case of better dispersed clays such as modified montmorillonite (mMMT), laponite (L) and modified

laponite (mL), the relaxation seems to present two steps: Marangoni stresses or variation in viscosity first induce a fast relaxation, then the interfacial tension dominates and slows down the relaxation at longer times.

Finally, the presence of clays in blends suppressed droplet breakup by either a viscosity variation if clay is dispersed in the matrix and by Marangoni stresses and/or Pickering effect if it is located at the interface.

# CONCLUSION & RECOMMENDATIONS

## A.     Summary of findings

The preliminary results of this thesis were presented in Chapter 3, entitled *"Compatibilization mechanism induced by organoclay in PMMA/PS blends"*. These first results were obtained using Cloisite 20A in PMMA/PS blends. The addition of clay led to a finer morphology as well as a decrease in interfacial tension. The novelty of this first article lies in the presence of Marangoni stresses evidenced for the first time in the case of nanoparticles. Marangoni stresses are usually associated to gradient of concentration of block copolymers at the droplets surface. Those results then suggested that nanoparticles are able to move around the droplets as well and may act similarly to block copolymers.

The second article, entitled *"Compatibilization mechanism induced by block copolymers with different molar masses in PMMA/PS blends"* aimed at investigating the compatibilization mechanism induced by block copolymers and especially study Marangoni stresses. Two block copolymers with different molar masses were chosen for this study. The results evidenced a decrease in interfacial tension but no refinement of the morphology. By further studying the compatibilization mechanism, relaxation caused by Marangoni stress was evidenced, indicating that block copolymers are located at least partially at the interface. However, Marangoni's relaxation evolution during coalescence suggested that block copolymers were not exclusively located at the interface initially but continued migrating during coalescence. Finally, the block copolymer with the higher molar mass was shown to be the most efficient at inhibiting coalescence most likely due to a combination of Marangoni stresses and steric hindrance.

In a third article, the compatibilization mechanism induced by clay nanoparticles of different sizes and shapes were studied. For this purpose, montmorillonite (MMT), laponite (L) and halloysite (H) were chosen and organically modified in such a manner that the surface chemistry remains similar from one type of blend to another. Each clay induced a decrease in interfacial tension and most of them a refinement of the morphology. Coalescence phenomena was more affected by the localization of clays:

- In the case of clays dispersed in the matrix (H, mH and MMT) the very limited influence on the coalescence originate from the variation of viscosity of the matrix due to the presence of nanoparticles.

- In the case of clays dispersed in the whole blend with no preference (L and mL), the small size of laponite might be the cause of a limited efficiency at inhibiting coalescence. Coalescence was slightly more affected by mL, most likely due to a more important quantity of nanoparticles located at the interface as suggested by the presence of Marangoni stresses.

- Finally, the most efficient at inhibiting coalescence was modified montmorillonite. Its localization at the interface between both polymers allowed Marangoni stresses and/or a Pickering effect to inhibit coalescence.

Finally, Chapter 6 offers preliminary results on the behavior nanocomposites and blends under elongational flow. The presence of clays in PMMA or PS nanocomposites exhibit a subtle strain hardening for modified clays most likely induced by a good dispersion of modified clays. The relaxation of PMMA/PS blends after elongation was then studied. The relaxation of the droplets was shown to be faster in the presence of clays in PMMA and attributed to a variation in the viscosity of the matrix. In the case of better dispersed clays: mMMT at the interface and mL and L in the whole blend, the relaxation presents two steps: a faster relaxation at small relaxation times most likely due to Marangoni stresses or variation in the viscosities, and a second step where the relaxation is slowed down by the interfacial tension. Finally, droplet breakup was noticed in pure PMMA/PS blends, but the presence of clays prevented this phenomenon.

## B. **Conclusions**

The main conclusion is that clay nanoparticles located at the interface, especially organo-modified montmorillonite (Cloisite 20A or mMMT), can behave similarly to block copolymers in terms of compatibilization mechanism and efficiency which is financially interesting because of the cheaper price of nanoparticles.

However, the initial objective of observing the influence of the shape and size of nanoparticles could not be studied as well as planed. Indeed, first, the large size of halloysite prevented it to locate at the interface and second, laponite was too easily dispersible to locate only at the interface. As such, the results were mainly influenced by the localization of clays instead of the shape and size. However, the results are still of interest and clearly evidenced that a localization of the nanoparticles at the interface induce a good compatibilization whereas a dispersion in the matrix phase lead to a limited compatibilization. Coalescence phenomenon is especially sensitive to the localization of

nanoparticles as its mechanism is induced by Marangoni stress, steric hindrance or Pickering effect which require the presence of compatibilizers at the interface. Droplets breakup was also suppressed with addition of nanoparticles but not sensitive to the localization of nanoparticles.

## C.    **Recommendations**

As most research works, some aspects could be further developed. The following recommendations are proposed for future works:

PMMA/PS blends are useful because their rheological behavior is well known, and they are appropriate for the use of models such as Palierne's model. However, PMMA/PS blends already have a fine dispersion of droplets and a low interfacial tension. Because of that, differences between the samples are too subtle to draw clear conclusions. As such, the first recommendation would be to use a less favorable blend for which compatibilization would induce more noticeable differences. To vary the viscosity ratio or the polarity of blends could also generate interesting results.

To be able to observe more frequently clay's localization with TEM would also have been of interest. Additional observations could have been interesting, for example, to confirm the localization of non-modified clays inferred with the wetting parameter. It would also have been of great interest to visualize Marangoni stresses. Theoretically, it would have been possible with highly deformed droplets were concentration gradients are supposed to appear.

Finally, measuring experimentally the surface tension between laponite, modified laponite, halloysite, modified halloysite and polymers would have been of interest in our study and would benefit many future works. As said previously, this kind of measurement is rare in the literature even if it would be very useful for modelling, calculating the wetting parameter for instance. Also, the influence of the modification of laponite and halloysite on the surface tension is of interest.

# LIST OF REFERENCES

[1]     S. R. Derkach, "Rheology of emulsions.," *Adv. Colloid Interface Sci.*, vol. 151, no. 1–2, pp. 1–23, Oct. 2009.

[2]     G. I. Taylor, "The viscosity of a fluid containing small drops of another fluid," *Proc. R. Soc. London. Ser. A, Contain. Pap. a Math. Phys. Character*, vol. 138, no. 834, pp. 41–48, 1932.

[3]     G. I. Taylor, "The Formation of Emulsions in Definable Fields of Flow," *Proc. R. Soc. A Math. Phys. Eng. Sci.*, vol. 146, no. 858, pp. 501–523, Oct. 1934.

[4]     F. D. Rumscheidt and S. G. Mason, "Particle motion in shared suspension - XII. Deformation and burst of fluid drops in shear and hyperbolic flow," *J. Colloid Sci.*, vol. 16, no. 3, pp. 238–261, 1961.

[5]     H. P. Grace, "Dispersion phenomena in high viscosity immiscible fluid systems and application of static mixers as dispersion devices in such systems," *Chem. Eng. Commun.*, vol. 14, no. 3–6, pp. 225–277, 1982.

[6]     C. L. Tucker and P. Moldenaers, "Microstructural evolution in polymer blends," *Annu. Rev. Fluid Mech.*, vol. 34, pp. 177–210, 2002.

[7]     U. Sundararaj and C. W. Macosko, "Drop breakup and coalescence in polymer blends : The effects of concentration and compatibilization," *Macromolecules*, vol. 28, no. 8, pp. 2647–2657, 1995.

[8]     P. Van Puyvelde, S. Velankar, J. Mewis, P. Moldenaers, and K. U. Leuven, "Effect of marangoni stresses on the deformation and coalescence in compatibilized immiscible polymer blends," *Polym. Eng. Sci. Sci.*, vol. 42, no. 10, pp. 1956–1964, 2002.

[9]     S.-P. Lyu, F. S. Bates, and C. W. Macosko, "Coalescence in polymer blends during shearing," *AIChE J.*, vol. 46, no. 2, pp. 229–238, Feb. 2000.

[10]    I. Vinckier, P. Moldenaers,  a. M. Terracciano, and N. Grizzuti, "Droplet size evolution during coalescence in semiconcentrated model blends," *AIChE J.*, vol. 44, no. 4, pp. 951–958, Apr. 1998.

[11]    C. L. DeLeo and S. S. Velankar, "Morphology and rheology of compatibilized polymer blends: diblock compatibilizers vs crosslinked reactive compatibilizers," *J. Rheol.* , vol. 52, no. 6, pp. 1385–1404, 2008.

[12]    N. C. Liu, H. Q. Xie, and W. E. Baker, "Comparison of the effectiveness of different basic functional groups for the reactive compatibilization of polymer blends," *Polymer* , vol. 34, pp. 4680–4687, 1993.

[13]    A. M. C. Souza and N. R. Demarquette, "Influence of coalescence and interfacial tension on the morphology of PP / HDPE compatibilized blends," *Polymer* , vol. 43, no. 14, pp. 3959–3967, 2002.

[14]    P. H. . Macaubas and N. . Demarquette, "Morphologies and interfacial tensions of immiscible polypropylene/polystyrene blends modified with triblock copolymers," *Polymer* , vol. 42, no. 6, pp. 2543–2554, 2001.

[15]    M. Yee, P. S. Calvão, and N. R. Demarquette, "Rheological behavior of poly(methyl methacrylate)/polystyrene (PMMA/PS) blends with the addition of PMMA-ran-PS," *Rheol. Acta*, vol. 46, no. 5, pp. 653–664, 2007.

[16]    A. M. C. de Souza, P. S. Calvão, and N. R. Demarquette, "Linear viscoelastic behavior of compatibilized PMMA/PP blends," *J. Appl. Polym. Sci.*, vol. 129, no. 3, pp. 1280–1289, 2013.

[17]  A. J. Ramic, J. C. Stehlin, S. D. Hudson, A. M. Jamieson, and I. Manas-Zloczower, "Influence of block copolymer on droplet breakup and coalescence in model immiscible polymer blends," *Macromolecules*, vol. 33, no. 2, pp. 371–374, 2000.

[18]  J. Huitric, M. Moan, P. J. Carreau, and N. Dufaure, "Effect of reactive compatibilization on droplet coalescence in shear flow," *J. Nonnewton. Fluid Mech.*, vol. 145, no. 2–3, pp. 139–149, 2007.

[19]  J. Vermant, G. Cioccolo, K. Golapan Nair, and P. Moldenaers, "Coalescence suppression in model immiscible polymer blends by nano-sized colloidal particles," *Rheol. Acta*, vol. 43, no. 5, pp. 529–538, 2004.

[20]  S. Lyu, T. D. Jones, F. S. Bates, and C. W. Macosko, "Role of block copolymers on suppression of droplet coalescence," *Macromolecules*, vol. 35, no. 20, pp. 7845–7855, 2002.

[21]  H. K. Jeon and C. W. Macosko, "Visualization of block copolymer distribution on a sheared drop," *Polymer*, vol. 44, no. 18, pp. 5381–5386, 2003.

[22]  A. Adedeji, S. Lyu, and C. W. Macosko, "Block copolymers in homopolymer blends: interface vs micelles," *Macromolecules*, vol. 34, no. 25, pp. 8663–8668, 2001.

[23]  E. Van Hemelrijck, P. Van Puyvelde, C. W. Macosko, and P. Moldenaers, "The effect of block copolymer architecture on the coalescence and interfacial elasticity in compatibilized polymer blends," *J. Rheol.*, vol. 49, no. 3, pp. 783–798, 2005.

[24]  P. V. Van Puyvelde and P. Moldenaers, "Rheology and morphology development in immiscible polymer blends," *Rheol. Rev.*, pp. 101–145, 2005.

[25]  I. Fortelný, "An analysis of the origin of coalescence suppression in compatibilized polymer blends," *Eur. Polym. J.*, vol. 40, no. 9, pp. 2161–2166, 2004.

[26]  A. Taguet, P. Cassagnau, and J.-M. Lopez-Cuesta, "Structuration, selective dispersion and compatibilizing effect of (nano)fillers in polymer blends," *Prog. Polym. Sci.*, vol. 39, no. 8, pp. 1526–1563, 2014.

[27]  F. Fenouillot, P. Cassagnau, and J.-C. Majesté, "Uneven distribution of nanoparticles in immiscible fluids: Morphology development in polymer blends," *Polymer*, vol. 50, no. 6, pp. 1333–1350, 2009.

[28]  N. R. Demarquette, "Evaluation of experimental techniques for determining interfacial tension between molten polymers," *Int. Mater. Rev.*, vol. 48, no. 4, pp. 247–269, Aug. 2003.

[29]  L. Elias, F. Fenouillot, J. C. Majesté, P. Alcouffe, and P. Cassagnau, "Immiscible polymer blends stabilized with nano-silica particles: Rheology and effective interfacial tension," *Polymer*, vol. 49, no. 20, pp. 4378–4385, 2008.

[30]  F. Gubbels, R. Jerome, E. Vanlathem, R. Deltour, S. Blacher, and F. Brouers, "Kinetic and Thermodynamic Control of the Selective Localization of Carbon Black at the Interface of Immiscible Polymer Blends," *Chem. Mater.*, vol. 10, no. 7, pp. 1227–1235, 1998.

[31]  L. Elias, F. Fenouillot, J.-C. Majesté, G. Martin, and P. Cassagnau, "Migration of Nanosilica Particles in Polymer Blends," *J. Polym. Sci. Part B Polym. Phys.*, vol. 46, pp. 1976–1983, 2008.

[32]  L. Elias, F. Fenouillot, J.-C. Majesté, and P. Cassagnau, "Morphology and rheology of immiscible polymer blends filled with silica nanoparticles," *Polymer*, vol. 48, pp. 6029–6040, 2007.

[33]  B. Du, U. A. Handge, M. Wambach, C. Abetz, S. Rangou, and V. Abetz, "Functionalization of MWCNT with P(MMA-co-S) copolymers via ATRP: Influence on localization of MWCNT in SAN/PPE 40/60 blends and on rheological

and dielectric properties of the composites," *Polymer* , vol. 54, no. 22, pp. 6165–6176, 2013.

[34]  K. Yurekli, A. Karim, E. J. Amis, and R. Krishnamoorti, "Influence of layered silicates on the phase-separated morphology of PS-PVME blends," *Macromolecules*, vol. 36, pp. 7256–7267, 2003.

[35]  M. Huang and H. Guo, "The intriguing ordering and compatibilizing performance of Janus nanoparticles with various shapes and different dividing surface designs in immiscible polymer blends," *Soft Matter*, vol. 9, no. 30, pp. 7356–7368, 2013.

[36]  Y. Xi, R. L. Frost, and H. He, "Modification of the surfaces of Wyoming montmorillonite by the cationic surfactants alkyl trimethyl, dialkyl dimethyl, and trialkyl methyl ammonium bromides," *J. Colloid Interface Sci.*, vol. 305, no. 1, pp. 150–158, 2007.

[37]  M. F. Delbem, T. S. Valera, F. R. Valenzuela-Diaz, and N. R. Demarquette, "Modification of a brazilian smectite clay with different quaternary ammonium salts," *Quim. Nova*, vol. 33, no. 2, pp. 309–315, 2010.

[38]  X. Tang and S. Alavi, "Structure and physical properties of starch/poly vinyl alcohol/laponite RD nanocomposite films," *J. Agric. Food Chem.*, vol. 60, pp. 1954–1962, 2012.

[39]  B. Wang, M. Zhou, Z. Rozynek, and J. O. Fossum, "Electrorheological properties of organically modified nanolayered laponite: influence of intercalation, adsorption and wettability," *J. Mater. Chem.*, vol. 19, no. 13, p. 1816, 2009.

[40]  C. A. Mitchell and R. Krishnamoorti, "Rheological properties of diblock copolymer/layered-silicate nanocomposites," *J. Polym. Sci. Part B Polym. Phys.*, vol. 40, no. 14, pp. 1434–1443, 2002.

[41]  T. Batista, A. M. Chiorcea-Paquim, A. M. O. Brett, C. C. Schmitt, and M. G. Neumann, "Laponite RD/polystyrenesulfonate nanocomposites obtained by photopolymerization," *Appl. Clay Sci.*, vol. 53, no. 1, pp. 27–32, 2011.

[42]  E. Joussein, S. Petit, J. Churchman, B. Theng, D. Righi, and B. Delvaux, "Halloysite clay minerals – a review," *Clay Miner.*, vol. 40, pp. 383–426, 2005.

[43]  P. Yuan, D. Tan, and F. Annabi-Bergaya, "Properties and applications of halloysite nanotubes: recent research advances and future prospects," *Appl. Clay Sci.*, vol. 112–113, pp. 75–93, 2015.

[44]  D. Rawtani and Y. K. Agrawal, "Multifarious applications of halloysite nanotubes: A review," *Rev. Adv. Mater. Sci.*, vol. 30, no. 3, pp. 282–295, 2012.

[45]  P. Pal, M. K. Kundu, A. Malas, and C. K. Das, "Compatibilizing effect of halloysite nanotubes in polar-nonpolar hybrid system," *J. Appl. Polym. Sci.*, vol. 131, 2014.

[46]  M. K. Kundu, P. Pal, G. Hatui, C. K. Das, and S. S. Kalra, "Investigation on crystallinity, performance and processability of naturally occurring halloysite nanotubes compatibilized sPS/LCP thermoplastic nanocomposites," *J. Polym. Res.*, vol. 22, 2015.

[47]  Y. Lvov, W. Wang, L. Zhang, and R. Fakhrullin, "Halloysite Clay Nanotubes for Loading and Sustained Release of Functional Compounds.," *Adv. Mater.*, vol. 20, no. 6, pp. 1227–1250, 2015.

[48]  R. Riemann, H. Cantow, and C. Friedrich, "Interpretation of a new interface-governed relaxation process in compatibilized polymer blends," *Macromolecules*, vol. 30, no. 18, pp. 5476–5484, 1997.

[49]  U. Jacobs, M. Fahrländer, J. Winterhalter, and C. Friedrich, "Analysis of Palierne's emulsion model in the case of viscoelastic interfacial properties," *J. Rheol.* , vol. 43, no. 6, pp. 1495–1509, 1999.

[50]  J. Honerkamp and J. Weese, "A nonlinear regularization method for the calculation of relaxation spectra," *Rheol. Acta*, vol. 32, no. 1, pp. 65–73, 1993.

[51]  D. Wu, Y. Zhang, L. Yuan, M. Zhang, and W. Zhou, "Viscoelastic interfacial properties of compatibilized poly(ε-caprolactone)/polylactide blend," *J. Polym. Sci. Part B Polym. Phys.*, vol. 48, no. 7, pp. 756–765, 2010.

[52]  J. F. Palierne, "Linear rheology of viscoelastic emulsions with interfacial tension," *Rheol. Acta*, vol. 29, no. 3, pp. 204–214, 1990.

[53]  E. Van Hemelrjick and P. Van Puyvelde, "Interfacial elasticity and coalescence suppression in compatibilized polymer blends," *J. Rheol.* , vol. 48, no. 1, pp. 143–158, 2004.

[54]  E. Van Hemelrijck, P. Van Puyvelde, S. Velankar, C. W. Macosko, and P. Moldenaers, "Interfacial elasticity and coalescence suppression in compatibilized polymer blends," *J. Rheol.* , vol. 48, no. 1, pp. 143–158, 2003.

[55]  D. Graebling, R. Muller, and J. F. Palierne, "Linear viscoelastic behavior of some incompatible polymer blends in the melt. Interpretation of data with a model of emulsion of viscoelastic liquids," *Macromolecules*, vol. 26, no. 2, pp. 320–329, 1993.

[56]  M. Bousmina, P. Bataille, S. Sapieha, and H. P. Schreiber, "Comparing the effect of corona treatment and block copolymer addition on rheological properties of polystyrene/polyethylene blends," *J. Rheol.* , vol. 39, no. 3, pp. 499–517, 1995.

[57]  C. Lacroix, M. Grmela, and P. J. Carreau, "Morphological evolution of immiscible polymer blends in simple shear and elongational flows," *J. Nonnewton. Fluid Mech.*, vol. 86, pp. 37–59, 1999.

[58]  H. M. Lee and O. O. Park, "Rheology and dynamics of immiscible polymer blends," *Journal of Rheology*, vol. 38, no. 1994. p. 1405, 1994.

[59]  M. Bousmina, "Rheology of polymer blends : linear model for viscoelastic emulsions," *Rheol. Acta*, vol. 38, pp. 73–83, 1999.

[60]  W. Yu, M. Bousmina, M. Grmela, and C. Zhou, "Modeling of oscillatory shear flow of emulsions under small and large deformation fields," *J. Rheol.* , vol. 46, p. 1401, 2002.

[61]  M. Grmela, M. Bousmina, and J. F. Palierne, "On the rheology of immiscible blends," *Rheol. Acta*, vol. 40, pp. 560–569, 2001.

[62]  E. Narimissa and M. H. Wagner, "A hierarchical multi-mode MSF model for long-chain branched polymer melts part III: shear flows," *Rheol. Acta*, vol. 55, no. 8, pp. 633–639, 2016.

[63]  M. Padmanabhan and C. W. Macosko, "Extensional viscosity from entrance pressure drop measurements," *Rheol. Acta*, vol. 36, no. 2, pp. 144–151, 1997.

[64]  J. Meissner and J. Hostettler, "A new elongational rheometer for polymer melts and other highly viscoelastic liquids," *Rheol. Acta*, vol. 33, no. 1, pp. 1–21, 1994.

[65]  H. Münstedt, "New Universal Extensional Rheometer for Polymer Melts. Measurements on a Polystyrene Sample," *J. Rheol.* , vol. 23, no. 4, p. 421, 1979.

[66]  M. L. Sentmanat, "Miniature universal testing platform: From extensional melt rheology to solid-state deformation behavior," *Rheol. Acta*, vol. 43, no. 6, pp. 657–669, 2004.

[67]  H. Münstedt and Z. Starý, "Steady states in extensional flow of strain hardening polymer melts and the uncertainties of their determination," *J. Rheol.* , vol. 57, no. 4, pp. 1065–1077, 2013.

[68]  H. Eslami and M. R. Kamal, "Effect of a chain extender on the rheological and mechanical properties of biodegradable poly(lactic acid)/poly[(butylene succinate)-

co-adipate] blends," *J. Appl. Polym. Sci.*, vol. 129, no. 5, pp. 2418–2428, 2013.

[69]   M. H. Wagner, S. Kheirandish, K. Koyama, A. Nishioka, A. Minegishi, and T. Takahashi, "Modeling strain hardening of polydisperse polystyrene melts by molecular stress function theory," *Rheol. Acta*, vol. 44, no. 3, pp. 235–243, 2005.

[70]   O. Akhlaghi, O. Akbulut, and Y. Z. Menceloglu, "Shear and extensional rheological characterization of poly(acrylonitrile)/halloysite nanocomposite solutions," *Eur. Polym. J.*, vol. 73, pp. 17–25, 2015.

[71]   K. Ogura and M. H. Wagner, "Rheological characterization of cross-linked poly(methyl methacrylate)," *Rheol. Acta*, vol. 52, no. 8–9, pp. 753–765, 2013.

[72]   M. Okamoto, P. H. Nam, P. Maiti, T. Kotaka, N. Hasegawa, and A. Usuki, "A House of Cards Structure in Polypropylene/Clay Nanocomposites under Elongational Flow," *Nano Lett.*, vol. 1, no. 6, pp. 295–298, 2001.

[73]   J. U. Park, J. L. Kim, K. H. Ahn, S. J. Lee, and K. S. Cho, "Rheological behavior of polymer/layered silicate nanocomposites under uniaxial extensional flow," *Macromol. Res.*, vol. 14, no. 3, pp. 318–323, 2006.

[74]   Q. Li, Q. Yang, Y. Huang, G. Chen, and Y. Lv, "Effect of Compatibilizer Content on the Shear and Extensional Rheology of Polypropylene/Clay Nanocomposites," *J. Macromol. Sci. Part B*, vol. 51, no. 9, pp. 1776–1793, 2012.

[75]   I. Delaby, B. Ernst, Y. Germain, and R. Muller, "Droplet deformation in polymer blends during uniaxial elongational flow: Influence of viscosity ratio for large capillary numbers," *J. Rheol.* , vol. 38, no. 6, pp. 1705–1720, 1994.

[76]   I. Delaby, B. Ernst, D. Froelich, and R. Muller, "Droplet deformation in immiscible polymer blends during transient uniaxial elongational flow," *Polym. Eng. Sci.*, vol. 36, no. 12, pp. 1627–1635, 1996.

[77]   M. Heindl, M. K. Sommer, and H. Münstedt, "Morphology development in polystyrene/polyethylene blends during uniaxial elongational flow," *Rheol. Acta*, vol. 44, no. 1, pp. 55–70, 2004.

[78]   H. Gramespacher and J. Meissner, "Melt elongation and recovery of polymer blends, morphology, and influence of interfacial tension," *J. Rheol.* , vol. 41, no. 1, pp. 27–44, 1997.

[79]   U. A. Handge and P. Pötschke, "Interplay of rheology and morphology in melt elongation and subsequent recovery of polystyrene/poly(methyl methacrylate) blends," *J. Rheol.* , vol. 48, no. 5, p. 1103, 2004.

[80]   U. A. Handge, "Modeling recovery of polymer blends after melt elongation," *J. Rheol.* , vol. 47, no. 4, pp. 969–978, 2003.

[81]   N. Mechbal and M. Bousmina, "Uniaxial deformation and relaxation of polymer blends: Relationship between flow and morphology development," *Rheol. Acta*, vol. 43, no. 2, pp. 119–126, 2004.

[82]   W. Yu, M. Bousmina, M. Grmela, J.-F. Palierne, and C. Zhou, "Quantitative relationship between rheology and morphology in emulsions," *J. Rheol.* , vol. 46, no. October, p. 1381, 2002.

[83]   Z. Starý and H. Münstedt, "Morphology development in PS/LLDPE blend during and after elongational deformation," *J. Polym. Sci. Part B Polym. Phys.*, vol. 46, no. 1, pp. 16–27, Jan. 2008.

[84]   Z. Starý, M. Musialek, and H. Münstedt, "Shape recovery versus breakup of deformed droplets in a polymer blend after uniaxial extension," *Macromol. Mater. Eng.*, vol. 296, no. 5, pp. 414–422, 2011.

[85]   Z. Starý, T. Pemsel, J. Baldrian, and H. Münstedt, "Influence of a compatibilizer on the morphology development in polymer blends under elongation," *Polymer* , vol.

53, no. 9, pp. 1881–1889, 2012.

[86]  N. Mechbal and M. Bousmina, "Effect of Copolymer Addition on Drop Deformation during Uniaxial Elongation and during Relaxation after Cessation of Flow," *Macromolecules*, vol. 40, no. 4, pp. 967–975, Feb. 2007.

[87]  H. A. Stone, B. J. Bentley, and L. G. Leal, "An experimental study of transient effects in the breakup of viscous drops," *J. Fluid Mech.*, vol. 173, no. 1, p. 131, 1986.

[88]  A. Monfared and A. Jalali-Arani, "Morphology and rheology of (styrene-butadiene rubber/acrylonitrile-butadiene rubber) blends filled with organoclay: The effect of nanoparticle localization," *Appl. Clay Sci.*, vol. 108, pp. 1–11, 2015.

[89]  T. Parpaite, B. Otazaghine, A. Taguet, R. Sonnier, a. S. Caro, and J. M. Lopez-Cuesta, "Incorporation of modified Stöber silica nanoparticles in polystyrene/polyamide-6 blends: Coalescence inhibition and modification of the thermal degradation via controlled dispersion at the interface," *Polymer*, vol. 55, no. 11, pp. 2704–2715, 2014.

[90]  T. Parpaite, B. Otazaghine, A. S. Caro, A. Taguet, R. Sonnier, and J. M. Lopez-Cuesta, "Janus hybrid silica/polymer nanoparticles as effective compatibilizing agents for polystyrene/polyamide-6 melted blends," *Polymer*, vol. 90, pp. 34–44, 2016.

[91]  G. Cavallaro, G. Lazzara, S. Milioto, F. Parisi, and V. Sanzillo, "Modified halloysite nanotubes: Nanoarchitectures for enhancing the capture of oils from vapor and liquid phases," *ACS Appl. Mater. Interfaces*, vol. 6, no. 1, pp. 606–612, 2014.

[92]  W. Jinhua *et al.*, "Rapid adsorption of Cr (VI) on modified halloysite nanotubes," *Desalination*, vol. 259, no. 1–3, pp. 22–28, 2010.

[93]  S. Sinha Ray, S. Pouliot, M. Bousmina, and L. A. Utracki, "Role of organically modified layered silicate as an active interfacial modifier in immiscible polystyrene/polypropylene blends," *Polymer*, vol. 45, no. 25, pp. 8403–8413, 2004.

[94]  V. Shaayegan, P. Wood-Adams, and N. R. Demarquette, "Linear viscoelasticity of immiscible blends: The application of creep," *J. Rheol.*, vol. 56, no. 5, pp. 1039–1056, 2012.

[95]  M. Yee, A. M. C. Souza, T. S. Valera, and N. R. Demarquette, "Stress relaxation behavior of PMMA/PS polymer blends," *Rheol. Acta*, vol. 48, no. 5, pp. 527–541, 2009.

[96]  S. A. Saltikov, "The Determination of the Size Distribution of Particles in an Opaque Material from a Measurement of the Size Distribution of Their Sections," in *Stereology*, Springer, Ed. Berlin, Heidelberg: Springer Berlin Heidelberg, 1967, pp. 163–173.

[97]  L. G. Amurin, D. J. Carastan, and N. R. Demarquette, "Morphological evolution of block copolymer nanocomposites submitted to extensionnal flows," *J. Rheol.*, vol. 60, no. 1, pp. 175–189, 2016.

[98]  B. Vergnes, "The use of apparent yield stress to characterize exfoliation in Polymer Nanocomposites," *Int. Polym. Process.*, vol. 26, no. 2, pp. 229–232, 2011.

[99]  W. Lertwimolnun and B. Vergnes, "Effect of processing conditions on the formation of polypropylene/organoclay nanocomposites in a twin screw extruder," *Polym. Eng. Sci.*, vol. 46, no. 3, pp. 314–323, 2006.

[100] P. S. Calvão, M. Yee, and N. R. Demarquette, "Effect of composition on the linear viscoelastic behavior and morphology of PMMA/PS and PMMA/PP blends," *Polymer*, vol. 46, no. 8, pp. 2610–2620, 2005.

[101] I. Labaume, P. Médéric, J. Huitric, and T. Aubry, "Comparative study of interphase viscoelastic properties in polyethylene/polyamide blends compatibilized with clay

nanoparticles or with a graft copolymer," *J. Rheol.* , vol. 57, no. 2, pp. 377–392, 2013.

[102] C. Friedrich and Y. Y. Antonov, "Interfacial relaxation in polymer blends and gibbs elasticity," *Macromolecules*, vol. 40, no. 4, pp. 1283–1289, 2007.

[103] J. Genoyer, M. Yee, J. Soulestin, and N. Demarquette, "Compatibilization mechanism induced by organoclay in PMMA/PS blends," *J. Rheol.* , vol. 61, no. 4, pp. 613–626, 2017.

[104] S. T. Milner and H. Xi, "How copolymers promote mixing of immiscible homopolymers," *J. Rheol.* , vol. 40, no. 4, p. 663, 1996.

[105] C. W. Macosko, P. Guégan, A. K. Khandpur, A. Nakayama, P. Marechal, and T. Inoue, "Compatibilizers for Melt Blending: Premade Block Copolymers," *Macromolecules*, vol. 29, no. 96, pp. 5590–5598, 1996.

[106] J. Genoyer, J. Soulestin, and N. R. Demarquette, "Influence of the molar masses on compatibilization mechanism induced by two block copolymers in PMMA/PS blends," *J. Rheol.* , no. Under Review.

[107] J. L. Sormana, S. Chattopadhyay, and J. C. Meredith, "Mechanical and thermal properties of poly(urethane urea) nanocomposites prepared with diamine-modified Laponite," *J. Nanomater.*, vol. 2008, no. 1, 2008.

[108] G. K. Dedzo, G. Ngnie, and C. Detellier, "PdNP Decoration of Halloysite Lumen via Selective Grafting of Ionic Liquid onto the Aluminol Surfaces and Catalytic Application," *ACS Appl. Mater. Interfaces*, vol. 8, no. 7, pp. 4862–4869, 2016.

[109] V. Khunova, J. Kristóf, I. Kelnar, and J. Dybal, "The effect of halloysite modification combined with in situ matrix modifications on the structure and properties of polypropylene/halloysite nanocomposites," *Express Polym. Lett.*, vol. 7, no. 5, pp. 471–479, 2013.

[110] J. Ren, A. S. Silva, and R. Krishnamoorti, "Linear viscoelasticity of disordered polystyrene-polyisoprene block copolymer based layered-silicate nanocomposites," *Macromolecules*, vol. 33, no. 10, pp. 3739–3746, 2000.

[111] J. Vermant, S. Ceccia, M. K. Dolgovskij, P. L. Maffettone, and C. W. Macosko, "Quantifying dispersion of layered nanocomposites via melt rheology," *J. Rheol.* , vol. 51, no. 3, pp. 429–450, 2007.

[112] R. Salehiyan, H. Y. Song, M. Kim, W. J. Choi, and K. Hyun, "Morphological Evaluation of PP/PS Blends Filled with Different Types of Clays by Nonlinear Rheological Analysis," *Macromolecules*, vol. 49, no. 8, pp. 3148–3160, 2016.

[113] J. Norris, R. F. Giese, P. M. Costanzo, and C. J. Vanoss, "The Surface Energies of Cation Substituted Laponite," *Clay Miner.*, vol. 28, no. 1, pp. 1–11, 1993.

[114] O. Monticelli, Z. Musina, A. Frache, F. Bellucci, G. Camino, and S. Russo, "Influence of compatibilizer degradation on formation and properties of PA6/organoclay nanocomposites," *Polym. Degrad. Stab.*, vol. 92, no. 3, pp. 370–378, 2007.

[115] J. Genoyer, N. R. Demarquette, and J. Soulestin, "Comparison of Montmorillonite, Laponite and Halloysite as Compatibilizers in PMMA/PS Blends," *Eur. Polym. J.*, vol. Submitted.

[116] M. Sentmanat, B. N. Wang, and G. H. McKinley, "Measuring the transient extensional rheology of polyethylene melts using the SER universal testing platform," *J. Rheol.* , vol. 49, no. 3, pp. 585–606, 2005.

[117] T. D. Fornes, P. J. Yoon, H. Keskkula, and D. R. Paul, "Nylon 6 nanocomposites: the effect of matrix molecular weight," *Polymer* , vol. 42, no. 25, pp. 09929–09940, 2001.

[118] S. Tanoue *et al.*, "Melt compounding of different grades of polystyrene with organoclay. Part 2: Rheological properties," *Polym. Eng. Sci.*, vol. 44, no. 6, pp. 1061–1076, Jun. 2004.

# Compatibilization of PMMA/PS blends by nanoparticles and block copolymers: effect on morphology and interfacial relaxation phenomena

## Abstract

In this thesis, the compatibilization mechanism induced by clay nanoparticles in polymer blends was investigated using rheology. To do so, montmorillonite, laponite and halloysite, modified or not, were added to PMMA/PS blends. Linear shear rheology showed that the compatibilization mechanism, especially the coalescence phenomenon, was greatly influenced by the localization of clay nanoparticles. Modified montmorillonite, which was located at the interface, was shown to be the most efficient at inhibiting coalescence among clays and as efficient as a block copolymer with a high molecular mass. The latter is particularly interesting as nanoparticles are cheaper than block copolymers. In this work, special attention was given to relaxations happening in blends. Using linear shear rheology, Marangoni stresses due to a gradient in compatibilizer concentration at the interface was evidenced for the first time in the case of organically modified clay nanoparticles when located at the interface. Finally, submitting blends to elongational flow and subsequent relaxation showed that the relaxation of the droplets after high deformations was faster in the case of clays dispersed in the matrix and slowed down by the interfacial tension in the case of a better dispersion of clays at the interface or in the whole blend.

*Keywords:* linear viscoelasticity, extensional rheology, polymer blends, compatibilization, nanoparticles, organoclay, Marangoni stresses

---

# Compatibilisation de mélanges PMMA/PS par des nanoparticules et des copolymères à bloc: effet sur la morphologie et les phénomènes de relaxations interfaciales

## Résumé

Ces travaux de thèse présentent une étude du mécanisme de compatibilisation induit par des nanoparticules d'argile dans les mélanges de polymères en utilisant la rhéologie. Pour cela, de la montmorillonite, la laponite et l'halloysite, modifiées ou non, ont été ajoutées à des mélanges PMMA/PS. Les résultats de rhéologie linéaire en cisaillement ont montré que le mécanisme de compatibilisation, particulièrement le phénomène de coalescence, dépendait beaucoup de la localisation des nanoparticules. La montmorillonite modifiée, présente à l'interface entre les polymères, est la plus efficace à inhiber la coalescence et est aussi efficace qu'un copolymère à bloc de haute masse molaire. Ceci est particulièrement intéressant car les nanoparticules d'argile représentent un coût moindre comparé aux copolymères à bloc. Dans ces travaux, une attention spéciale a été portée aux relaxations présentes dans les mélanges. En utilisant la rhéologie linéaire en cisaillement, un effet Marangoni a été mis en évidence pour la première fois dans le cas de nanoparticules d'argile modifiées présentes à l'interface. Enfin, les mélanges soumis à un flux élongationnel puis relaxation ont montré que la relaxation des gouttes de phase dispersée après une importante déformation était plus rapide par ajout d'argiles dispersées dans la matrice et ralentie par des argiles mieux dispersées soit à l'interface, soit dans l'ensemble du mélange.

*Mots clés :* viscoélasticité linéaire, rhéologie extensionnelle, mélange de polymères, compatibilisation, nanoparticules, argiles modifiées, effet Marangoni